学位論文

Higgs Dynamics in the Early Universe

(初期宇宙におけるヒッグス場のダイナミクス)

平成29年12月博士(理学)申請

東京大学大学院理学系研究科

物理学専攻

江間 陽平

Higgs Dynamics in the Early Universe

Yohei Ema

Department of Physics, Faculty of Science,
University of Tokyo, Bunkyo-ku, Tokyo 113-0033, Japan

Abstract

According to the current measurement of the standard model parameters, the Higgs potential may develop a true minimum deeper than the electroweak vacuum in a large field value region, indicating that the electroweak vacuum is metastable. In this thesis, we study cosmological implications of the electroweak vacuum metastability in the context of the inflationary universe. We pay special attention to the Higgs-inflaton preheating dynamics after inflation, and find that the electroweak vacuum can be destabilized due to resonant Higgs particle production. We study this process in detail both analytically and numerically, and specify the parameter region where the electroweak vacuum destabilization happens.

Contents

List of Figures

List of Tables

Chapter 1

Introduction

1.1 Overview

After the Higgs mass measurement by the large hadron collider (LHC), all the parameters in the standard model (SM) are now fixed. One of the most important consequences is probably the so-called electroweak (EW) vacuum metastability. Assuming that the SM is valid up to high energy scale, we can compute the high energy behavior of the Higgs quartic self coupling by using the renormalization group (RG) equation. With the current center values of the Higgs and top quark masses, it actually turns to negative at around the renormalization scale of 10^{10} GeV, which we call an instability scale. It indicates that the SM Higgs potential develops a true minimum deeper than the EW vacuum at a large field value region. It does not necessarily contradict with the present universe since the lifetime of the EW vacuum is longer than the age of the universe. This situation is called the EW vacuum metastability.

If the EW vacuum is indeed metastable, we should carefully follow the dynamics of the Higgs field during the whole cosmological history. The universe, especially in its early state, is controlled by high energy phenomena, and hence it is possible that the Higgs field rolls down to the true minimum at some cosmological epoch. Once it happens, it is expected to be difficult to realize the present universe where the Higgs field lies in the EW vacuum. Thermal effects are not likely to cure this situation since particles that couple to the Higgs field must be quite heavy due to the large Higgs field value once the Higgs rolls down to the true minimum. Thus the EW vacuum metastability has non-trivial implications on the cosmology, especially in the early universe, and this is the main topic of this thesis.

In this dissertation, we study implications of the EW vacuum metastability in the context of the inflationary cosmology. In particular we pay attention to the Higgs-inflaton dynamics after inflation. An inflaton typically oscillates at around its potential minimum after inflation, and it causes resonant Higgs particle production if there are sizable couplings between the inflaton/gravity sector and the Higgs sector. Provided that the inflaton mass scale is higher than the instability scale, the produced Higgs particles induce a tachyonic mass to the Higgs itself due to finite density effect, and push the Higgs to roll down to the true minimum. Thus we can obtain bounds on the strength of the interaction between the inflaton/gravity sector and the Higgs sector by requiring that the EW vacuum survives such a "preheating"

epoch. More specifically, we assume that there exists the following interaction between the inflaton/gravity sector and the Higgs sector:

$$\mathcal{L}_{\rm int} = -\lambda_{h\phi}\phi^2 |H|^2 - \sigma_{h\phi}\phi |H|^2 - \xi_h R |H|^2 , \tag{1.1.1}$$

where H is the SM Higgs doublet, ϕ is the inflaton, R is the Ricci scalar, and $\lambda_{h\phi}$, ξ_h and $\sigma_{h\phi}$ are coupling constants. These couplings are expected to be present in general, and are also useful to stabilize the Higgs during inflation for high-scale inflation models. Thus our primary goal of this dissertation is to determine in what parameter region the EW vacuum destabilization occurs during the preheating epoch with the above interaction for both high-scale/low-scale inflation models.

1.2 Organization of this dissertation

Chaps. 2 and 3 are the review part of this dissertation. In Chap. 2, we review the global structure of the Higgs potential. We first briefly explain the idea of the effective potential and the renormalization group (RG) improvement in Sec. 2.1. Then we move on to the SM Higgs potential in Sec. 2.2. There we show the RG evolution of the Higgs quartic self coupling. We shall see that it turns to negative at high energy scale, indicating that the EW vacuum is metastable. This chapter is the basis of the subsequent chapters.

In Chap. 3, we review the Higgs dynamics during inflation. Light scalar fields including the Higgs experience stochastic dynamics during inflation whose noise term is controlled by the Hubble parameter. In Sec. 3.1 we introduce the Fokker-Planck equation that describes this stochastic dynamics. In Sec. 3.2 we study the Higgs dynamics during inflation. In particular, if the inflationary scale is high enough, the noise term may push the Higgs to roll down to the true minimum during inflation. Thus we obtain bounds on the Hubble parameter from the EW vacuum stability during inflation. We slightly extend previous studies by including the time-dependence of the Hubble parameter there. In Sec. 3.3, we discuss one possible way to avoid the constraint. If the Higgs acquires an effective mass during inflation from, *e.g.* the interaction (1.1.1), it stabilizes the Higgs at the origin of its potential during inflation. Hence we can indeed avoid the constraint, and this fact motivates us to study the interaction (1.1.1) in detail. It typically induces, however, resonant Higgs particle production after inflation, which may cause the EW vacuum destabilization during the preheating epoch. This is the main topic of this thesis.

Chaps. 4 and 5 are the main parts of this dissertation, based on the author's original works [1–3] in collaboration with Mindaugas Karčiauskas, Oleg Lebedev, Kyohei Mukaida, Kazunori Nakayama and Marco Zatta. We study the Higgs-inflaton dynamics after inflation for a high-scale inflation model in Chap. 4. We first give an overview of this system in Sec. 4.1. We then study effects of the Higgs-inflaton quartic coupling $\lambda_{h\phi}$ or the Higgs-curvature non-minimal coupling ξ_h after inflation, and derive bounds on $\lambda_{h\phi}$ or ξ_h both analytically and numerically in Secs. 4.2 and 4.3, respectively. In Sec. 4.4, we study the case with both $\lambda_{h\phi}$ and ξ_h being present. We shall find that the resonance is actually suppressed for some finite parameter region, and relatively large values of $\lambda_{h\phi}$ and ξ_h are allowed in such a case. In

Sec. 4.5, we study the Higgs-inflaton trilinear coupling $\sigma_{h\phi}$. We derive bound on $\sigma_{h\phi}$ almost independently of $\lambda_{h\phi}$ and ξ_h. In Sec. 4.6, we study effects of the couplings between the Higgs and the other SM particles. We will find that they do not significantly affect the preheating dynamics of the EW vacuum.

In Chap. 5, we study the Higgs-inflaton dynamics after inflation for a low-scale inflation model. We take the hill-top inflation model as a representative example of low-scale inflation models in this chapter. We first explain the setup in Sec. 5.1. In Sec. 5.2, we briefly explain the Higgs dynamics during inflation. For low-scale inflation models with the Hubble parameters being sufficiently small, the Higgs dynamics during inflation is rather trivial. Still, we have some constraints on the couplings in order not to induce a tachyonic mass to the Higgs during inflation. In Sec. 5.3, we analytically discuss particle production of the Higgs and the inflaton after inflation. For low-scale inflation models such as the hill-top inflation model, not only the Higgs but also the inflaton particles are resonantly produced. Indeed, the latter determines the end of the preheating. We roughly estimate bounds on the couplings from the EW vacuum stability by taking these effects into account there. In Sec. 5.4, we perform numerical simulation to study the EW vacuum destabilization during the preheating epoch more precisely, and confirm our analytical estimation.

In Chap. 6, we summarize this dissertation with some possible future directions.

The appendices are organized as follows. In App. A, we summarize the notations and conventions used in this dissertation. App. B is devoted to supplementary materials on the EW vacuum metastability. In particular, we derive one-loop RG equations of the relevant SM parameters there. In App. C, we review the basis of inflation. We shall derive the power spectrum of the scalar and tensor perturbations that are the primary observables used to constrain the inflationary models. We also discuss derivation of the Langevin and the Fokker-Planck equations that are used extensively in Chap. 3. In App. D, we review resonant particle production after inflation, or the preheating epoch. The idea of the broad/tachyonic resonance is extensively discussed there. Finally in App. E, we review some basics about the classical lattice simulation. We also give some details on the practical implementation of our numerical simulations there.

Chapter 2

Electroweak vacuum metastability

In this chapter we review the global structure of the SM Higgs potential. We pay special attention to the large field value region of the Higgs potential. Indeed, the effective Higgs potential turns to negative at a large field value region, indicating that the EW vacuum is not absolutely stable. It is called the EW vacuum metastability, and is the fundamental subject of this dissertation.

2.1 Lightning review on effective potential

In order to understand the EW vacuum metastability, the idea of the effective potential and the renormalization group (RG) improvement plays the key role, and hence we briefly review them at first. We refer Coleman-Weinberg's original paper [4] for more details.

2.1.1 Definition

In this section we review the theoretical foundations on the effective potential. For simplicity, we consider only a real scalar field ϕ in this section. We define $Z[J]$ as

$$Z[J] = \int \mathcal{D}\phi \exp\left[i \int d^4x \left(\mathcal{L} + J\phi \right) \right], \tag{2.1.1}$$

where the boundary states are taken as the in/out vacua, $\mathcal{L}$ is the Lagrangian for ϕ, and J is a c-number external source term. We define the generating functional for the connected Green's function $W[J]$ as

$$W \equiv -i \log Z. \tag{2.1.2}$$

Note that

$$\left. \frac{\delta W}{\delta J(x)} \right|_{J=0} = \left\langle \phi(x) \right\rangle. \tag{2.1.3}$$

More generally we define a background field value $\bar{\phi}$ as

$$\bar{\phi}(x) \equiv \frac{\delta W}{\delta J(x)}, \tag{2.1.4}$$

that is, $\bar{\phi}$ is the expectation value of ϕ in the presence of the source term J. Now we define the effective action $\Gamma[\bar{\phi}]$ as the Legendre transformation of $W[J]$ as

$$\Gamma[\bar{\phi}] \equiv W[J] - \int d^4x J(x)\bar{\phi}(x). \tag{2.1.5}$$

In this formula, J should be understood as the solution of Eq. (2.1.4) (or Eq. (2.1.6) below) for a given $\bar{\phi}$, as it is usual for the Legendre transformation. Then we obtain

$$\frac{\delta\Gamma}{\delta\bar{\phi}} = -J. \tag{2.1.6}$$

In particular, if we find a configuration $\phi_{\rm sol}$ that satisfies

$$\left.\frac{\delta\Gamma}{\delta\bar{\phi}}\right|_{\bar{\phi}=\phi_{\rm sol}} = 0, \tag{2.1.7}$$

we do not need any external force J to keep the configuration of ϕ as $\phi_{\rm sol}$. In other words, $\phi = \phi_{\rm sol}$ is the configuration realized by the Lagrangian $\mathcal{L}$ with quantum effects taken into account. In this sense, Eq. (2.1.7) is understood as the quantum version of the equation of motion of the scalar field ϕ. For a generic field configuration $\bar{\phi}$ that does not satisfy Eq. (2.1.7), we need an external force J determined by Eq. (2.1.6) to keep it as it is. Indeed, as we shall see below, the source term J is used to cancel tad-pole terms in the effective potential in practical computations.

Now we perform the gradient expansion as

$$\Gamma[\bar{\phi}] = \int d^4x \left[-V_{\rm eff}(\bar{\phi}) - \frac{Z(\bar{\phi})}{2}\left(\partial\bar{\phi}\right)^2 + ...\right], \tag{2.1.8}$$

where the leading term $V_{\rm eff}$ is called the effective potential. Then a constant $\bar{\phi}$ is the expectation value of ϕ at a vacuum if it satisfies

$$\frac{\partial V_{\rm eff}}{\partial\bar{\phi}} = 0. \tag{2.1.9}$$

Thus the effective potential characterizes locations of vacua for a given theory including quantum effects. It is this effective potential that is the main target in this chapter.

2.1.2 Example

In this subsection we consider the following action

$$\mathcal{L} = -\frac{1}{2}\left(\partial\phi\right)^2 - V(\phi), \quad V(\phi) \equiv \frac{\lambda_b}{4}\phi^4, \tag{2.1.10}$$

as an example, and demonstrate how to obtain the effective potential by means of perturbative expansion. The effective potential is defined as

$$\exp\left(-i\int d^4x V_{\rm eff}(\bar{\phi})\right) = \int \mathcal{D}\phi \exp\left[i\int d^4x \left(\mathcal{L} + J(\phi-\bar{\phi})\right)\right], \tag{2.1.11}$$

where $\bar{\phi}$ is now constant. We define $\chi \equiv \phi - \bar{\phi}$, and expand the Lagrangian up to quadratic order in χ. It is rewritten as

$$\exp\left(-i\int d^4x V_{\rm eff}(\bar{\phi})\right) = \int \mathcal{D}\chi \exp\left[i\int d^4x \left(-V(\bar{\phi}) + \mathcal{L}_\chi\right)\right] \tag{2.1.12}$$

where the quadratic Lagrangian for χ is given by

$$\mathcal{L}_\chi = -\frac{1}{2}(\partial\chi)^2 - \frac{1}{2}m_\chi^2(\bar{\phi})\chi^2 + \left(J - \lambda_b\bar{\phi}^3\right)\chi + O(\chi^3), \tag{2.1.13}$$

with the mass term of χ being given by

$$m_\chi^2(\bar{\phi}) = 3\lambda_b\bar{\phi}^2. \tag{2.1.14}$$

Here the source term J is fixed such that the expectation value of ϕ is equal to $\bar{\phi}$, and thus it just erases the term linear in χ up to the quadratic level, which means $J = \lambda_b\bar{\phi}^3$. Now the integration over χ is trivial since it is Gaussian, and we obtain

$$V_{\rm eff}(\bar{\phi}) = \frac{1}{4}\left[\lambda + \frac{9\lambda^2}{16\pi^2}\left(\ln\left(\frac{\bar{\phi}^2}{M^2}\right) - \frac{25}{6}\right)\right]\bar{\phi}^4, \tag{2.1.15}$$

where the counter terms are determined by the conditions

$$\left.\frac{d^2V_{\rm eff}}{d\bar{\phi}^2}\right|_{\bar{\phi}=0} = 0, \quad \text{and} \quad \left.\frac{d^4V_{\rm eff}}{d\bar{\phi}^4}\right|_{\bar{\phi}=M} = 6\lambda, \tag{2.1.16}$$

with M being some field value. For more details on the computation, see App. B.1. Note that the correction comes with the factor $\lambda\ln(\bar{\phi}^2/M^2)$, not λ, and hence it is applicable only at around $\bar{\phi} \sim M$. In order to make it applicable for larger field value region, we have to perform the RG improvement of the effective potential. After the RG improvement, the effective potential is valid as long as the (running) coupling is small enough.

2.1.3 RG improvement

Now we discuss the RG improvement procedure of the effective potential. As we saw in the previous subsection, perturbations come with the factor $\lambda\ln(\bar{\phi}^2/M^2)$, and hence the effective potential in the previous section is valid only when this factor is small, not λ. In order to remedy this point, we consider the following equation:

$$0 = M\frac{dV_{\rm eff}}{dM} = \left[M\frac{\partial}{\partial M} + \sum_i \beta_i\frac{\partial}{\partial g_i} - \sum_a \gamma_a\frac{\partial}{\partial\ln\phi_a}\right]V_{\rm eff}, \tag{2.1.17}$$

where we have defined the beta functions and the anomalous dimensions as

$$\beta_i \equiv \frac{dg_i}{d\ln M} \quad \text{and} \quad \gamma_a \equiv -\frac{d\ln\phi_a}{d\ln M}. \tag{2.1.18}$$

It means that the effective potential should not depend on the renormalization scale M, or different choices of M can be compensated by corresponding changes/rescalings of the parameters/fields. This equation is exact, and once we know the shape of V_{eff} at some M, then we can know the shape of V_{eff} for any M by using it. Of course we usually use perturbative expansions to obtain β_i and γ_a, but they are expansions with respect to couplings, not to couplings times $\ln(\bar{\phi}^2/M^2)$. Hence it is valid for any $\bar{\phi}$ as long as the couplings remain small enough, which is the virtue of the RG improvement procedure. In order to illustrate this procedure more concretely, we consider again the ϕ^4 theory as an example in the following.

From now we consider the ϕ^4 theory as an example. Just from the dimensional analysis, the effective potential must be parametrized by

$$V_{\text{eff}}(\bar{\phi}) = \frac{Y(t,\lambda)}{4}\bar{\phi}^4, \tag{2.1.19}$$

where t is defined as

$$t \equiv \ln\left(\frac{\bar{\phi}}{M}\right), \tag{2.1.20}$$

with M being some renormalization scale. Here λ is the renormalized coupling defined by the renormalization condition as

$$6\lambda \equiv \left.\frac{d^4V_{\text{eff}}}{d\bar{\phi}^4}\right|_{\bar{\phi}=M}. \tag{2.1.21}$$

If we instead impose a renormalization condition at $\bar{\phi} = M' \neq M$, then we should use a different numerical value λ' to make the theory intact. In this sense, the renormalized coupling depends on M. It is governed by

$$\frac{d\lambda}{d\ln M} = \beta(\lambda). \tag{2.1.22}$$

It just tells us how to reparameterize λ. Then the prefactor Y satisfies

$$\left[\frac{\partial}{\partial t} - \bar{\beta}(\lambda)\frac{\partial}{\partial\lambda} + 4\bar{\gamma}(\lambda)\right]Y = 0, \tag{2.1.23}$$

where we have defined

$$\bar{\beta}(\lambda) \equiv \frac{\beta}{1+\gamma} \quad \text{and} \quad \bar{\gamma}(\lambda) \equiv \frac{\gamma}{1+\gamma}. \tag{2.1.24}$$

Note that β and γ depend on t only through λ, and hence commute with the partial derivative $\partial/\partial t$. In general, the solution to this equation is given by

$$Y(t,\lambda) = f\left(\bar{\lambda}(t,\lambda)\right) \exp\left[-4\int_0^t dt' \bar{\gamma}\left(\bar{\lambda}(t',\lambda)\right)\right], \tag{2.1.25}$$

where $\bar{\lambda}$ satisfies

$$\frac{\partial \bar{\lambda}}{\partial t} = \bar{\beta}(\bar{\lambda}). \tag{2.1.26}$$

The boundary condition of $\bar{\lambda}$ at $t = 0$ is given as a function of λ by the renormalization condition. In order to show Eq. (2.1.25), it is useful to note that

$$\int_\lambda^{\bar{\lambda}(t)} \frac{d\lambda'}{\bar{\beta}(\lambda')} = t. \tag{2.1.27}$$

By taking derivative with respect to λ, we obtain

$$\frac{\partial \bar{\lambda}}{\partial \lambda} = \frac{\bar{\beta}(\bar{\lambda})}{\bar{\beta}(\lambda)}. \tag{2.1.28}$$

Once we have this relation, it is trivial to show that Eq. (2.1.25) is indeed a solution by substituting it directly to Eq. (2.1.23). The functional form of f is fixed by the renormalization condition at $t = 0$, and hence we finally obtain the effective potential as

$$V_{\rm eff}(\bar{\phi}) = \frac{\bar{\lambda}(t,\lambda)}{4}\bar{\phi}^4 \exp\left[-4\int_0^t dt' \bar{\gamma}\left(\bar{\lambda}(t',\lambda)\right)\right]. \tag{2.1.29}$$

From this expression, it is clear that the beta function plays a crucial role to determine the global structure of the effective potential, and hence the vacuum structure of the theory. For this reason, we discuss in detail the RG evolution of the Higgs quartic self coupling in the next section.

So far we have not used any information of the one-loop effective potential we obtained in the previous subsection, but it is indeed useful to determine the beta function. In order to see this point, we first expand Eq. (2.1.29) by t assuming that t is small:

$$V_{\rm eff}(\bar{\phi}) \simeq \frac{1}{4}\left[\lambda + \frac{\bar{\beta}(\lambda) - 4\lambda\bar{\gamma}(\lambda)}{2}\ln\left(\frac{\bar{\phi}^2}{M^2}\right)\right]\bar{\phi}^4, \tag{2.1.30}$$

where we have concentrated only on the coefficient of t. On the other hand, Eq. (2.1.15) should also be valid as long as t is small, and hence we obtain

$$\beta(\lambda) = \frac{9}{8\pi^2}\lambda^2 + 4\lambda\gamma, \tag{2.1.31}$$

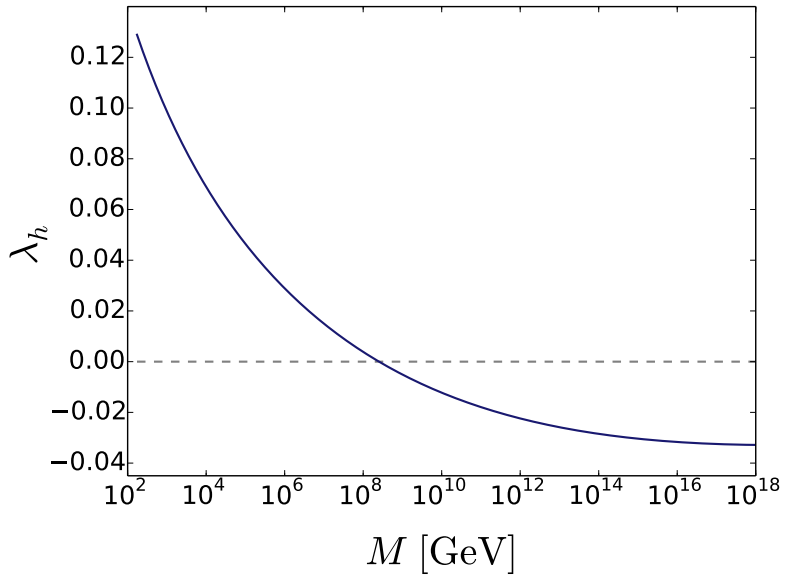

Figure 2.1: The RG evolution of the Higgs quartic self coupling at the one-loop level within the SM. We take the Higgs/top quark masses as $m_h = 125\,\text{GeV}$ and $m_t = 173.1\,\text{GeV}$, respectively. It turns to negative at around $M \simeq 10^9\,\text{GeV}$ at the one-loop level, while it occurs at around $M \simeq 10^{10}\,\text{GeV}$ once we include higher order corrections [5].

by matching the coefficient of t. Note that $\bar{\beta} \simeq \beta$ and $\bar{\gamma} \simeq \gamma$ at the one-loop level. Since $\gamma = 0$ in the ϕ^4 theory as we see in App. B.2.1, we get

$$\beta(\lambda) = \frac{9}{8\pi^2}\lambda^2. \tag{2.1.32}$$

Thus, the loop expansion of the effective potential is useful to determine the RG running of the parameters in the scalar potential. We shall use the same method to compute the one-loop beta function of the Higgs quartic self coupling in the SM in App. B.2.2. The effective potential with the one-loop beta function (2.1.32) being used to find $\bar{\lambda}$ is called the RG improved one-loop effective potential.

2.2 Electroweak vacuum metastability

As we discussed in the previous section, RG evolutions of couplings are crucial in understanding the vacuum structure of a system. In particular, the RG running of the quartic coupling is most important for the simplest ϕ^4 theory. The situation is similar in the SM model, where the Higgs potential is almost purely quartic for a field value much larger than the EW scale. For this reason, in Fig. 2.1, we show the RG evolution of the Higgs quartic coupling λ_h computed within the vanilla SM. It includes the one-loop contributions, and the input Higgs/top quark masses are $m_h = 125\,\text{GeV}$ and $m_t = 173.1\,\text{GeV}$, respectively. For the derivation of the one-loop beta functions, see App. B. For higher-loop contributions, we refer the readers to Ref. [5]. From Fig. 2.1, we can see that the Higgs quartic coupling λ_h turns to

negative at high energy scale. It indicates that the Higgs effective potential develops a deeper minimum in a larger field value region. It does not contradict with the present universe, since the lifetime of the EW vacuum is likely to be longer than the age of the universe, as calculated in detail in Refs. [6–8]. Thus we call this situation as the EW vacuum metastability [5,6,9–19], and we assume that it is indeed the case throughout this dissertation. For the one-loop case, the Higgs quartic self coupling λ_h turns to negative at around $M \simeq 10^9$ GeV, but it happens at $M \simeq 10^{10}$ GeV after including higher loop effects [5], where M is the renormalization scale. Hence we denote the latter scale as $M_{\rm inst}$, and use it as a rough estimation of the instability scale.[þ1]

As we said above, the EW vacuum decay rate is small enough for the current center values of the SM parameters. However, in order to check whether the EW vacuum metastability is truly consistent with the present universe, it is mandatory to study not only the vacuum tunneling rate, but also the whole cosmological evolution of the Higgs field. The universe, in particular in its early stage such as inflation, is controlled by high energy phenomena. Hence it may be possible that the Higgs tends to roll down to the deeper region during some cosmological epoch, resulting in difficulty to realize the present universe. Thus the EW vacuum metastability has deep implications on the dynamics in the early universe, which is the main subject of this dissertation. In particular, we study in detail the Higgs dynamics during/after inflation in the presence of the EW vacuum metastability in the following chapters.

[þ1] The instability scale here is an energy scale, not a field value of the Higgs.

Chapter 3

Metastability during inflation

In this chapter, we review the dynamics of the Higgs field during inflation, following mainly the discussion in Ref. [20]. In particular, we derive constraints on the Hubble parameter during inflation by requiring that the EW vacuum is stable during inflation.

3.1 Fokker-Planck equation

In this section we briefly explain the Langevin and the Fokker-Planck equations that describe the dynamics of the super-horizon mode of a spectator field [21, 22]. Homogeneous modes of a light[þ1] scalar field χ obey the following Langevin equation during inflation:

$$\dot{\chi} = -\frac{1}{3H}\frac{\partial V}{\partial \chi} + f(t, \vec{x}), \tag{3.1.1}$$

where H is the Hubble parameter and V is the scalar potential of χ. Here χ should be understood as a homogeneous mode where the modes with the momentum $k/a < \epsilon H$ are summed over, and $\epsilon < 1$ is a numerical factor with ϵH being constant during inflation. The noise term f satisfies

$$\langle f(t, \vec{x}) f(t', \vec{x}') \rangle = \frac{H^3}{4\pi^2}\frac{\sin z}{z}\delta(t - t'), \quad z = \epsilon a H \left|\vec{x} - \vec{x}'\right|, \tag{3.1.2}$$

where $\langle ... \rangle$ denotes the average over possible noise configurations. It originates from the quantum fluctuations during inflation. In particular, within the same Hubble patch it satisfies

$$\langle f(t) f(t') \rangle = \frac{H^3}{4\pi^2}\delta(t - t'). \tag{3.1.3}$$

It may be instructive to rewrite the Langevin equation in terms of the number of e-folds N as

$$\frac{\partial \chi}{\partial N} = -\frac{1}{3H^2}\frac{\partial V}{\partial \chi} + \frac{H}{2\pi}\zeta(N), \tag{3.1.4}$$

[þ1] Here "light" means that a mass is much smaller than the Hubble parameter during inflation.

where ζ now satisfies

$$\langle \zeta(N)\zeta(N')\rangle = \delta(N - N'). \tag{3.1.5}$$

Thus the light field χ experiences the Brownian motion with the step size of $H/2\pi$ for each one e-fold. For the derivation of the Langevin equation, see App. C.3.2

For our purpose, it is more convenient to rewrite the Langevin equation to the time evolution equation for the probability density function of χ. We define $P(\chi, N)$ as

$$P(\tilde{\chi}, N) \equiv \langle \delta\left(\chi(N) - \tilde{\chi}\right)\rangle . \tag{3.1.6}$$

Note that

$$\langle F\left(\chi(N)\right)\rangle = \int d\tilde{\chi}\, P(\tilde{\chi}, N)\, F(\tilde{\chi}), \tag{3.1.7}$$

and hence P should be indeed understood as the probability density function of χ. Then the Langevin equation is written in terms of P as

$$\frac{\partial P}{\partial N} = \frac{\partial}{\partial \chi}\left[\frac{\partial V}{\partial \chi}\frac{P}{3H^2} + \frac{H^2}{8\pi^2}\frac{\partial P}{\partial \chi}\right], \tag{3.1.8}$$

where we have dropped the tildes for notational ease. It is the Fokker-Planck equation that describes the time evolution of the probability distribution function of a light scalar field during inflaiton. For more details on the derivation, see again App. C.3.2. In the next section we extensively use it to study the stochastic dynamics of the Higgs during inflation.

3.2 Higgs dynamics during inflation

As we reviewed in Chap. 2, the EW vacuum may be metastable according to the current measurement of the SM parameters. In such a case the EW vacuum can be destabilized during inflation, and hence we can obtain an upper bound on the inflationary energy scale by requiring that the EW vacuum be stable during inflation [20, 23–32]. In the following, we first describe qualitative properties of this system, and then perform numerical computation to derive the upper bound. We follow the discussion in Ref. [20] in this section.

3.2.1 Preliminary

Without any Hubble induced mass terms, the Higgs is light during inflation, and hence its superhorizon mode grows stochastically due to the quantum fluctuations. The size of the noise term is controlled by the Hubble parameter (see Eq. (3.1.3)). If the noise term is much larger than the instability scale of the Higgs potential ($\sim 10^{10}$ GeV), it easily kicks the Higgs to roll down to the deeper region of the potential. Thus, in order to avoid such a catastrophe, we obtain an upper bound on the Hubble parameter during inflation. Below we quantify this idea.

The stochastic dynamics of the Higgs is well described by the Fokker-Planck equation introduced in the previous section:

$$\frac{\partial P}{\partial N} = \frac{\partial}{\partial h}\left[\frac{\partial V}{\partial h}\frac{P}{3H^2} + \frac{H^2}{8\pi^2}\frac{\partial P}{\partial h}\right], \tag{3.2.1}$$

where h is the radial component of the Higgs. In the following analysis we approximate the Higgs potential as that around $M_{\rm inst}^2$, or

$$V \simeq -b_0 \log\left(\frac{H^2+h^2}{M_{\rm inst}^2}\right)\frac{h^4}{4}, \tag{3.2.2}$$

where $b_0 \simeq 0.12/16\pi^2$.[b2] Here we take the renormalization scale as $M^2 = H^2 + h^2$ following Ref. [28]. This is because the dispersion relation of the SM particles is modified in the de-Sitter space, and its effect appears as an additional H^2 factor in the logarithms when computing the one-loop effective potential. For more details, see *e.g.* Refs. [28, 33] and references therein.[b3] In this system, there are two important quantities in addition to $M_{\rm inst}$. One is the field value $h_{\rm cl}$ above which the classical drift term overcomes the quantum noise term. It is defined as

$$\left|\frac{\partial V}{\partial h}(h_{\rm cl})\right| \equiv \frac{3H^3}{2\pi}. \tag{3.2.3}$$

It is derived as follows. The displacement of Higgs due to the potential within one e-folding is estimated with the slow-roll approximation as $h/H \simeq -(\partial V/\partial h)/3H^2$, while that due to the quantum noise is $H/2\pi$. Hence we obtain the above expression for $h_{\rm cl}$ by equating them. The other is the field value $h_{\rm srv}$ at which the slow-roll condition is violated:

$$h_{\rm srv} \equiv -\frac{1}{3H^2}\frac{\partial V}{\partial h}(h_{\rm srv}). \tag{3.2.4}$$

They satisfy

$$M_{\rm inst} < h_{\rm cl} < h_{\rm srv}, \tag{3.2.5}$$

as long as $M_{\rm inst} \ll H$ and $|\lambda_h| \ll 1$. For $h < h_{\rm cl}$, the Higgs just experiences the Brownian motion without feeling the potential. Once the Higgs grows due to the quantum noise term so that $h_{\rm cl} < h < h_{\rm srv}$, the potential dominates over the quantum noise, and hence the Higgs rolls down along the potential. Still, it takes some e-foldings for the Higgs to reach the region $h_{\rm srv} < h$ since the slow-roll condition is satisfied. After the Higgs reaches the region $h_{\rm srv} < h$, it rapidly rolls down to the deeper region. Thus, we may require[b4]

$$P(|h| > h_{\rm srv}, N)\, e^{3N} < 1, \quad \text{where} \quad P(|h| > h_{\rm srv}, N) \equiv 2\int_{h_{\rm srv}}^{\infty} dh\, P(h, N), \tag{3.2.6}$$

[b2] Here we are dealing with the super-horizon mode, and it may justify to use the effective potential for the Higgs equation of motion in the sense of the gradient expansion.

[b3] We must include a non-minimal coupling between the Higgs and the Ricci scalar to renormalize a logarithmic divergence as well. Its size at the inflationary scale depends on the boundary condition. Here we simply ignore it assuming that it is small. Its effect is discussed separately in Sec. 3.3 and Chap. 4.

[b4] See Ref. [30] for the gauge invariance of this requirement.

during the whole inflationary history for the EW vacuum stability during inflation.[b5] In other words, we require that there is no single Hubble patch where the Higgs rolls down to the true minimum during inflation in our past light-cone. This is because a Hubble patch in which the Higgs rolls down to the true minimum is expected to expand with the speed of light after inflation, and hence even single such patch would eventually swallow our entire universe. For more details on the dynamics of such a patch, see Refs. [20,30]. Thus we should multiply e^{3N}, or the number of the independent Hubble patches in our past light-cone, since h in the Fokker-Planck equation describes the Higgs field value averaged over one Hubble patch. Note that thermal potential after inflation is unlikely to change the situation much. This is because the Higgs rapidly rolls down to the large field value region once it exceeds $h_{\rm srv}$, and hence particles that couple to the Higgs must be decoupled from thermal bath due to large masses coming from the large Higgs field value.

3.2.2 Numerical analysis

Now we numerically solve the Fokker-Planck equation to obtain an upper bound on the Hubble parameter during inflation. In order to check the requirement (3.2.6), we should treat a tiny value of $P(|h| > h_{\rm srv}, N)$ precisely due to the large factor e^{3N}. For this reason, we change the variable as

$$X(h, N) \equiv \log\left(\frac{P(h, N)}{P(0, 0)}\right), \tag{3.2.7}$$

and solve the Fokker-Planck equation for $X(h, N)$ in our numerical code following Ref. [20]. We assume that the Higgs is initially set at the origin of its potential to obtain a conservative bound. More explicitly, we take the initial condition as Gaussian:

$$P = \frac{1}{\sqrt{2\pi\sigma^2}} \exp\left(-\frac{h^2}{2\sigma^2}\right), \quad \text{where} \quad \sigma^2 = \frac{1}{\sqrt{2\,|\lambda_h|}} \frac{H^2}{2\pi} \tanh\left(\frac{\sqrt{2\lambda_h}}{16\pi}\right), \tag{3.2.8}$$

with $|\lambda_h| = 0.01$. The precise value of σ is unimportant as long as $\sigma^2 \ll H^2$ since it quickly spread with its size determined by H. The boundary condition is taken as

$$h\frac{\partial P}{\partial h} = \frac{\partial^2 P}{\partial h^2}, \tag{3.2.9}$$

at the end-point, but the precise form is again unimportant. We have used the Crank-Nicolson (implicit) method as a differential equation solver.

The numerical results are shown in Fig. 3.1. In the left panel we fix the Hubble parameter at the beginning of the inflation $H_{\rm ini}$, and plot the maximal number of e-foldings with which the condition (3.2.6) is not violated. In the right panel we instead fix the Hubble parameter at the end of the inflation $H_{\rm end}$. We have included the time-dependence of the Hubble parameter

[b5] In a strict sense, we cannot rely on the Fokker-Planck equation for $h_{\rm srv} < h$ since it uses the slow-roll approximation. However, the Higgs never comes back to $h < h_{\rm srv}$ once it exceed $h_{\rm srv}$ even if we (wrongly) use the Fokker-Planck equation. Thus we safely ignore this subtlety to obtain $P(|h| > h_{\rm srv})$.

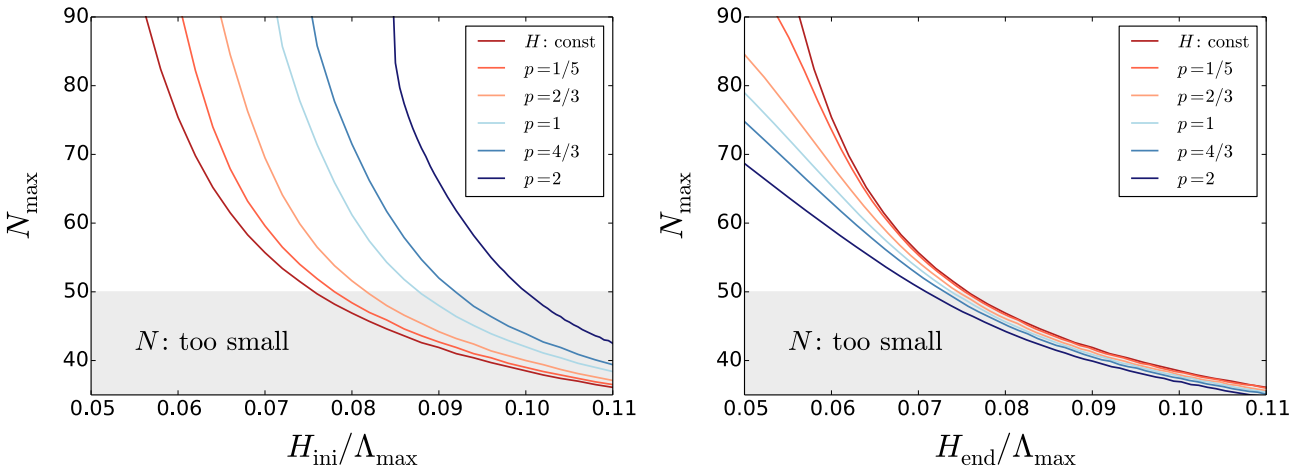

Figure 3.1: The constraints on the inflationary scale from the EW vacuum stability. The initial Hubble parameter $H_{\rm ini}$ is fixed in the left panel, while the final Hubble parameter $H_{\rm end}$ is fixed in the right panel. Here we have defined $\Lambda_{\max} \equiv M_{\rm inst}/\sqrt{e}$.

in the case where the inflaton potential is monomial: $V(\phi) \propto \phi^p$ where ϕ is the inflaton. In this case the Hubble parameter is estimated by using the slow-roll approximation as

$$H(N) = H_{\rm end}\left(1 + \frac{4}{p}(N_e - N)\right)^{p/4}, \tag{3.2.10}$$

where N_e is the e-folding at which $M_p^2 V'^2/2V^2 = 1$ with the prime denoting the derivative with respect to ϕ. In Fig. 3.1, the gray regions are excluded since inflation must last at least 50-60 e-folds depending on the reheating temperature. The plot of the pure de-Sitter case (the red one) agrees well with Ref. [20]. The plots with finite p are also easy to understand qualitatively. If we fix $H_{\rm ini}$, H is smaller in later time for larger p, and hence the constraint must be weaker. If we instead fix $H_{\rm end}$, H is larger in earlier time for larger p, and hence the constraint must be stronger. Anyway, the instability scale is of order 10^{10} GeV, and hence the upper bound is roughly given by

$$H \lesssim 10^9\,{\rm GeV}. \tag{3.2.11}$$

Thus it is a tight constraint on high-scale inflation models. For instance, the simple chaotic and the R^2-type inflation models are excluded since the Hubble parameters of these models are of order 10^{12}-10^{14} GeV fixed by the cosmic microwave background (CMB) observations.

It might also be instructive to see the time evolution of $P(h, N)$ shown in Fig. 3.2. The probability $P(|h| > h_{\rm srv}, N)$ always increases with time, so does the right-hand-side of Eq. (3.2.6). Thus although we require Eq. (3.2.6) during the whole history of inflation, it is actually equivalent to require Eq. (3.2.6) just at the end of inflation. As another thing, we can see that $P(|h| > h_{\rm srv}, N)$ is indeed quite tiny. Nevertheless it has a dramatic consequence due to the large factor e^{3N} in Eq. (3.2.6).

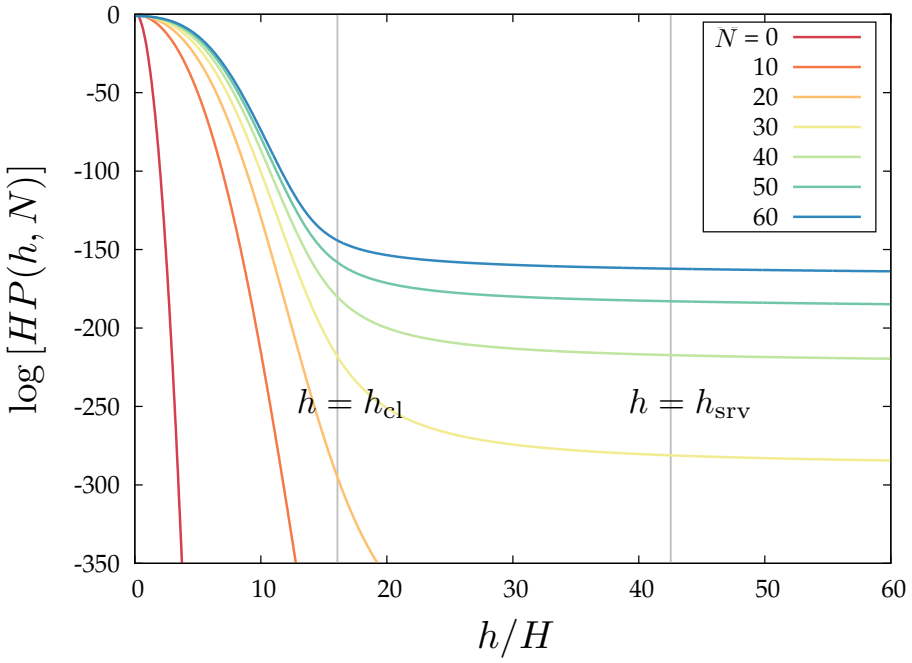

Figure 3.2: Time evolution of the probability distribution function $P(h, N)$ for $H/\Lambda_{\rm max} = 0.07$ in the pure de-Sitter space. The gray lines show the field values $h = h_{\rm cl}$ and $h_{\rm srv}$ in the unit of the Hubble parameter during inflation.

3.3 Stabilization by effective mass

As we saw in the previous sections, the EW vacuum metastability puts a tight constraint on the Hubble parameter during inflation. Still, there are several ways to avoid this constraint. Probably the simplest way is to introduce an effective mass to the Higgs during inflation. The noise term in the Langevin equation originates from the quantum fluctuations, and hence it is suppressed if the Higgs is massive (see App. C.3.1). Such an effective mass is induced if there are, *e.g.* the following couplings [23, 34]:

$$\mathcal{L}_{\rm int} = -\left(\frac{\lambda_{h\phi}}{2}\phi^2 + \frac{\xi_h}{2}R\right)h^2, \tag{3.3.1}$$

where ϕ is the inflaton, R is the Ricci scalar, $\lambda_{h\phi}$ is the Higgs-inflaton quartic coupling and ξ_h is the Higgs-curvature non-minimal coupling, respectively. It induces a Higgs effective mass as

$$m_h^2 = \lambda_{h\phi}\Phi^2 + 12\xi_h H^2, \tag{3.3.2}$$

where Φ is the inflaton field value and $R \simeq 12H^2$ during inflation. Thus it suppresses the quantum fluctuations if

$$\lambda_{h\phi} \gtrsim \frac{H^2}{\Phi^2}, \quad \text{and/or} \quad \xi_h \gtrsim 0.1, \tag{3.3.3}$$

so that we can avoid the tight constraint on the Hubble parameter during inflation.

Once we consider the dynamics of the Higgs after inflation, however, the situation is totally different: the very couplings (3.3.1) that stabilize the EW vacuum during inflation may cause the EW vacuum destabilization after inflation. This is because the induced effective mass term oscillates during the inflaton oscillation epoch after inflation (or the "preheating" epoch), resulting in Higgs particle production. If the couplings are large enough, the Higgs production is so efficient that it can kick the Higgs to roll down to the deeper region. Thus in the following chapters, we study the dynamics of the Higgs after inflation in detail. We assume that the inflaton/gravity sector and the Higgs sector is connected by the following interaction:

$$\mathcal{L}_{\rm int} = -\frac{1}{2}\left[\lambda_{h\phi}\phi^2 + \sigma_{h\phi}\phi + \xi_h R\right]h^2. \tag{3.3.4}$$

We also include the trilinear coupling $\sigma_{h\phi}$ in our discussion since it is allowed in general, to say the least. The typical energy scale of the system after inflation is controlled by the inflaton mass m_ϕ, and hence the EW vacuum may be destabilized even for low-scale inflation models as long as $m_\phi \gg M_{\rm inst}$. Thus we study high-scale and low-scale inflation models in Chaps. 4 and 5, respectively.

Chapter 4

Metastability after high-scale inflation

In Chap. 3, we have seen that the Higgs-inflaton and/or Higgs-gravity non-minimal couplings help to stabilize the Higgs during inflation for high-scale inflation models. After inflation, however, the same couplings may cause the EW vacuum destabilization due to resonant particle production as long as $m_\phi \gg M_{\rm inst}$, where m_ϕ is the inflaton mass scale. Thus, we study the Higgs dynamics after inflation, or during the inflaton oscillation epoch, with such couplings and with $m_\phi \gg M_{\rm inst}$ in this and next chapters. In this chapter we concentrate on a high-scale inflation model, and obtain upper bounds on the couplings by requiring that the EW vacuum survives the preheating epoch. This chapter is based on the author's original works [1, 2].

The organization of this chapter is as follows. In Sec. 4.1 we give an overview of our study in this chapter. In Secs. 4.2 and 4.3, we study the cases where there is only the Higgs-inflaton quartic coupling $\lambda_{h\phi}$ and the Higgs-curvature non-minimal coupling ξ_h, respectively. Then we study the case where there exist both $\lambda_{h\phi}$ and ξ_h in Sec. 4.4. In Sec. 4.5 we study effects of the Higgs-inflaton trilinear coupling $\sigma_{h\phi}$. Finally in Sec. 4.6, we discuss effects of the interaction between the Higgs and the other SM particles.

4.1 Overview

4.1.1 Setup

First we summarize our setup. In this chapter we consider the following Lagrangian:

$$\mathcal{L} = \frac{M_{\rm Pl}^2}{2} R + \mathcal{L}_\phi + \mathcal{L}_h + \mathcal{L}_{\rm int}, \tag{4.1.1}$$

where $M_{\rm Pl}$ is the reduced Planck scale, R is the Ricci scalar, $\mathcal{L}_\phi$ ($\mathcal{L}_h$) is the Lagrangian for the inflaton (Higgs) sector, and $\mathcal{L}_{\rm int}$ is the interaction between the Higgs and the inflaton/gravity. We explain each term in detail in the following.

■ **Inflaton sector**

We take the inflaton sector as the simplest one,

$$\mathcal{L}_\phi = -\frac{1}{2}\left(\partial\phi\right)^2 - V(\phi), \tag{4.1.2}$$

where the inflaton potential at around its origin is assumed to be quadratic:

$$V(\phi) = \frac{1}{2}m_\phi^2\phi^2, \tag{4.1.3}$$

with m_ϕ being the inflaton mass. This is just for simplicity, and our analysis can be extended to more generic inflaton sectors. We assume that inflation occurs in the $\phi > 0$ region without loss of generality, and $m_\phi \gg M_{\rm inst}$ that holds in most of high-scale inflation models. Indeed, the mass scale m_ϕ is typically of order 10^{12}–10^{13} GeV for high-scale inflation models in order to be consistent with the CMB observations as we see in App. C.2.3.

■ Higgs sector

The Higgs sector is given by

$$\mathcal{L}_h = -\frac{1}{2}\left(\partial h\right)^2 - \frac{\lambda_h}{4}h^4, \tag{4.1.4}$$

where λ_h is the Higgs quartic self coupling.[b1] We ignore the bare mass term since it is much smaller than the typical energy scale m_ϕ. As we have seen in Sec. 2.2, the quartic coupling λ_h becomes negative at a high energy (or large field value) region. The precise shape is not important for our purpose, and hence we approximate it as

$$\lambda_h\left(M\right) = -0.01 \times \mathrm{sgn}\left(M - M_{\rm inst}\right). \tag{4.1.5}$$

We take the renormalization scale M as $M = \max\left(H, \sqrt{\langle h^2\rangle}\right)$ with H being the Hubble parameter. The Higgs obtains a dispersion of order $\langle h^2\rangle \gtrsim m_\phi^2$ after the first oscillation of the inflaton, and hence it is almost equivalent to take $M \simeq m_\phi$. In other words, we simply use the tree-level Higgs potential with the renormalization scale chosen at the typical energy scale of the preheating dynamics in this (and next) chapter.

■ Interaction sector

We take the interaction sector as

$$\mathcal{L}_{\rm int} = -\frac{\lambda_{h\phi}}{2}\phi^2h^2 - \frac{\sigma_{h\phi}}{2}\phi h^2 - \frac{\xi_h}{2}R\,h^2, \tag{4.1.6}$$

where $\lambda_{h\phi}$ is the Higgs-inflaton quartic coupling, $\sigma_{h\phi}$ is the Higgs-inflaton trilinear coupling and ξ_h is the Higgs-gravity non-minimal coupling, respectively. As we have seen in Sec. 3.3, they stabilize the EW vacuum during inflation as long as they are large enough with the correct sign, and we concentrate on such a case in the following.

[b1] We consider only one degree of freedom for simplicity, but the results change only logarithmically even if we take into account the full SU(2) doublet.

4.1.2 Main idea

The inflaton typically oscillates at around the origin after inflation. In our setup it is well described as

$$\phi = \Phi(t)\cos\left(m_\phi t\right), \tag{4.1.7}$$

before the back-reaction is effective, where the inflaton oscillation amplitude $\Phi(t)$ gradually decreases due to the Hubble expansion as

$$\Phi(t) = \frac{\Phi_{\rm ini}}{a^{3/2}(t)}. \tag{4.1.8}$$

Here we take the scale factor at the beginning of the inflaton oscillation as unity. For more details, see App. D.1. The inflaton oscillation acts as a time-dependent background for the Higgs since we introduce the interaction terms (4.1.6), and hence Higgs particle production is triggered. In our case the typical energy scale ($\sim m_\phi$) is well beyond the instability scale, and hence such produced Higgs particles induce a tachyonic mass to the Higgs itself though the Higgs self quartic coupling. It is estimated as

$$m_{\rm tac}^2 \simeq -3\,|\lambda_h|\left\langle h^2\right\rangle, \tag{4.1.9}$$

in the mean field approximation. It pushes the Higgs to roll down to the true minimum, and hence destabilizes the EW vacuum. In order to prevent such a catastrophe, the couplings $\lambda_{h\phi}$, ξ_h and $\sigma_{h\phi}$ are required to be small enough. This is the main idea of our study.

In the following we elaborate this idea, and obtain quantitative upper bounds on $\lambda_{h\phi}$, ξ_h and $\sigma_{h\phi}$. We study four cases separately: $\lambda_{h\phi} > 0$, $\sigma_{h\phi} = \xi_h = 0$ in Sec. 4.2, $\xi_h > 0$, $\lambda_{h\phi} = \sigma_{h\phi} = 0$ in Sec. 4.3, $\lambda_{h\phi},\ \xi_h \neq 0$, $\sigma_{h\phi} = 0$ in Sec. 4.4 and $\lambda_{h\phi},\ \sigma_{h\phi},\ \xi_h \neq 0$ in Sec. 4.5, respectively.

4.2 Higgs-inflaton quartic coupling

Here we consider the case $\lambda_{h\phi} > 0$, $\sigma_{h\phi} = \xi_h = 0$. First we analytically estimate an upper bound on $\lambda_{h\phi}$, and then perform numerical simulations to confirm it.

Analytical estimation

We expand the Higgs field by modes as

$$h(x) = \int \frac{d^3k}{(2\pi a(t))^{3/2}}\left[\hat{a}_{\vec{k}} h_k(t) e^{i\vec{k}\cdot\vec{x}} + \hat{a}^\dagger_{\vec{k}} h_k^*(t) e^{-i\vec{k}\cdot\vec{x}}\right]. \tag{4.2.1}$$

The linearized equation of motion for the mode function is given by

$$\ddot{h}_{\vec{k}} + \left[\omega_k^2(t) + \Delta(t)\right] h_{\vec{k}} = 0, \tag{4.2.2}$$

where the dot denotes the derivative with respect to t, $\Delta(t) = -9H^2/4 - 3\dot{H}/2$, and the frequency $\omega_k(t)$ is given by

$$\omega_k^2(t) = \frac{k^2}{a^2} + \lambda_{h\phi}\Phi^2(t)\cos^2\left(m_\phi t\right). \tag{4.2.3}$$

It is rewritten as

$$\left[\frac{d^2}{dz^2} + A_k + 2q\cos(2z)\right]h_k = 0, \tag{4.2.4}$$

where

$$z = m_\phi t, \quad A_k = \frac{k^2}{a^2 m_\phi^2} + \frac{\lambda_{h\phi}\Phi^2}{2m_\phi^2}, \quad q = \frac{\lambda_{h\phi}\Phi^2}{4m_\phi^2}. \tag{4.2.5}$$

It is the so-called Mathieu equation. Here we keep only leading terms in H^2/ω_k^2 expansion, which is justified for $q \gg 1$. In this system, the Higgs fluctuations with $k/a \lesssim p_*$ are efficiently produced if the following inequality holds:

$$p_*(t) \gtrsim m_\phi, \quad p_*(t) \equiv m_\phi q^{1/4}, \tag{4.2.6}$$

or equivalently

$$q \gtrsim O(1), \tag{4.2.7}$$

where $p_*(= k_*/a)$ is a typical momentum scale of the produced Higgs particles (see App. D.3 for details). We assume that the above inequality is indeed satisfied at the onset of the inflaton oscillation. Hence the quartic coupling should satisfy $\lambda_{h\phi}\Phi_{\rm ini}^2 > m_\phi^2$, or

$$\lambda_{h\phi} > 2\times 10^{-11}\left[\frac{m_\phi}{1.5\times 10^{13}\,{\rm GeV}}\right]^2\left[\frac{\sqrt{2}\,M_{\rm Pl}}{\Phi_{\rm ini}}\right]^2, \tag{4.2.8}$$

where $\Phi_{\rm ini}$ is the initial inflaton amplitude. This inequality implies $\lambda_{h\phi}\Phi_{\rm ini}^2 > H_{\rm end}^2$ since $m_\phi^2 \gtrsim H_{\rm end}^2$ holds generically. Thus the Higgs is stabilized during inflation, [♭2] and we consider this situation hereafter. We may define the comoving number density of Higgs for each mode as

$$n_{k;h}(t) \equiv \frac{1}{2\omega_{k;h}(t)}\left[\left|\dot{h}_{\vec{k}}(t)\right|^2 + \omega_{k;h}^2(t)\left|h_{\vec{k}}(t)\right|^2\right] - \frac{1}{2}. \tag{4.2.9}$$

The total physical number density is given as

$$n_h(t) \equiv \int \frac{d^3k}{(2\pi a)^3} n_{k;h}(t). \tag{4.2.10}$$

[♭2] If there is a hierarchy $m_\phi \gg H_{\rm end}$ (or $\Phi_{\rm ini} \ll M_{\rm pl}$), it is possible to choose $H_{\rm end}^2 < \lambda_{h\phi}\Phi_{\rm ini}^2 < m_\phi^2$. In such a case, the Higgs is stabilized during inflation while there is no violent Higgs production after inflation.

In the case where Eq. (4.2.8) holds, it grows exponentially after several times of the inflaton oscillation as (see Apps. D.3 and D.7 for more details)

$$n_h(t) \simeq \int \frac{d^3k}{(2\pi a)^3} \frac{e^{2\mu_k m_\phi t}}{2} \sim \frac{1}{32\pi^2} \sqrt{\frac{\pi}{2\mu_{\rm qtc} m_\phi t}}\, e^{2\mu_{\rm qtc} m_\phi t} p_*^3(t), \tag{4.2.11}$$

where μ_k is a momentum dependent function, which has a maximum value $\mu_{\rm qtc} \simeq \mathcal{O}(0.1)$ at $k/a \simeq p_*/2$. We have used the steepest descent method to evaluate the integral, and estimated the second derivative of μ_k as $\mu''_{k_*} \sim 2\mu_{\rm qtc}/\delta k^2$ with $\delta k/a \sim p_*/2$.

As the Higgs particles are continuously produced, the finite density effect of the produced particles starts to play a role. It affects the dynamics of the inflaton and the Higgs itself via $\lambda_{h\phi}\phi^2 h^2$ and $\lambda_h h^4$, respectively. In our case, $|\lambda_h|$ is much larger than $\lambda_{h\phi}$,[b3] and hence we need to consider only the latter effect. The coupling λ_h is negative in the case of our interest since $m_\phi \gg M_{\rm inst}$. Therefore, the self coupling induces a tachyonic mass term $m_{\rm tac}^2$ as

$$m_{\rm tac}^2(t) \equiv -3\,|\lambda_h| \int \frac{d^3k}{(2\pi a)^3} |h_{\boldsymbol{k}}(t)|^2 \sim -3\,|\lambda_h|\, \frac{n_h(t)}{\omega_{k/a=p_*}(t)}. \tag{4.2.12}$$

It forces the Higgs to roll down to the true minimum.

Now let us derive the condition where the Higgs rolls down to the true vacuum. There are two important contributions to the Higgs effective mass: $\lambda_{h\phi}\phi^2$ from the quartic coupling, and $m_{\rm tac}^2$ from the Higgs self coupling. The former is oscillating, and hence the latter inevitably overcomes the former for some small time interval Δt as ϕ approaches the origin even if $\lambda_{h\phi}\Phi^2 \gg |m_{\rm tac}|^2$. The time interval Δt is estimated as

$$m_\phi^2 q (m_\phi \Delta t)^2 \sim |m_{\rm tac}|^2\,, \quad \text{or} \quad \Delta t^2 \sim \frac{|m_{\rm tac}|^2}{p_*^4}, \tag{4.2.13}$$

where we have used $\phi \simeq \Phi m_\phi \Delta t$ around the potential origin. The tachyonic mass $m_{\rm tac}^2$ enhances the Higgs during this time interval. The growth rate is estimated as $|m_{\rm tac}|\,\Delta t \sim |m_{\rm tac}|^2/p_*^2$. If it exceeds unity, the Higgs field increases by a large amount due to $m_{\rm tac}^2$, and the EW vacuum is destabilized. Thus the EW vacuum is destabilized at

$$\left|m_{\rm tac}^2(t)\right|_{\phi\sim 0} \simeq p_*^2(t) \quad \Rightarrow \quad \frac{3\,|\lambda_h|}{16\pi^2} \sqrt{\frac{\pi}{2\mu_{\rm qtc} m_\phi t}}\, e^{2\mu_{\rm qtc} m_\phi t} \simeq 1, \tag{4.2.14}$$

where the subscript $\phi \sim 0$ indicates that the effective mass is evaluated at the passage of $\phi \sim 0$.[b4] It implies that the EW vacuum decays at

$$t_{\rm dec} \sim \frac{1}{2\mu_{\rm qtc} m_\phi} \ln\left(\frac{16\pi^{\frac{3}{2}}}{3\,|\lambda_h|}\right). \tag{4.2.15}$$

[b3] Otherwise the radiative correction from $\lambda_{h\phi}$ easily spoils the flatness of the inflaton potential.

[b4] All the modes with $p \lesssim p_*$ tend to grow due to the tachyonic effective mass at this time. The transition is hence expected to be dominated by the scale below p_*.

Before this time, the resonant Higgs production should be killed due to the cosmic expansion for the EW vacuum to survive the preheating epoch. The cosmic expansion kills the resonance at $p_*(t_{\rm end}) \sim m_\phi$, or

$$t_{\rm end}^2 \sim \frac{8}{3m_\phi^2}\frac{\lambda_{h\phi}M_{\rm Pl}^2}{m_\phi^2}, \tag{4.2.16}$$

where we have used Eq. (D.1.8). Thus the EW vacuum survives the preheating for $t_{\rm end} \lesssim t_{\rm dec}$, which yields the following upper bound:

$$\lambda_{h\phi} \lesssim \frac{3}{32\mu_{\rm qtc}^2}\frac{m_\phi^2}{M_{\rm Pl}^2}\left[\ln\left(\frac{16\pi^{\frac{3}{2}}}{3\tilde{\lambda}}\right)\right]^2 \simeq 10^{-8}\left[\frac{0.1}{\mu_{\rm qtc}}\right]^2\left[\frac{m_\phi}{10^{13}\,{\rm GeV}}\right]^2. \tag{4.2.17}$$

Note that $\mu_{\rm qtc} \sim O(0.1)$ almost independently of $\Phi_{\rm ini}$ and q in the case with only $\lambda_{h\phi}$ as we see in App. D.7. In the following we verify it by using the classical lattice simulation.

Numerical simulation

Now we show the results of the classical lattice simulations for the case with $\lambda_{h\phi}$. The main purpose here is to confirm the upper bound given in Eq. (4.2.17).

We solve the following classical equations of motion numerically in the configuration space:

$$0 = \ddot{\phi} + 3H\dot{\phi} - \frac{1}{a^2}\partial_i^2\phi + \left(m_\phi^2 + \lambda_{h\phi}h^2\right)\phi, \tag{4.2.18}$$

$$0 = \ddot{h} + 3H\dot{h} - \frac{1}{a^2}\partial_i^2 h + \left(\lambda_{h\phi}\phi^2 + \lambda_h h^2\right)h, \tag{4.2.19}$$

for the scalar fields, and

$$H^2 = \frac{\langle\rho\rangle}{3M_{\rm Pl}^2}, \tag{4.2.20}$$

for the metric, where the total energy density is given by

$$\rho = \frac{1}{2}\left(\dot{\phi}^2 + \frac{1}{a^2}\left(\partial_i\phi\right)^2 + m_\phi^2\phi^2\right) + \frac{1}{2}\left(\dot{h}^2 + \frac{1}{a^2}\left(\partial_i h\right)^2\right) + \frac{\lambda_h}{4}h^4 + \frac{1}{2}\lambda_{h\phi}\phi^2h^2, \tag{4.2.21}$$

and $\langle ...\rangle$ denotes the spatial average. We ignore fluctuations of the metric because their effects are suppressed by $M_{\rm Pl}$. Actually there is another equation of motion in the metric sector, and it is redundant. We have checked that our numerical calculation satisfies the redundancy at least at $O(10^{-3})$ precision. The simulation parameters are summarized in Tab. 4.1. The inflaton mass is fixed as $m_\phi = 1.5\times10^{13}\,{\rm GeV}$. We show results for $\lambda_{h\phi} = 10^{-8}$ and $\lambda_{h\phi} = 4\times10^{-8}$.

Now we explain some details of the lattice simulation. We solved the discretized version of the classical equations of motion with the initial inflaton amplitude $\Phi_{\rm ini} = \sqrt{2}\,M_{\rm Pl}$ or

d	N_g	L	$\mathrm{d}t$
3+1	128	$10 m_\phi^{-1}$	$10^{-3} m_\phi^{-1}$

Table 4.1: The parameters of the classical lattice simulation, where d is the spacetime dimension, N_g is the number of grid in each spatial dimension, L is the size of the lattice, $\mathrm{d}t$ is the size of the each time step.

$\sqrt{0.2}\,M_{\rm Pl}$. By changing $\Phi_{\rm ini}$, we tested whether the inflation scale changes the bounds on the coupling strength. We took $\dot{\Phi}_{\rm ini} = 0$, but our results are insensitive to this choice. We also introduced gaussian initial fluctuations on the inflaton and Higgs field following Refs. [35, 36], which mimic the quantum fluctuations. We renormalized the inflaton and the Higgs masses originating from the initial fluctuations. We also added an h^6 term to the Higgs potential to avoid numerical divergence. We took the coefficient of the h^6 term such that the Higgs field value $h_{\rm min}$ at the true minimum is $|\lambda_h|\, h_{\rm min}^2 = 5\times 10^{-8} M_{\rm Pl}^2$. We verified that the EW vacuum decay is not affected by the additional h^6 term. See App. E.3 for more details.

In Fig. 4.1, we show the time evolution of $\langle\phi\rangle^2$ (black), $\langle\phi^2\rangle - \langle\phi\rangle^2$ (red) and $\langle h^2\rangle$ (blue). They are multiplied by a^3 with the initial value taken as $a_{\rm ini} = 1$. We take the coupling as $\lambda_{h\phi} = 10^{-8}$ for the left panels and $\lambda_{h\phi} = 4\times 10^{-8}$ for the right panels, respectively. The initial inflaton amplitudes are $\Phi_{\rm ini} = \sqrt{2}\,M_{\rm Pl}$ in the upper panels and $\Phi_{\rm ini} = \sqrt{0.2}\,M_{\rm Pl}$ in the lower panels, respectively. As it is clear from Fig. 4.1, the Higgs stays at the EW vacuum for $\lambda_{h\phi} = 10^{-8}$, while it rolls down to the true vacuum for $\lambda_{h\phi} = 4\times 10^{-8}$, independent of the initial inflaton amplitude. It is consistent with Eq. (4.2.17). Indeed, an interesting feature of Eq. (4.2.17) is that it does not depend on the initial inflaton amplitude as long as Eq. (4.2.6) is satisfied initially. This is because the growth rate $\mu_{\rm qtc}$ does not much depend on the inflaton amplitude for the broad resonance.[b5] Thus, the Higgs fluctuations are efficiently produced at the latest epoch independent of $\Phi_{\rm ini}$, since the number of the inflaton oscillation is dominated by that epoch.

We also plot the time evolution of the comoving number density of the Higgs defined in Eq. (4.2.9) for $\Phi_{\rm ini} = \sqrt{2}\,M_{\rm Pl}$ in Fig. 4.2. For the motivation of this definition, see the discussion around Eq. (D.2.12). The left panel shows the case with $\lambda_{h\phi} = 10^{-8}$ and the right panel does the case with $\lambda_{h\phi} = 4\times 10^{-8}$. In the left panel, the Higgs is efficiently produced at the beginning of the oscillation, but the resonance shuts off due to the Hubble expansion. After $t \simeq 30/m_\phi$, the comoving number density of the Higgs remains almost constant. On the other hand, in the right panel, the comoving number density of the Higgs continues to grow resonantly. As a result, Higgs rolls down to the true vacuum once the condition (4.2.14) is satisfied. Also, we can see that modes below p_* is efficiently produced as expected. The time evolution of the number density for $\Phi_{\rm ini} = \sqrt{0.2}\,M_{\rm Pl}$ is quite similar.

[b5] As we shall see below, the situation is completely different for the tachyonic resonance case.

Summary

In summary, we obtain an upper bound on the Higgs-inflaton quartic coupling $\lambda_{h\phi}$ by requiring that the EW vacuum be stable during the preheating epoch. Since $\lambda_{h\phi}$ is also bounded from below from the requirement of the EW vacuum during inflation, the favorable $\lambda_{h\phi}$ is limited in a finite parameter region. For instance, if we consider a quadratic chaotic inflation model with $\Phi_{\rm ini} \simeq M_{\rm Pl}$ and $m_\phi \simeq 10^{13}\,{\rm GeV}$, the quartic coupling $\lambda_{h\phi}$ must be within the following window:

$$10^{-10} \lesssim \lambda_{h\phi} \lesssim 10^{-8}, \tag{4.2.22}$$

where the upper (lower) bound comes from the EW vacuum stability during the preheating (inflation). See Eqs. (3.3.3) and (4.2.17). The allowed region can be larger for an inflation model with $\Phi_{\rm ini} \ll M_{\rm Pl}$ (or $H_{\rm inf} \ll m_\phi$), since the resonance does not happen if the condition (4.2.8) is violated, which may make the upper bound looser.

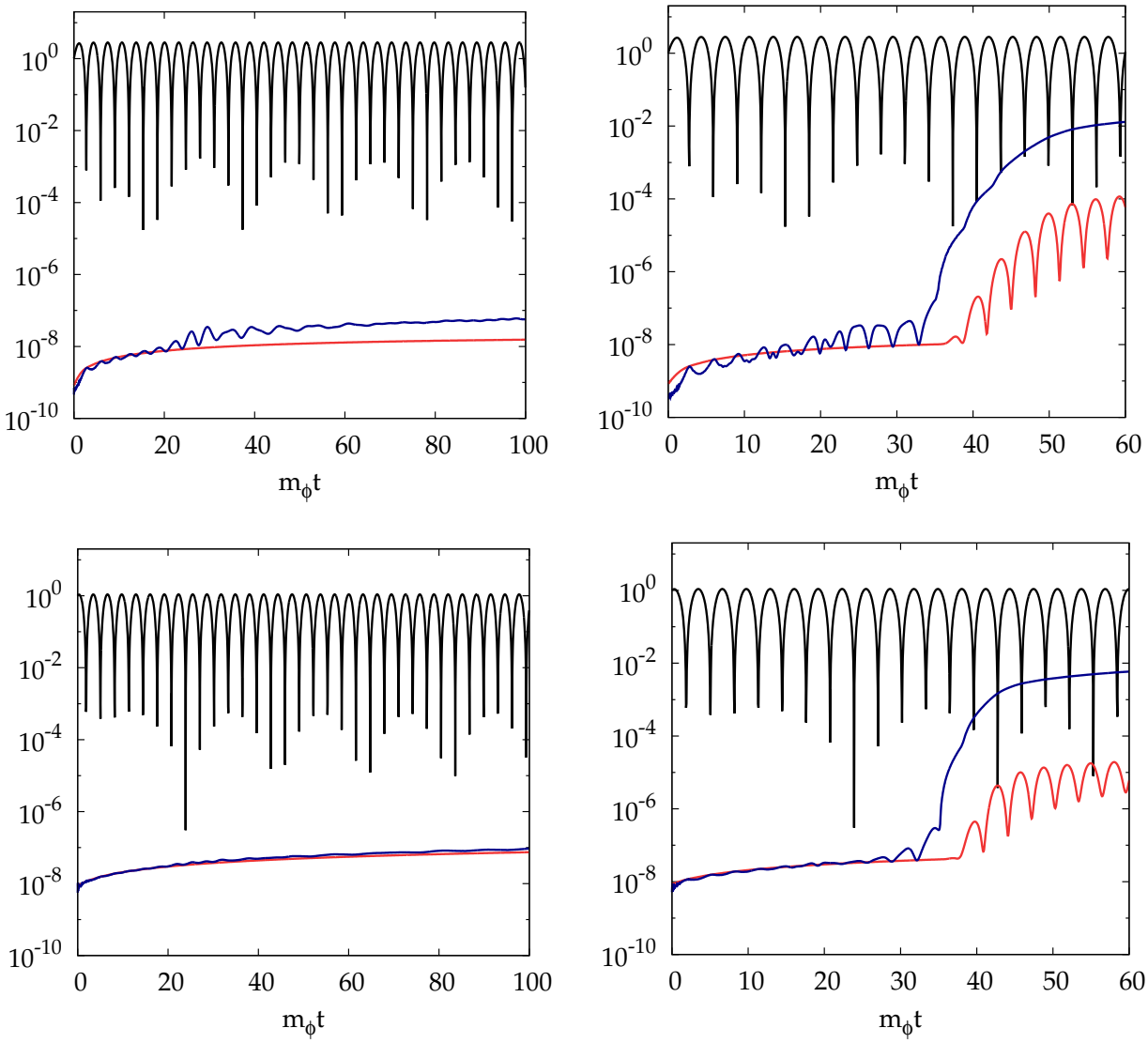

Figure 4.1: The time evolution of the inflaton and the Higgs. The black line is $\langle\phi\rangle^2$, the red line is $\langle\phi^2\rangle - \langle\phi\rangle^2$ and the blue line is $\langle h^2\rangle$, where the angle brackets denote the spatial average. They are multiplied by a^3, and normalized by $\Phi_{\rm ini}$. Upper left: $\lambda_{h\phi} = 10^{-8}, \Phi_{\rm ini} = \sqrt{2}\,M_{\rm Pl}$, upper right: $\lambda_{h\phi} = 4\times10^{-8}, \Phi_{\rm ini} = \sqrt{2}\,M_{\rm Pl}$, lower left: $\lambda_{h\phi} = 10^{-8}, \Phi_{\rm ini} = \sqrt{0.2}\,M_{\rm Pl}$, lower right: $\lambda_{h\phi} = 4\times10^{-8}, \Phi_{\rm ini} = \sqrt{0.2}\,M_{\rm Pl}$.

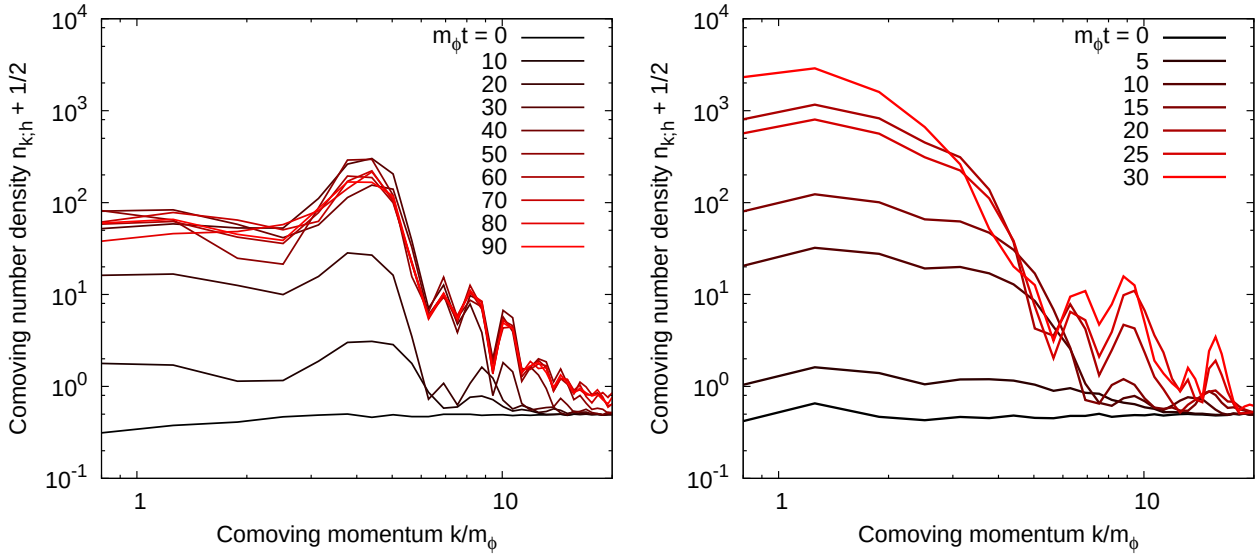

Figure 4.2: The Higgs comoving number density. The parameters are $m_\phi = 1.5 \times 10^{13}\,\mathrm{GeV}$ and $\Phi_{\mathrm{ini}} = \sqrt{2}M_{\mathrm{Pl}}$. Left: $\lambda_{h\phi} = 10^{-8}$. Right: $\lambda_{h\phi} = 4 \times 10^{-8}$.

4.3 Higgs-gravity non-minimal coupling

in this section we consider the case $\xi_h > 0$, $\lambda_{h\phi} = \sigma_{h\phi} = 0$. First we analytically estimate an upper bound on ξ_h, and then perform numerical simulations to confirm it.

Analytical estimation

In the present case, the linearized equation of motion for the Higgs mode function is

$$\ddot{h}_{\vec{k}} + \left[\omega_k^2(t) + \Delta(t)\right] h_{\vec{k}} = 0, \tag{4.3.1}$$

where the frequency $\omega_k(t)$ is given by

$$\omega_k^2(t) = \frac{k^2}{a^2} + \xi_h R. \tag{4.3.2}$$

Assuming that the inflaton condensation dominates the universe, the Ricci scalar is given as

$$R = \frac{1}{M_{\rm Pl}^2}\left[-\dot{\phi}^2 + 2m_\phi^2\phi^2\right], \tag{4.3.3}$$

and hence the frequency is rewritten as

$$\omega_k^2(t) \simeq \frac{k^2}{a^2} + \frac{\xi_h m_\phi^2}{2M_{\rm Pl}^2}\Phi^2 + \frac{3\xi_h m_\phi^2}{2M_{\rm Pl}^2}\Phi^2\cos\left(2m_\phi t\right). \tag{4.3.4}$$

where we have kept only leading terms in H^2/ω_k^2. Thus, the modes can be tachyonic in one oscillation in contrast to the case with $\lambda_{h\phi}$. An efficient resonance occurs only when $\xi_h\Phi^2/M_{\rm Pl}^2 > O(1)$, and hence we concentrate on the case with[b6]

$$\xi_h > \left[\frac{\sqrt{2}M_{\rm Pl}}{\Phi_{\rm ini}}\right]^2. \tag{4.3.5}$$

In this case an efficient particle production occurs via the tachyonic instability, which we call tachyonic resonance. For more details, see App. D.4. If this condition is satisfied, the EW vacuum stability during inflation is ensured since $\Phi_{\rm ini} \lesssim M_{\rm pl}$ leads to $\xi_h \gtrsim O(1)$.[b7] The linearized equation of motion is rewritten in the form of the Mathieu equation as

$$\left[\frac{d^2}{dz^2} + A_k + 2q\cos\left(2z\right)\right] h_k = 0, \tag{4.3.6}$$

where

$$z = m_\phi t, \quad A_k = \frac{k^2}{a^2 m_\phi^2} + \frac{\xi_h\Phi^2}{2M_{\rm Pl}^2}, \quad q = \frac{3\xi_h\Phi^2}{4M_{\rm Pl}^2}. \tag{4.3.7}$$

[b6] We do not consider the case with $-\xi_h \gtrsim O(1)$ since it destabilize the EW vacuum during inflation.

[b7] If $\Phi_{\rm ini} \ll M_{\rm Pl}$, it is possible that $O(0.1) < \xi_h < (M_{\rm Pl}/\Phi_{\rm ini})^2$. In such a case, Higgs is stable during inflation while no tachyonic resonance occurs after inflation.

The growth rate of the number density $X_k(t)$ is estimated as [37]:

$$X_k(t) \simeq -\frac{x}{\sqrt{q}} A_k + 2x\sqrt{q}, \tag{4.3.8}$$

with $x \simeq 0.85$. Recalling that $\Phi(t) \propto 1/t$, the first a few oscillations play the dominant role in the tachyonic resonance. The typical physical momentum enhanced by the tachyonic resonance is given by

$$p_*^{(\mathrm{tac})}(t) \equiv \frac{1}{\sqrt{x}} m_\phi q^{1/4}(t). \tag{4.3.9}$$

In terms of $p_*^{(\mathrm{tac})}$, the condition for the resonant particle production is similar to Eq. (4.2.6):

$$p_*^{(\mathrm{tac})}(t) \gtrsim m_\phi, \quad \text{or} \quad q \gtrsim \mathcal{O}(1). \tag{4.3.10}$$

The number density of the Higgs produced after the j-th passage of $\phi = 0$ is estimated as

$$\begin{aligned} n_h(t_j) = \int \frac{d^3k}{\left(2\pi a(t_j)\right)^3} n_k(t_j) &\simeq \int \frac{d^3k}{\left(2\pi a(t_j)\right)^3} e^{2\sum_{i=1}^{j} X_k(t_i)} \\ &\sim \frac{1}{16\pi^2}\sqrt{\frac{\pi}{2}} e^{n_{\mathrm{eff}}(t_j)\,\mu_{\mathrm{crv}}\sqrt{\xi_h}\Phi_{\mathrm{ini}}/M_{\mathrm{Pl}}} \frac{a^3(t_{\mathrm{ini}})}{a^3(t_j)} p_*^{(\mathrm{tac})^3}(t_{\mathrm{ini}}), \end{aligned} \tag{4.3.11}$$

where $\mu_{\mathrm{crv}} \simeq 2x\sqrt{4/3} \simeq 2$ for $\xi_h \gtrsim \mathcal{O}(1)$, and Φ_{ini} is the initial inflaton amplitude. The effective number of times of oscillation $n_{\mathrm{eff}}(t_j) \equiv \sum_{i=1}^{j} \Phi(t_i)/\Phi_{\mathrm{ini}}$ grows logarithmically in time. We estimate $n_{\mathrm{eff}} \simeq 1$ for $\Phi_{\mathrm{ini}} \gtrsim M_{\mathrm{Pl}}$. This is because the amplitude drastically decreases within the first oscillation, and hence the first one or two oscillations dominate the Higgs production. On the other hand, for $\Phi_{\mathrm{ini}} \lesssim M_{\mathrm{Pl}}$, the later oscillations can also be important since the amplitude decreases rather slowly. For $\Phi_{\mathrm{ini}} = \sqrt{0.2}\,M_{\mathrm{Pl}}$, for instance, we roughly estimate $n_{\mathrm{eff}} \simeq 1.5$–$2$. See also App. D.7. Once the Higgs particles are produced, they induce the tachyonic mass to the Higgs itself as

$$m_{\mathrm{tac}}^2(t) \equiv -3\,|\lambda_h| \int \frac{d^3k}{(2\pi a)^3} |h_{\boldsymbol{k}}(t)|^2 \sim -3\,|\lambda_h| \frac{n_h(t)}{\omega_{k/a=p_*^{(\mathrm{tac})}}(t)}. \tag{4.3.12}$$

in the same way as the case with $\lambda_{h\phi}$.

Now we derive the condition where the EW vacuum is stable during the preheating. Contrary to the case with $\lambda_{h\phi}$, the Higgs effective mass from $\xi_h R$ becomes tachyonic every crossing around $\phi \sim 0$. Thus, the effect of $|m_{\mathrm{tac}}|^2$ overcomes that from the curvature coupling only when $|m_{\mathrm{tac}}|^2 \gtrsim q m_\phi^2$. Once this condition is satisfied, the tachyonic mass $|m_{\mathrm{tac}}|^2$ exceeds the effective mass $\xi_h R$ even at around the end point of the inflaton oscillation, and the EW vacuum decay is triggered. Thus, we may conservatively estimate the condition for the EW vacuum stability as[þ8]

$$\left|m_{\mathrm{tac}}^2(t_j)\right|_{\xi_h R \sim 0} \lesssim q m_\phi^2 \quad \Rightarrow \quad \frac{3\,|\lambda_h|}{16\pi^2}\sqrt{\frac{\pi}{2q(t_{\mathrm{ini}})}} \frac{a(t_{\mathrm{end}})}{a(t_{\mathrm{ini}})} e^{n_{\mathrm{eff}}(t_{\mathrm{end}})\,\mu_{\mathrm{crv}}\sqrt{\xi_h}\Phi_{\mathrm{ini}}/M_{\mathrm{Pl}}} \lesssim 1, \tag{4.3.13}$$

[þ8] Not only the long wave length mode but all the modes below $q^{1/2} m_\phi$ grows towards the deeper minimum if this condition is violated.

d	N_g	L	$\mathrm{d}t$
3+1	128	$20m_\phi^{-1}$ or $40m_\phi^{-1}$	$10^{-3}m_\phi^{-1}$

Table 4.2: The parameters of the classical lattice simulation, where d is the spacetime dimension, N_g is the number of grid in each spatial dimension, L is the size of the lattice, $\mathrm{d}t$ is the size of the each time step. We take $L = 20/m_\phi$ for $\Phi_{\rm ini} = \sqrt{2}\,M_{\rm Pl}$ and $L = 40/m_\phi$ for $\Phi_{\rm ini} = \sqrt{0.2}\,M_{\rm Pl}$

where the end time of the preheating $t_{\rm end}$ is estimated from the condition $p_*^{(\rm tac)}(t_{\rm end}) \simeq m_\phi$. As a result, the EW vacuum survives the tachyonic resonance for

$$\xi_h \lesssim \frac{1}{n_{\rm eff}^2\,\mu_{\rm crv}^2}\left[\frac{M_{\rm Pl}}{\Phi_{\rm ini}}\right]^2\left[\ln\left(\frac{16\pi^2}{3\,|\lambda_h|}\sqrt{\frac{2}{\pi}}\right)\right]^2 \simeq 10\left[\frac{2}{n_{\rm eff}\,\mu_{\rm crv}}\right]^2\left[\frac{\sqrt{2}\,M_{\rm Pl}}{\Phi_{\rm ini}}\right]^2, \tag{4.3.14}$$

where we have taken $q \simeq 1$ in the logarithm and ignored the scale factor dependence.

Numerical simulation

In the following, we show the results of the classical lattice simulations for the case with ξ_h. The main purpose is to confirm Eq. (4.3.14).

We numerically solve the following classical equations of motion in the Einstein frame in the configuration space:

$$0 = \ddot{\phi} + 3H\dot{\phi} - \frac{1}{a^2}\partial_i^2\phi + 2\frac{\xi_h}{M_{\rm Pl}^2}\left[\dot{\phi}\dot{h} - \frac{1}{a^2}\partial_i\phi\partial_i h\right]h + \left(1 + \frac{\xi_h h^2}{M_{\rm Pl}^2}\right)m_\phi^2\phi, \tag{4.3.15}$$

$$0 = \ddot{h} + 3H\dot{h} - \frac{1}{a^2}\partial_i^2 h + \frac{\xi_h}{M_{\rm Pl}^2}\left[2m_\phi^2\phi^2 - \dot{\phi}^2 + \frac{1}{a^2}\left(\partial_i\phi\right)^2\right]h + \lambda h^3, \tag{4.3.16}$$

for the scalar fields, and

$$H^2 = \frac{\langle\rho\rangle}{3M_{\rm Pl}^2}, \tag{4.3.17}$$

for the metric, where the energy density is given by

$$\rho = \frac{1}{2}\left(1 + \frac{\xi_h h^2}{M_{\rm Pl}^2}\right)\left(\dot{\phi}^2 + \frac{1}{a^2}\left(\partial_i\phi\right)^2\right) + \frac{1}{2}\left(1 + 2\frac{\xi_h h^2}{M_{\rm Pl}^2}\right)m_\phi^2\phi^2 + \frac{1}{2}\left(\dot{h}^2 + \frac{1}{a^2}\left(\partial_i h\right)^2\right) + \frac{\lambda}{4}h^4. \tag{4.3.18}$$

We retain terms only up to first-order in $\xi_h h^2/M_{\rm Pl}^2$ and $\xi_h^2 h^2/M_{\rm Pl}^2$. It is justified because $\xi_h h^2/M_{\rm Pl}^2, \xi_h^2 h^2/M_{\rm Pl}^2 \ll 1$ always holds in our numerical calculation. Again we have verified that our numerical calculation satisfies the redundancy for the equations of motion at least at $O(10^{-3})$ precision. The parameters of the classical lattice simulation are summarized in Tab. 4.2. The inflaton mass is fixed as $m_\phi = 1.5 \times 10^{13}$ GeV.

Now we explain some details of the lattice simulation. We solved the discretized version of the classical equations of motion with $\Phi_{\rm ini} = \sqrt{2}\,M_{\rm Pl}$ or $\sqrt{0.2}\,M_{\rm Pl}$. We set $\dot{\Phi}_{\rm ini} = 0$. We

introduced gaussian initial fluctuations in the inflaton and the Higgs fields which arise from the quantum fluctuations. Concerning the interaction terms, we again renormalized the inflaton and the Higgs masses originating from the initial fluctuations. We added an h^6 term to the Higgs potential to stabilize it in our calculation as well. We took the coefficient such that the Higgs field value at the true minimum is $|\lambda_h| h_{\rm min}^2 = 5 \times 10^{-8} M_{\rm Pl}^2$, and checked that it does not affect the EW vacuum decay. For more details, we again refer the readers to App. E.3.

In Fig. 4.3, we show the time evolution of $\langle\phi\rangle^2$ (black), $\langle\phi^2\rangle - \langle\phi\rangle^2$ (red) and $\langle h^2\rangle$ (blue). They are multiplied by a^3 whose initial value is $a_{\rm ini} = 1$, and normalized by $\Phi_{\rm ini}$. We take ξ_h and $\Phi_{\rm ini}$ as follows: $\xi_h = 10$ and $\Phi_{\rm ini} = \sqrt{2}\, M_{\rm Pl}$ for the upper left panel, $\xi_h = 20$ and $\Phi_{\rm ini} = \sqrt{2}\, M_{\rm Pl}$ for the upper right panel, $\xi_h = 20$ and $\Phi_{\rm ini} = \sqrt{0.2}\, M_{\rm Pl}$ for the lower left panel and $\xi_h = 30$ and $\Phi_{\rm ini} = \sqrt{0.2}\, M_{\rm Pl}$ for the lower right panel, respectively. For the $\Phi_{\rm ini} = \sqrt{2}\, M_{\rm Pl}$ cases (the upper panels), the Higgs remains in the EW vacuum for $\xi_h = 10$, while it rolls down to the true vacuum for $\xi_h = 20$. Thus, the condition (4.3.14) is consistent with our numerical calculation within a factor of two.[b9] On the contrary to the case with $\lambda_{h\phi}$, the upper bound on ξ_h depends on $\Phi_{\rm ini}$. Indeed, for the $\Phi_{\rm ini} = \sqrt{0.2}\, M_{\rm Pl}$ cases (the lower panels), the Higgs remains in the EW vacuum for $\xi_h = 20$, while it rolls down to the true vacuum for $\xi_h = 30$. Again, it is consistent with Eq. (4.3.14) once we include the effect of $n_{\rm eff} \simeq 1.5$-2.

In Fig. 4.4, we plot the time evolution of the comoving number density of the Higgs (defined in Eq. (4.2.9)) for $\Phi_{\rm ini} = \sqrt{2}\, M_{\rm Pl}$. The curvature coupling is $\xi_h = 10$ for the left panel and $\xi_h = 20$ for the right panel, respectively. We evaluated the number density at the end points of the oscillations since it is well-defined only at around these points. The Higgs particles are created dominantly within the first a few oscillations. This is because the growth rate depends on Φ. The result for $\Phi_{\rm ini} = \sqrt{0.2}\, M_{\rm Pl}$ is quite similar.

Summary

In summary, we obtain an upper bound on the non-minimal coupling ξ_h by requiring that the EW vacuum be stable during the preheating epoch. Again it is also bounded from below from the requirement of the EW vacuum during inflation, and hence the favorable ξ_h is limited in a finite parameter region. For instance, if we consider a quadratic chaotic inflation model with $\Phi_{\rm ini} \simeq M_{\rm Pl}$ and $m_\phi \simeq 10^{13}\,$GeV, the non-minimal coupling ξ_h must be within the following window:

$$0.1 \lesssim \xi_h \lesssim 10. \tag{4.3.19}$$

where the upper (lower) bound comes from the EW vacuum stability during the preheating (inflation). See Eqs. (3.3.3) and (4.3.14). As in the case of the quartic coupling $\lambda_{h\phi}$, the allowed region is larger for an inflation model with $\Phi_{\rm ini} \ll M_{\rm Pl}$ (or $H_{\rm inf} \ll m_\phi$). In particular, the lower bound does not change while the upper bound becomes looser by a factor of $M_{\rm Pl}^2/\Phi_{\rm ini}^2$.

[b9] The difference between Eq. (4.3.14) and our numerical calculation may be due to the fact that the inflaton amplitude decreases drastically within the first oscillation for $\Phi_{\rm ini} = \sqrt{2}\, M_{\rm Pl}$, while we assume that the amplitude is constant to derive Eq. (4.3.14). Our main purpose is, however, an order estimation of the bound on ξ_h, and hence Eq. (4.3.14) is enough.

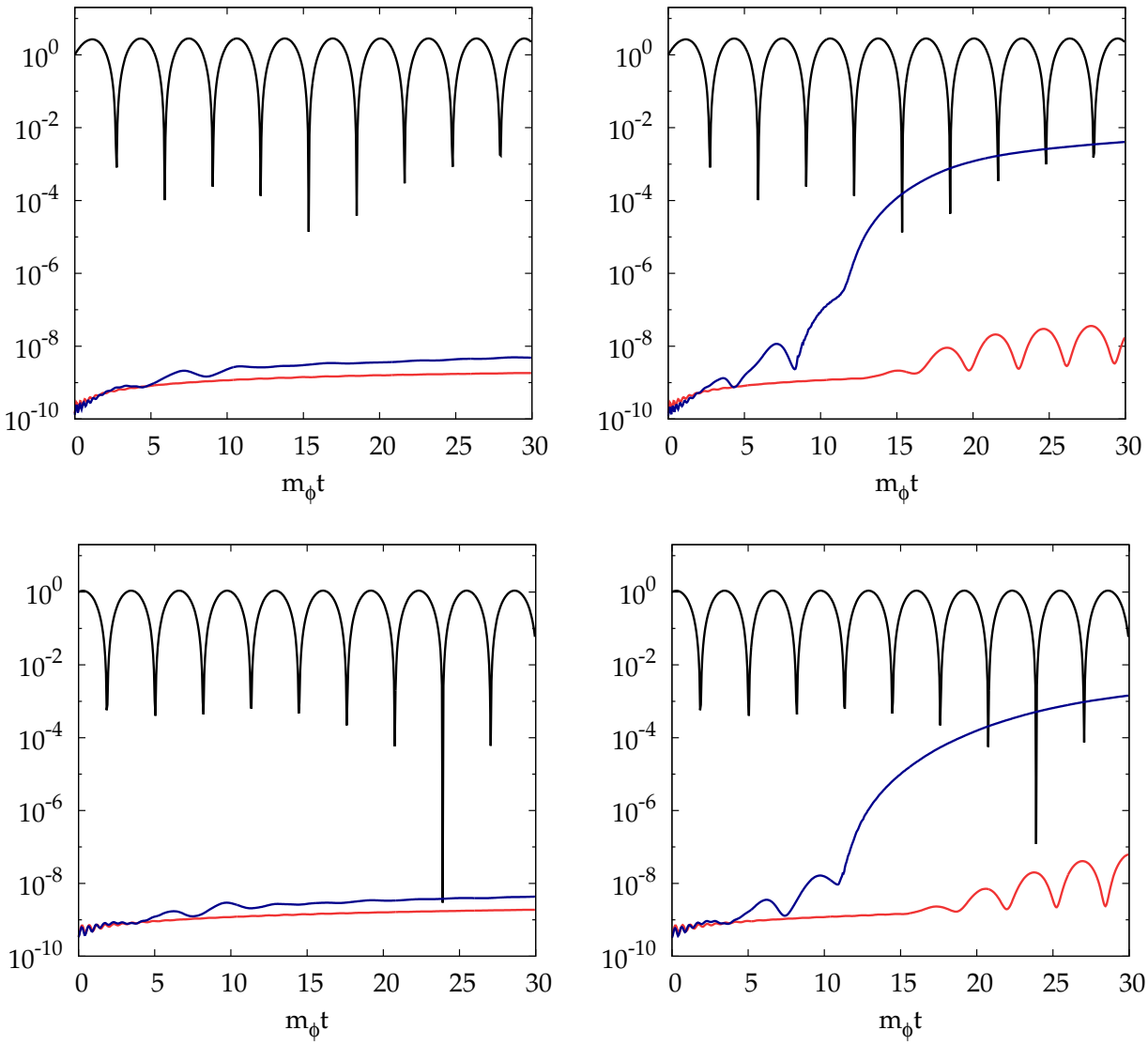

Figure 4.3: Time evolution of the inflaton and the Higgs. The black line is $\langle\phi\rangle^2$, the red line is $\langle\phi^2\rangle - \langle\phi\rangle^2$ and the blue line is $\langle h^2\rangle$, where the angle brackets denote the spatial average. They are multiplied by a^3, and normalized by the initial inflaton amplitude $\Phi_{\rm ini} = \sqrt{2}\,M_{\rm Pl}$. Upper left: $\xi_h = 10, \Phi_{\rm ini} = \sqrt{2}\,M_{\rm Pl}$, upper right: $\xi_h = 20, \Phi_{\rm ini} = \sqrt{2}\,M_{\rm Pl}$, lower left: $\xi_h = 20, \Phi_{\rm ini} = \sqrt{0.2}\,M_{\rm Pl}$, lower right: $\xi_h = 30, \Phi_{\rm ini} = \sqrt{0.2}\,M_{\rm Pl}$.

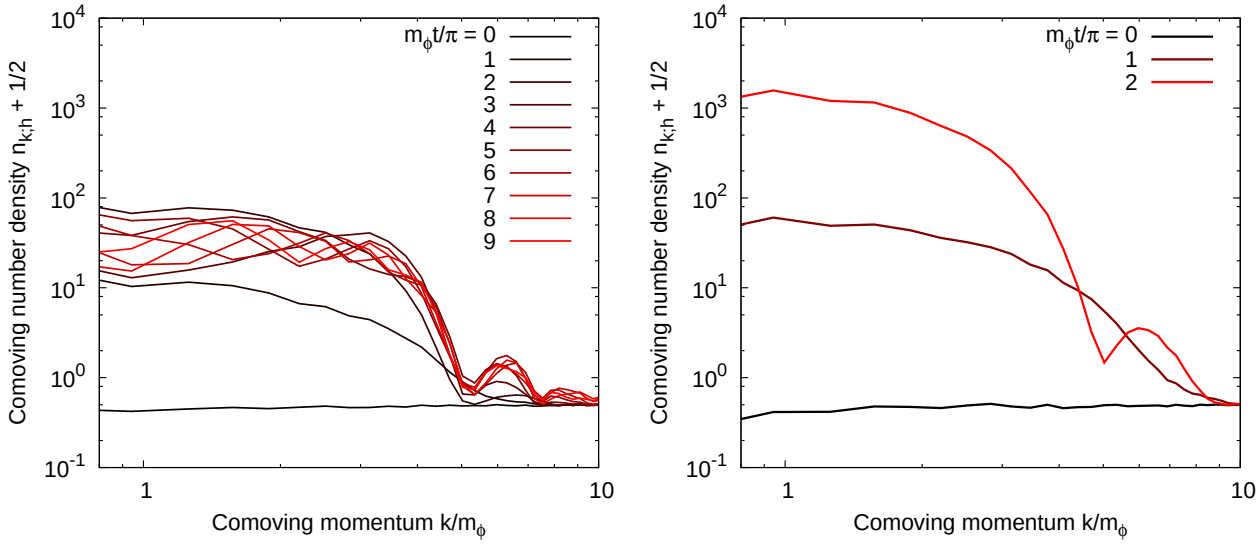

Figure 4.4: The Higgs comoving number density. The parameters are $m_\phi = 1.5 \times 10^{13}\,\mathrm{GeV}$ and $\Phi_{\mathrm{ini}} = \sqrt{2}M_{\mathrm{Pl}}$. Left: $\xi_h = 10$, right: $\xi_h = 20$.

4.4 Both quartic and non-minimal couplings

Now we consider the case $\lambda_{h\phi},\ \xi_h \neq 0$ and $\sigma_{h\phi} = 0$. We first give a qualitative overview of this system, and then show results of numerical simulations.

Qualitative discussion

In the presence of $\lambda_{h\phi}$ and ξ_h, the linearized equation of motion of the Higgs is given by the Mathieu equation as

$$\left[\frac{d^2}{dz^2} + A_k + 2q\cos(2z)\right] h_k = 0, \tag{4.4.1}$$

where

$$z = m_\phi t,\ \ A_k = \frac{k^2}{a^2 m_\phi^2} + \left[\lambda_{h\phi} + \frac{\xi_h m_\phi^2}{M_{\rm Pl}^2}\right]\frac{\Phi^2}{2m_\phi^2},\ \ q = \left[\lambda_{h\phi} + \frac{3\xi_h m_\phi^2}{M_{\rm Pl}^2}\right]\frac{\Phi^2}{4m_\phi^2}. \tag{4.4.2}$$

Here again we have kept only leading order terms in H^2/ω_k^2. Note that A_k and q can vary independently for fixed k since we have now two parameters: $\lambda_{h\phi}$ and ξ_h. The stability during inflation requires that

$$A_k + 2q \gtrsim O(1), \tag{4.4.3}$$

or

$$\lambda_{h\phi} + 2\xi_h \frac{m_\phi^2}{M_{\rm Pl}^2} \gtrsim 10^{-10}, \tag{4.4.4}$$

for $m_\phi \simeq 10^{13}\,\text{GeV}$ and $\Phi_{\rm ini} \simeq M_{\rm Pl}$, and hence we concentrate on this parameter region in the following. Without the Hubble expansion, the Mathieu equation is characterized by the stability/instability chart of Fig. 4.5. If the point (A_k, q) lies in the white regions, the corresponding solution grows exponentially with time as $h_k \propto e^{\mu m_\phi t}$ with μ called the Floquet exponent. On the other hand, the shaded regions lead to stable solutions. For more details, see App. D. With the Hubble expansion, both A_k and q decrease with time crossing many instability regions. The resonance ends when the system enters the last stability region at $q \lesssim 1$. In particular, an interesting feature of Fig. 4.5 is that a larger $A/|q|$ leads to a weaker resonance, where A is defined as

$$A \equiv A_{k=0} = \left[\lambda_{h\phi} + \frac{\xi_h m_\phi^2}{M_{\rm Pl}^2}\right]\frac{\Phi^2}{2m_\phi^2}. \tag{4.4.5}$$

In particular, $q \simeq 0$ or

$$\lambda_{h\phi} + 3\xi_h \frac{m_\phi^2}{M_{\rm Pl}^2} \simeq 0, \tag{4.4.6}$$

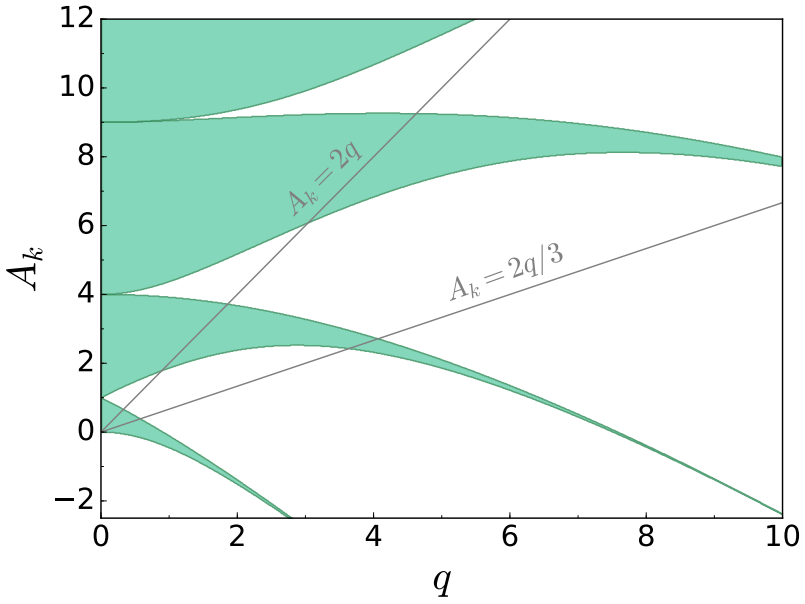

Figure 4.5: The stability/instability chart of the Mathieu equation. An exponentially growing mode exits in the white region, which means that the resonance occurs in that region. The gray lines are $A_k = 2q$ and $2q/3$ that correspond to the mode $k = 0$ with $\lambda_{h\phi}$ and ξ_h, respectively. The chart is even with respect to q.

kills the resonance completely. It is actually sufficient to have $A/|q| \sim$ a few to avoid the EW vacuum destabilization. Such a relation is not quite unnatural: since $m_\phi^2/M_{\rm Pl}^2 \sim 10^{-10}$, $|\xi_h|$ between 1-10^4 corresponds to $\lambda_{h\phi}$ between 10^{-10}-10^{-6}. In reality, the Mathieu equation gives only an approximate description of the system due to the Hubble expansion, and hence we perform the classical lattice simulations to determine the stability region in the the following.

Numerical simulation

Now we show the results of the classical lattice simulation. Our main concern is the parameter region with larger $A/|q|$. The results are presented in Fig. 4.6. These show maximal allowed $|q|$ for a given A and the corresponding range of $\xi_h m_\phi^2/M_{\rm Pl}^2$ for a given $\lambda_{h\phi}$. The orange points correspond to stable configurations in the sense that the EW vacuum does not decay before the end of the resonance. As we can see from Fig. 4.6, a wide range of positive $\lambda_{h\phi}$ and negative ξ_h is allowed. On the other hand, a negative $\lambda_{h\phi}$ leads to smaller A/q, and hence are ruled out (apart from small values around the origin). The line $A = 2|q|$ separates the broad resonance from the tachyonic one.

The qualitative behavior of our bound can be understood as follows. We are mostly interested in a region with a substantial ratio $A/|q|$. At $A/|q| > 2.3$ or so, the broad resonance with the Hubble expansion simplifies. Whether the EW vacuum is destabilized or not is mostly determined by the last instability region closest to the origin. This is because, in the parameter range of interest, the system spends little time in other instability bands since

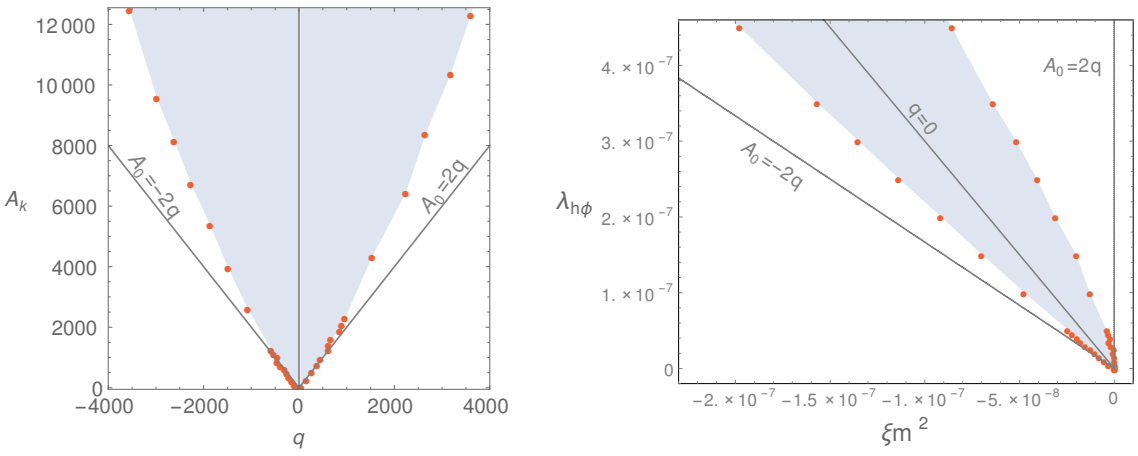

Figure 4.6: The EW vacuum stability region (the shaded region) in the q–A plane (left) and the ξ_h–$\lambda_{h\phi}$ plane (right) with $m_\phi \simeq 10^{13}$ GeV. The red points represent the numerical results for the boundary of the stability/instability region for fixed $\lambda_{h\phi}$. The shaded region is the interpolation of the red points, indicating the stability region.

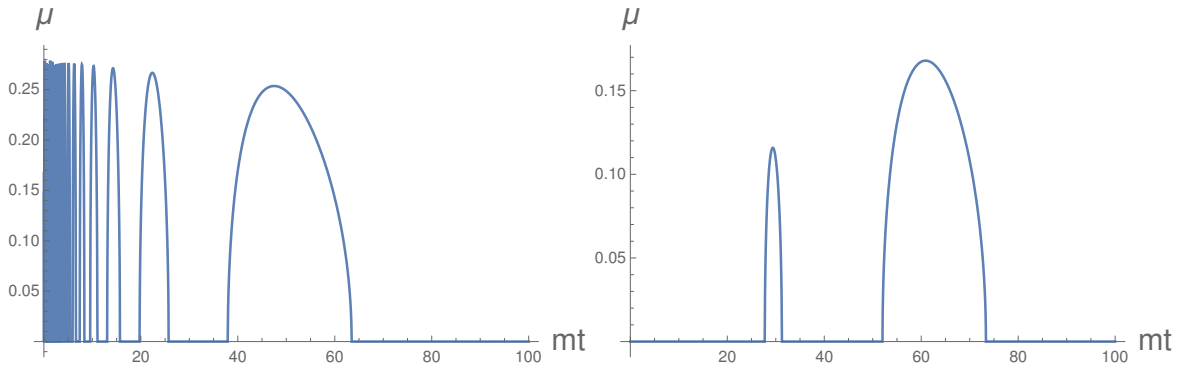

Figure 4.7: The Floquet exponent μ along the trajectory $A/q = 2$ (left) and $A/q = 3$ (right). The initial value of q is taken as $q = 2000$. See App. D.6 for the computation of the Floquet exponent.

the band widths get narrower (Fig. 4.5) and the inflaton evolves faster at earlier times. This tendency is clearly seen in Fig. 4.7: at $A/q = 3$ only the last band contributes significantly, whereas in the usual case of $A/q = 2$ many bands are important. The growth rate of the Higgs for a given k, which can be taken $k = 0$ as a representative value, is determined approximately by the Floquet exponent

$$h_{k=0} \propto e^{\mu_{\rm eff} m_\phi \Delta t} \tag{4.4.7}$$

where $\mu_{\rm eff}$ is an averaged Floquet parameter μ along the relevant trajectory in the last instability band and Δt is the time the system spends there. Since both A and q are proportional to Φ^2, the system evolves along a straight line in the (A, q) plane.[þ10] The resonance becomes inefficient for $\mu_{\rm eff} m_\phi \Delta t \lesssim O(1)$. The quantity $m_\phi \Delta t$ depends on two factors: (1) the width Δq

[þ10] We have verified that it also applies to the relevant range of $k \neq 0$.

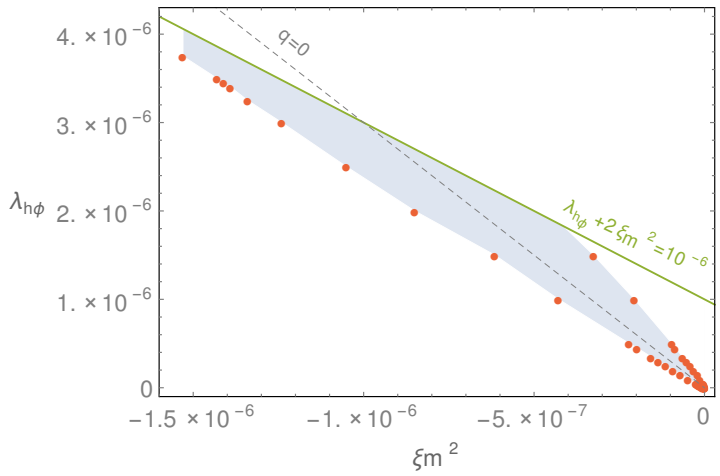

Figure 4.8: The EW vacuum stability region (the shaded region). The horizontal axis is $\xi_h m_\phi^2/M_{\rm Pl}^2$, while the vertical axis is $\lambda_{h\phi}$. The EW vacuum is stable during the preheating epoch in the shaded region. The red dots indicate the boundary of the stability region obtained with the lattice simulations.

of the last instability band determined by A/q with larger A/q leading to smaller Δq; (2) the rate of the decrease of Φ in the last band which is controlled by the initial q, or $q_{\rm ini}$. We have $\Delta q/q \simeq 2\Delta t/t_{\rm end}$ and $m_\phi t_{\rm end} \propto q_{\rm ini}^{1/2}$, and thus get the following scaling relation:

$$\mu_{\rm eff} m_\phi \Delta t \propto \sqrt{\lambda_{h\phi} + 3\xi_h \frac{m_\phi^2}{M_{\rm Pl}^2}}\, \mu_{\rm eff} \Delta q. \tag{4.4.8}$$

This shows that the resonance can be suppressed at larger couplings $\lambda_{h\phi} + 3\xi_h m_\phi^2/M_{\rm Pl}^2$ (or larger $q_{\rm ini}$) by increasing A/q (which decreases Δq and $\mu_{\rm eff}$). For instance, a tenfold increase in $q_{\rm ini}$ can be compensated by increasing A/q from 2 to 3. This is roughly what we observe in Fig. 4.6. While for larger A/q the above scaling works well, at $A/q \leq 2.3$ this approximation breaks down and many instability bands contribute to the resonance.

The final result of our numerical study is shown in Fig. 4.8. The shaded region corresponds to the parameter region where the EW vacuum is stable during and after inflation. The region is finite due to the large couplings being cut off by the constraint of sufficiently flat inflaton potential. Negative $\lambda_{h\phi}$ and positive ξ_h lead to stronger resonance and thus are excluded except close to the origin. The red dots indicate the boundary of the stability region obtained with the lattice simulations. These center around the $q = 0$ line. The allowed parameter region extends to about $\lambda_{h\phi} \sim 6 \times 10^{-6}$, although the tip of this region is not shown in the plot. The Higgs stability during inflation (Eq. (4.4.4)) is satisfied in the shaded region.

4.5 Higgs-inflaton trilinear coupling

Finally we consider the case $\lambda_{h\phi},\ \xi_h,\ \sigma_{h\phi} \neq 0$. We give a brief overview first, and then show numerical results.

Qualitative discussion

The trilinear coupling $\sigma_{h\phi}\phi h^2$ can be ignored during inflation as long as $|\sigma_{h\phi}|\Phi < \lambda_{h\phi}\Phi^2, 12\xi_h H^2$, but it can be dominant as Φ decreases in the preheating epoch. Actually the quartic as well as the curvature interactions decrease as t^{-2}, while the trilinear one decreases only as t^{-1} since it is linear in ϕ. Hence it dominates at late times resulting in a tachyonic resonance. Thus we can obtain a strong bound on $\sigma_{h\phi}$ almost independently of $\lambda_{h\phi}$ and ξ_h. See also App. D.5 and Ref. [38].

Ignoring the Hubble expansion and the Higgs self-interaction, the Higgs dynamics are described by the so-called Whittaker-Hill equation:

$$\left[\frac{d^2}{dz^2} + A_k + 2p\cos 2z + 2q\cos 4z\right] h_k = 0, \tag{4.5.1}$$

where the resonance parameters are defined as

$$z \equiv \frac{m_\phi t}{2}, \quad A_k \equiv \frac{4k^2}{m_\phi^2} + 2\left(\lambda_{h\phi} + \xi_h\frac{m_\phi^2}{M_{\rm Pl}^2}\right)\frac{\Phi^2}{m_\phi^2}, \quad p \equiv \frac{2\sigma_{h\phi}\Phi}{m_\phi^2}, \quad q \equiv \left(\lambda_{h\phi} + 3\xi_h\frac{m_\phi^2}{M_{\rm Pl}^2}\right)\frac{\Phi^2}{m_\phi^2}. \tag{4.5.2}$$

This is a good approximation as long as A_k, p and q change adiabatically. The relevant stability charts for the Whittaker-Hill equation are shown in Fig. 4.9. If the parameters are in the white region, there exits an exponentially growing mode, resulting in the resonant particle production. See App. D.5 for more details.

Numerical simulation

In order to obtain a bound on $\sigma_{h\phi}$, we have performed the classical lattice simulation. We have chosen $\lambda_{h\phi}$ and ξ_h such that they are in the shaded region in Fig. 4.6, and see whether the trilinear coupling $\sigma_{h\phi}$ destabilizes the EW vacuum or not. The results are shown in Fig. 4.10. The EW vacuum is stable in the shaded region, while it is destabilized in the white region. From this figure, we may require that

$$\left|\sigma_{h\phi}\right| \lesssim 10^9\ {\rm GeV}, \tag{4.5.3}$$

for $m_\phi \simeq 10^{13}$ GeV, in order for the EW vacuum to be stable during the preheating epoch. It is almost independent of $\lambda_{h\phi}$ and ξ_h since the trilinear coupling eventually dominates over the other terms as we explained just above. The constraint is expected to scale as $\propto m_\phi^2$ since the end of the preheating is estimated as $m_\phi t_{\rm end} \sim |\sigma_{h\phi}| M_{\rm Pl}/m_\phi^2$, assuming that the dependence of the Floquet exponent on $\sigma_{h\phi}$ is mild. Positive and negative $\sigma_{h\phi}$ are slightly inequivalent due to the Universe expansion.

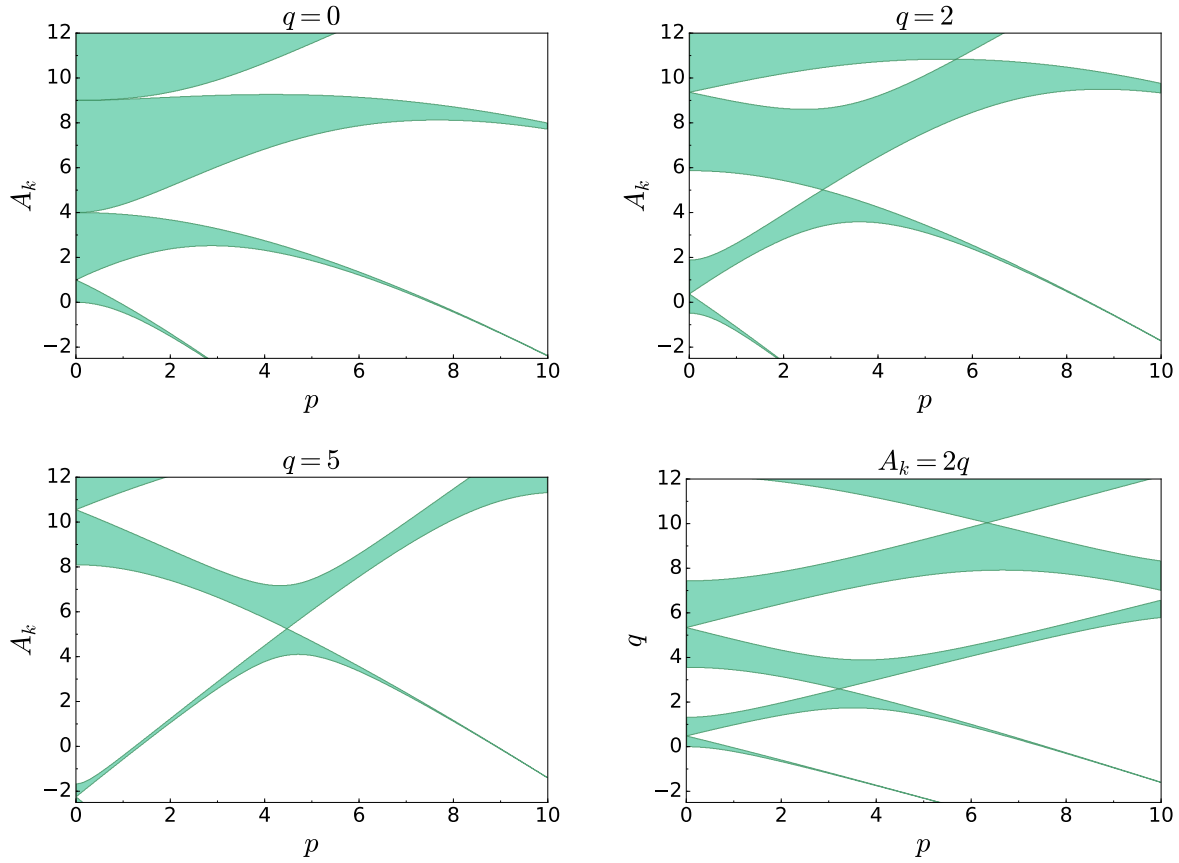

Figure 4.9: The stability/instability chart of the Whittaker-Hill equation. The green shaded (white) region corresponds to the stability (instability) region. The first three panels fix q as $q = 0$ (upper left, equivalent to the Mathieu equation), $q = 2$ (upper right) and $q = 5$ (lower left). The last panel (lower right) shows the result with $A_k = 2q$. The charts are even with respect to p.

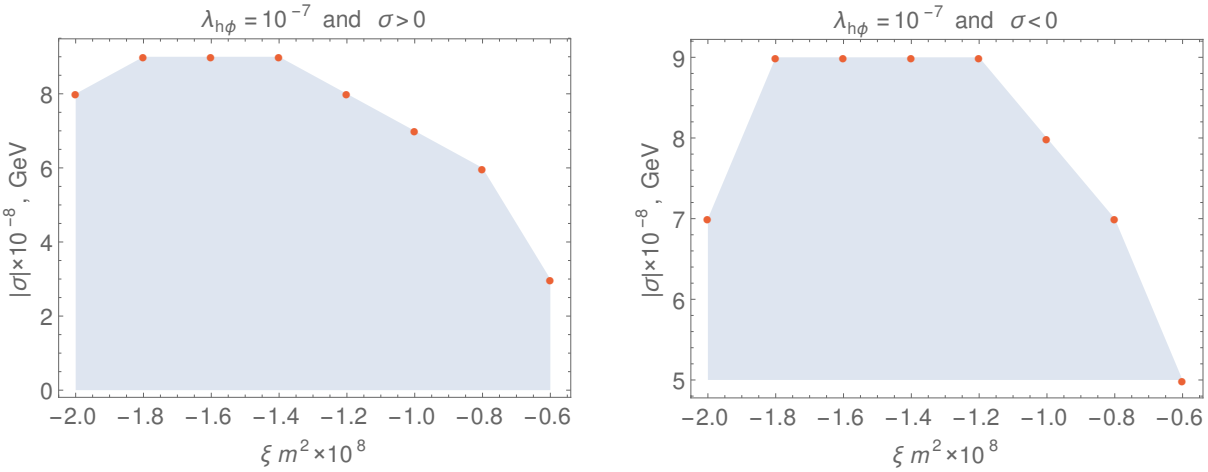

Figure 4.10: The EW vacuum stability region (shaded region) with $\sigma_{h\phi}$. Left: $\sigma_{h\phi} > 0$, right: $\sigma_{h\phi} < 0$. The red dots indicate the boundary of the stability region obtained with the lattice simulations.

4.6 Higgs-radiation coupling

In the previous sections, we have neglected effects of the SM Yukawa and gauge couplings. In this section, we investigate whether these couplings modify the above analysis or not. In particular, we discuss the instant preheating and the annihilation processes that might affect the Higgs dynamics during preheating. Here we concentrate on the cases where there is only $\lambda_{h\phi}$ or ξ_h, but a generalization to the case with all the couplings should be straightforward.

■ Instant preheating

For a relatively large $\lambda_{h\phi}$, the Higgs particles produced at $\phi \sim 0$ decay into top quarks at a large field value of the inflaton where the Higgs is heavy [39]. If it is prompt, the efficiency of the resonance is reduced and the decay products may stabilize the EW vacuum.

■ Annihilation

If the number density of the Higgs grows, the annihilation of the produced Higgs into top quarks and EW gauge bosons may become significant [40, 41]. It reduces the efficiency of the resonance, and the produced particles may stabilize the EW vacuum as well.

4.6.1 Instant preheating

Since the Higgs couples with the top quark via the sizable Yukawa coupling, it decays into top quarks at a large field value region of the inflaton where the Higgs effective mass is large. We first give an overview of this process.

At the early stage of the preheating, effects of the top Yukawa coupling significantly differ depending on whether we consider $\lambda_{h\phi}$ or ξ_h. For the quartic coupling $\lambda_{h\phi}$, the growth rate of the resonance is almost independent of $\lambda_{h\phi}$. Hence the Higgs decay ($\propto \lambda_{h\phi}$) overcomes the resonance at the early stage. Radiation is effectively produced at this epoch, which may stabilize the EW vacuum. For the curvature coupling ξ_h, on the contrary, both the growth rate of the resonance and the decay rate are proportional to $\sqrt{\xi_h}$. Thus, the resonance always dominates over the Higgs decay. At the late stage, the Higgs resonant production dominates over the Higgs decay even in the case with $\lambda_{h\phi}$, and hence the Higgs decay just reduces the efficiency of the resonance.

From now we first discuss its effect in the early stage for the case only with $\lambda_{h\phi}$. Then we move on to the discussion in the late stage.

■ Instant decay of Higgs [Early stage with $\lambda_{h\phi}$]

At the early stage of the preheating, the Higgs decay may dominate over the resonant Higgs production in the broad resonance case. If $\lambda_{h\phi}$ is so large that the decay is efficient enough, then the EW vacuum can be stabilized by the produced particles. In the following we estimate the boundary of $\lambda_{h\phi}$ above which it occurs.

The Higgs obtains the effective mass of $m_h^2 = \lambda_{h\phi}\Phi^2 \cos^2\left(m_\phi t\right)$, and hence it is heavy enough to decay into the top quarks when the inflaton is away from its potential origin. The

oscillation averaged decay rate is roughly estimated as

$$\bar{\Gamma}_{h\to t\bar{t}} \simeq \frac{3\alpha_t}{2}\bar{m}_h \sim \lambda_{h\phi}^{1/2}\,\alpha_t\Phi, \tag{4.6.1}$$

where the bar indicates the oscillation average, and $\alpha_t \equiv y_t^2/4\pi$ with y_t being the SM top Yukawa coupling. If it satisfies $\bar{\Gamma}_{h\to t\bar{t}} \gg m_\phi/\pi$, the Higgs particles produced at $\phi \sim 0$ decay completely before the inflaton moves back to its potential origin. While this condition holds, the Higgs particles decay at

$$\int_{t_c}^{t_{\rm dec}} dt\Gamma_{h\to t\bar{t}} \sim 1, \quad \text{or} \quad m_\phi^2\,(t_{\rm dec}-t_c)^2 \sim \frac{m_\phi}{\lambda_{h\phi}^{1/2}\,\alpha_t\Phi}, \tag{4.6.2}$$

where t_c is the time at which the inflaton crosses the origin. The Higgs is non-relativistic due to the factor $\alpha_t^{1/2} \ll 1$ at its decay, and hence the Higgs energy density at its decay is given by

$$\rho_h(t_{\rm dec}) \sim \frac{p_*^3}{8\pi^3}m_h(t_{\rm dec}) \sim \frac{\lambda_{h\phi}}{8\pi^3\alpha_t^{1/2}}m_\phi^2\Phi^2. \tag{4.6.3}$$

Note that $n_h \sim p_*^3/(2\pi)^3$ for the large inflaton field value region since the adiabaticity is satisfied in that region (see App. D.3). The top Yukawa coupling comes in the denominator since the Higgs is heavier at its decay for smaller α_t as long as $\bar{\Gamma}_{h\to t\bar{t}} \gg m_\phi/\pi$ is satisfied. This energy density is converted to the top quarks within one oscillation of the inflaton, and hence we can define an effective inflaton decay rate as [42, 43]

$$\Gamma_{\rm inst} \equiv \frac{m_\phi}{\pi}\frac{\rho_h(t_{\rm dec})}{\rho_\phi} \sim \frac{\lambda_{h\phi}}{8\pi^4\alpha_t^{1/2}}m_\phi. \tag{4.6.4}$$

If the conditions $\bar{\Gamma}_{h\to t\bar{t}} \gg m_\phi/\pi$ and $p_*^2 > m_{\rm th}^2$ are satisfied until $\Gamma_{\rm inst} \simeq H$, with $m_{\rm th}$ being the thermal mass of the Higgs from the produced SM particles, the inflaton condensation completely decays before the Higgs resonant production overcomes the Higgs decay. Hence the EW vacuum is stable in such a case. The former condition is satisfied if

$$\lambda_{h\phi} \gg 5\times 10^{-2}\left(\frac{m_\phi}{10^{13}\,{\rm GeV}}\right)^{2/3}\left(\frac{0.02}{\alpha_t}\right)^{1/3}, \tag{4.6.5}$$

while the latter is satisfied if

$$\lambda_{h\phi} > 0.1\left(\frac{100}{g_*}\right). \tag{4.6.6}$$

Thus, the instant preheating process can kill the inflaton condensation for the case with $\lambda_{h\phi}$ as large as $\lambda_{h\phi} \gtrsim 0.1$. Otherwise we expect that the inflaton condensation survives the instant preheating epoch, and the Higgs resonant production eventually dominates over the decay in the late time. Here note that the coupling as large as $\lambda_{h\phi} \gtrsim 0.1$ is unlikely for the

vanilla chaotic inflation model. The quartic coupling $\lambda_{h\phi}$ induces the Coleman-Weinberg potential [4] as

$$V_{\rm CW} = \frac{\lambda_{h\phi}^2 \phi^4}{64\pi^2} \ln\left(\frac{\lambda_{h\phi}\phi^2}{m_\phi^2}\right). \tag{4.6.7}$$

If we stick to the quadratic inflaton potential, $\lambda_{h\phi}$ should satisfy $\lambda_{h\phi} \lesssim 10^{-6}$ [34] for the flatness of the inflaton potential. In this case the instant preheating is not efficient. It may be possible to have $\lambda_{h\phi} \gtrsim 0.1$ for other inflation models such as with the non-minimal coupling [44] or the modified kinetic terms [45–47], but we do not dig into these models here to avoid model dependent discussions.

■ **Slow decay of Higgs [Late stage with $\lambda_{h\phi}$, or with ξ_h]**

Now we discuss the case where the resonance dominates over the Higgs decay. More specifically, we consider the case where

$$\bar{\Gamma}_{h\to t\bar{t}} \ll \frac{m_\phi}{\pi}, \tag{4.6.8}$$

in this subsection. Then only a part of the Higgs produced by the inflaton oscillation decays within one inflaton oscillation, and hence the decay reduces the efficiency of the resonance. We study its effect here. We consider the case with $\lambda_{h\phi}$ in detail. A similar discussion holds in the case with ξ_h.

A typical decay rate of the Higgs is given by

$$\bar{\Gamma}_{h\to t\bar{t}} \simeq \frac{3\alpha_t}{2\sqrt{2}} \lambda_{h\phi}^{1/2} \Phi. \tag{4.6.9}$$

It reduces the growth rate of Higgs as

$$\ln n_h \propto 2\mu_{\rm qtc} m_\phi t - \bar{\Gamma}_{h\to t\bar{t}} t. \tag{4.6.10}$$

As a result, the decay time in Eq. (4.2.15) becomes slightly longer:

$$m_\phi t_{\rm dec} \sim \frac{1}{2\mu_{\rm qtc}} \ln\left(\frac{16\pi^{\frac{3}{2}}}{3\tilde{\lambda}}\right) + \frac{\sqrt{3}\alpha_t}{2\mu_{\rm qtc}} \frac{\lambda_{h\phi}^{1/2} M_{\rm Pl}}{m_\phi}. \tag{4.6.11}$$

By comparing it with $t_{\rm end}$ given in Eq. (4.2.16), we estimate the impacts of the Higgs decay on the upper bound as follows:

$$\lambda_{h\phi} \lesssim 10^{-8} \left[\frac{0.1}{\mu_{\rm qtc}}\right]^2 \left[\frac{m_\phi}{10^{13}\,{\rm GeV}}\right]^2 \left[1 - 0.1\left(\frac{\alpha_t}{0.02}\right)\left(\frac{0.1}{\mu_{\rm qtc}}\right)\right]^{-2}. \tag{4.6.12}$$

Similarly, in the case with ξ_h, we find

$$\xi_h \lesssim 10 \times \left[\frac{2}{n_{\rm eff}\,\mu_{\rm crv}}\right]^2 \left[\frac{\sqrt{2}\,M_{\rm Pl}}{\Phi_{\rm ini}}\right]^2 \left[1 - 0.04\left(\frac{\alpha_t}{0.02}\right)\left(\frac{2}{\mu_{\rm crv}}\right)\right]^{-2}. \tag{4.6.13}$$

Thus it does not significantly change the upper bound. Note that the decay of Higgs into the top quarks may be much suppressed in reality. This is because the typical life time of the Higgs should be longer since the Higgs is relativistic, and because the top quarks acquire a finite density mass correction from the Higgs fluctuations. Since our estimation is not affected drastically even if we optimistically estimate the Higgs decay rate, we do not investigate these effects further.

4.6.2 Annihilation

In the broad/tachyonic resonance, the number density of the Higgs grows exponentially. If the number density is large enough, the Higgs can annihilate into top quarks and EW gauge bosons. In particular, the Higgs may rapidly excite the gauge bosons to exponentially large number densities [48]. If the number densities of the gauge bosons become comparable to the Higgs before the EW vacuum destabilization, they might stabilize the EW vacuum.

In order to see whether the annihilation can indeed stabilize the EW vacuum or not, we consider the following simplified Lagrangian:

$$\mathcal{L} = \mathcal{L}_\phi + \mathcal{L}_h + \mathcal{L}_\chi + \mathcal{L}_{\rm int} + \mathcal{L}_{\rm ann}, \tag{4.6.14}$$

where $\mathcal{L}_\phi$, $\mathcal{L}_h$ and $\mathcal{L}_{\rm int}$ are the same as Eqs. (4.1.2), (4.1.4) and (4.1.6) with the couplings being $\lambda_{h\phi} \neq 0, \xi_h = \sigma_{h\phi} = 0$ or $\xi_h \neq 0, \lambda_{h\phi} = \sigma_{h\phi} = 0$. In addition, we take the Lagrangian for a light scalar field χ as

$$\mathcal{L}_\chi = \frac{1}{2}\partial_\mu\chi\partial^\mu\chi - \frac{1}{4}g_{\chi\chi}^2\chi^4, \tag{4.6.15}$$

$$\mathcal{L}_{\rm ann} = -\frac{1}{2}g_{h\chi}^2 h^2\chi^2. \tag{4.6.16}$$

Here χ schematically represents the SM gauge bosons, where we model the gauge interactions as the quartic interactions.

We have solved the classical equations of motion derived from the Lagrangian (4.6.14) numerically. We take $d = 3+1$, $N_g = 128$, $dt = 10^{-3}/m_\phi$, $m_\phi = 1.5\times10^{13}\,\text{GeV}$, $\Phi_{\rm ini} = \sqrt{2}M_{\rm Pl}$, $a_{\rm ini} = 1$, $\dot\Phi_{\rm ini} = 0$ and $g_{h\chi} = g_{\chi\chi} = 0.5$. In Fig. 4.11, we show the time evolution of $\langle\phi\rangle^2$ (black), $\langle\phi^2\rangle - \langle\phi\rangle^2$ (red), $\langle h^2\rangle$ (blue) and $\langle\chi^2\rangle$ (orange). They are multiplied by a^3, and normalized by $\Phi_{\rm ini}$. The left panel is the result of the quartic coupling case with $\lambda_{h\phi} = 4\times10^{-8}$ and $L = 10/m_\phi$, and the right panel is that of the curvature coupling case with $\xi_h = 20$ and $L = 20/m_\phi$. As we can see from Fig. 4.11, the Higgs rolls down to the true vacuum well before χ is sufficiently produced. In fact, the dynamics of the Higgs is almost the same as those in Figs. 4.1 and 4.3. Thus, the annihilation process cannot stabilize the EW vacuum in our simplified setup. The results do not change even if we take the couplings of χ larger, say $g_{h\chi} = g_{\chi\chi} = 1$.

Now let us take a closer look at Fig. 4.11. In the case with ξ_h (the right panel), the Higgs rolls down to the true vacuum at the first a few oscillations of the inflaton, regardless of the existence of the annihilation channel. It seems that this is because the time scale of the EW vacuum decay is too short for the annihilation to be effective. We believe that the same argument holds for the realistic model where the Higgs couples to the EW gauge bosons,

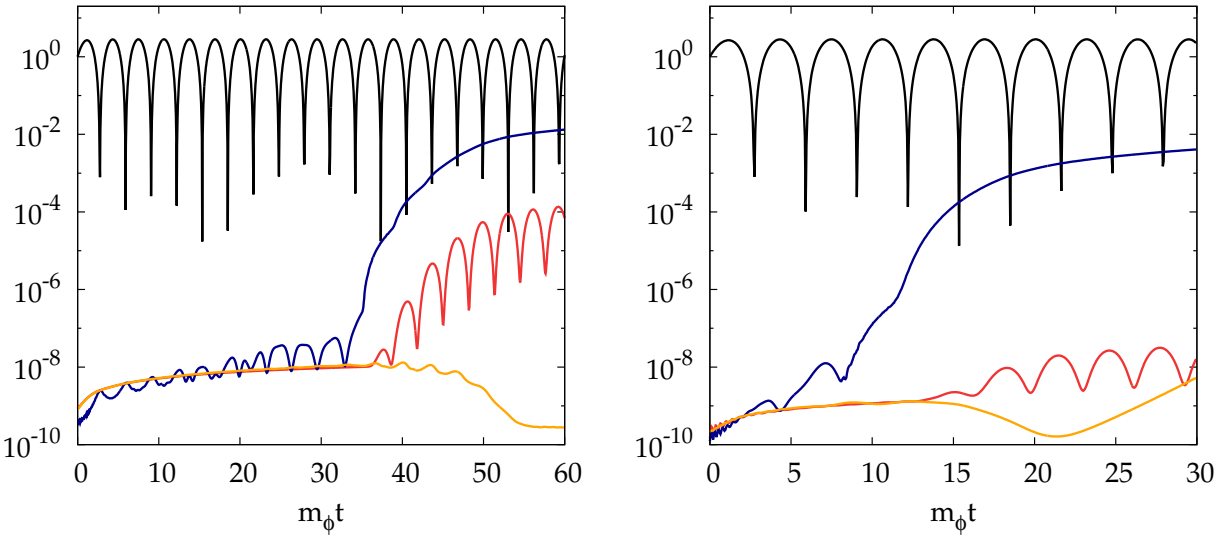

Figure 4.11: The time evolution of the inflaton and the Higgs. The black line is $\langle\phi\rangle^2$, the red line is $\langle\phi^2\rangle - \langle\phi\rangle^2$, the blue line is $\langle h^2\rangle$ and the orange line is $\langle\chi^2\rangle$, where the angle brackets denote the spatial average. They are multiplied by a^3 and normalized by $\Phi_{\rm ini} = \sqrt{2}M_{\rm Pl}$. Left: $\lambda_{h\phi} = 4\times10^{-8}, \xi_h = 0$, right: $\lambda_{h\phi} = 0, \xi_h = 20$.

since the annihilation rate is not much different from our simplified model. In the case with $\lambda_{h\phi}$, the Higgs remains in the EW vacuum for the first O(1-10) times of oscillation of inflaton. Even in such a case χ is not efficiently produced via the annihilation process. It might be understood as follows. If the Higgs is produced, it induces an effective mass to χ as

$$m^2_{{\rm eff};\chi}(t) \simeq g^2_{h\chi}\frac{n_h(t)}{\omega_{k_*;h}(t)}. \tag{4.6.17}$$

The phase space of the produced χ is kinematically restricted by the effective mass $m^2_{{\rm eff};\chi}$, and hence it might suppress the annihilation rate. Provided that this description is correct, the dynamics should be similar for the realistic case where the Higgs couples to the gauge bosons. Thus, we may expect that the annihilation process cannot stabilize the EW vacuum during the preheating stage in the realistic case either. More rigorous analysis requires lattice simulations including the gauge bosons [49–51], which is beyond the scope of this dissertation.

Even if we properly take into account the degrees of freedom of the gauge bosons and the Higgs, the situation is not expected to change. In order for the gauge boson to stabilize the EW vacuum, its dispersion must satisfy

$$g^2\sum\left\langle A^2\right\rangle \gtrsim |\lambda_h|\sum\left\langle h^2\right\rangle, \tag{4.6.18}$$

where g is the EW gauge coupling, A is the gauge boson and h is the Higgs. The sums are for the six degrees of freedom for A and the four degrees of freedom for h, respectively. Expecting that $\langle A^2\rangle \simeq \langle\chi^2\rangle$, we can see from Fig. 4.11 that the produced amount of the gauge boson is far below Eq. (4.6.18).

Chapter 5

Metastability after low-scale inflation

In Chap. 4, we have seen that the EW vacuum can be destabilized during the preheating epoch once the inflaton mass scale m_ϕ is larger than the instability scale $M_{\rm inst}$. There we have concentrated on the high-scale inflation models. However, m_ϕ can be larger than $M_{\rm inst}$ even for low-scale inflation models with $M_{\rm inst} \gg H_{\rm inf}$ where $H_{\rm inf}$ is the Hubble parameter during inflation. Actually it is usually the case that $m_\phi \gg H_{\rm inf}$ for low-scale inflation models. Thus, in this chapter, we study the EW vacuum stability during the preheating epoch for a low-scale inflation model. This chapter is based on the author's original work [3].

5.1 Setup

First we summarize our setup. We take the Lagrangian as

$$\mathcal{L} = \frac{M_{\rm Pl}^2}{2}R - \frac{1}{2}\left(\partial\phi\right)^2 - \frac{1}{2}\left(\partial h\right)^2 - U(\phi, h), \tag{5.1.1}$$

where $M_{\rm Pl}$ is the reduced Planck scale, R is the Ricci scalar, ϕ is the inflaton, and h is the Higgs.[b1] We assume that the inflaton is singlet under the SM gauge group, and hence the trilinear as well as quartic portal couplings between the inflaton and Higgs are allowed in general. Thus we take the following generic form for the potential:

$$U(\phi, h) = V(\phi) + \frac{\tilde{\sigma}_{h\phi}}{2}\phi h^2 + \frac{\lambda_{h\phi}}{2}\phi^2 h^2 + \frac{m_h^2}{2}h^2 + \frac{\lambda_h}{4}h^4, \tag{5.1.2}$$

where V is the inflaton potential, m_h^2 is the bare mass of Higgs, and $\tilde{\sigma}_{h\phi}$, $\lambda_{h\phi}$, and λ_h are coupling constants.[b2] Note that the inflaton can have some gauge charges other than the SM such as $\mathrm{U}(1)_{\rm B-L}$. In that case, ϕ should be regarded as a radial component of the complex scalar, and $\tilde{\sigma}_{h\phi} = 0$. In this chapter, however, we keep $\tilde{\sigma}_{h\phi} \neq 0$ to make our discussion generic. Below we explain each term in detail.

[b1] Again we consider only one degree of freedom for simplicity.

[b2] We can consider the non-minimal Higgs-curvature interaction $\xi_h R h^2$ as well, but it is effective only when the non-minimal coupling ξ_h is quite sizable: $|\xi_h| \gtrsim m_\phi^2/H_{\rm inf}^2 \gg 1$.

Inflaton potential

As a representative example of low-scale inflation models, we consider the hilltop model [52–55] (see Refs. [56–59] for supergravity embeddings):

$$V(\phi) = \Lambda^4 \left[1 - \left(\frac{\phi}{v_\phi}\right)^n\right]^2, \tag{5.1.3}$$

where $n > 2$ is an integer and $v_\phi > 0$ is the vacuum expectation value (VEV) of the inflaton at the minimum of its potential. The inflaton mass around the minimum is

$$m_\phi = \frac{\sqrt{2}n\Lambda^2}{v_\phi}. \tag{5.1.4}$$

Since we are interested in small field inflation models, we assume that $v_\phi \ll M_{\rm Pl}$. Otherwise, the model would be rather similar to high-scale inflation models. Inflation takes place in the region $|\phi| \ll v_\phi$. Here and in what follows, we concentrate on the region $\phi > 0$ without loss of generality. The Hubble parameter at the end of inflation $H_{\rm end}$ is indeed much smaller than the inflaton mass m_ϕ in this case:

$$\frac{H_{\rm end}}{m_\phi} \simeq \frac{v_\phi}{\sqrt{6}nM_{\rm Pl}} \ll 1. \tag{5.1.5}$$

The CMB constraints on this model are discussed in App. C.2.3.

Higgs-inflaton couplings and bare mass term

In terms of $\varphi \equiv v_\phi - \phi$, the potential is given as

$$\begin{aligned} U(\phi, h) =& V(v_\phi - \varphi) + \frac{1}{2}\left(m_h^2 + \tilde{\sigma}_{h\phi} v_\phi + \lambda_{h\phi} v_\phi^2\right) h^2 \\ &+ \frac{\sigma_{h\phi}}{2}\varphi h^2 + \frac{\lambda_{h\phi}}{2}\varphi^2 h^2 + \frac{\lambda_h}{4} h^4, \end{aligned} \tag{5.1.6}$$

where we have defined

$$\sigma_{h\phi} \equiv -\left(\tilde{\sigma}_{h\phi} + 2\lambda_{h\phi} v_\phi\right). \tag{5.1.7}$$

Note that $\varphi = 0$ at the minimum of the inflaton potential. Here comes our crucial observation. In order to realize the EW scale, the bare Higgs mass and the mass coming from v_ϕ must be cancelled:[b3]

$$m_h^2 + \tilde{\sigma}_{h\phi} v_\phi + \lambda_{h\phi} v_\phi^2 = 0. \tag{5.1.8}$$

[b3] We have ignored the EW scale since the typical energy scale of our interest is much higher.

It is of course a tuning, but it is inevitable since we assume that the SM is valid up to some high energy scale aside from the inflaton sector. Thus, the potential is now given by

$$U(\phi, h) = V(v_\phi - \varphi) + \frac{\sigma_{h\phi}}{2}\varphi h^2 + \frac{\lambda_{h\phi}}{2}\varphi^2 h^2 + \frac{\lambda_h}{4}h^4. \tag{5.1.9}$$

In particular, the Higgs is almost massless at $\varphi = 0$.

Now we discuss quantum corrections to the inflaton potential. The potential of the low-scale inflation model has to be extremely flat, and hence only a small change might spoil the successful inflation. Suppose that the effective potential around the vacuum $\langle\phi\rangle \sim v_\phi$ is given by Eq. (5.1.9) at the end of inflation for some renormalization scale M. We will take M as the typical scale of the preheating dynamics ($M \gtrsim m_\phi$), and put bounds on the couplings defined at this scale. At the one-loop level, the radiative correction induces the Coleman-Weinberg effective potential,

$$V_{\rm CW}(\phi) \simeq \frac{m_h^4(\phi)}{64\pi^2}\ln\left(\frac{m_h^2(\phi)}{M^2}\right), \tag{5.1.10}$$

where we define $m_h^2(\phi) \equiv m_h^2 + \tilde{\sigma}_{h\phi}\phi + \lambda_{h\phi}\phi^2$, and the couplings are evaluated at M. We have assumed $m_h^2(\phi) > 0$ during inflation. Otherwise, the Higgs potential might be destabilized during inflation (see Sec. 5.2). In order not to change the tree-level inflaton potential too much during inflation, we need $|\partial V_{\rm CW}/\partial\phi| \lesssim |\partial V/\partial\phi|$. It roughly indicates

$$\left|\sigma_{h\phi}\right| \lesssim m_\phi\left(\frac{v_\phi}{M_{\rm Pl}}\right)^{\frac{n-1}{n-2}}, \qquad \left|\lambda_{h\phi}\right| \lesssim \frac{m_\phi}{M_{\rm Pl}}\left(\frac{v_\phi}{M_{\rm Pl}}\right)^{\frac{1}{n-2}}, \tag{5.1.11}$$

for $\tilde{\sigma}_{h\phi} \neq 0$ and

$$\left|\sigma_{h\phi}\right| \lesssim m_\phi\frac{v_\phi}{M_{\rm Pl}}, \qquad \left|\lambda_{h\phi}\right| \lesssim \frac{m_\phi}{M_{\rm Pl}}, \tag{5.1.12}$$

for $\tilde{\sigma}_{h\phi} \simeq 0$. We require these conditions in the following.

Higgs potential

Finally, we discuss the Higgs quartic coupling λ_h. In the present case, in order to understand the high-energy behavior of λ_h, we must carefully consider the mixing between φ and h [60–62]. Once we ignore $\lambda_{h\phi}$, the potential at around the minimum is written as

$$U \simeq \frac{m_\phi^2}{2}\left(\varphi + \frac{\sigma_{h\phi}h^2}{2m_\phi^2}\right)^2 + \frac{1}{4}\left(\lambda_h - \frac{\sigma_{h\phi}^2}{2m_\phi^2}\right)h^4. \tag{5.1.13}$$

Thus the Higgs potential below the energy scale of m_ϕ is

$$V_{\rm SM}(h) = \frac{\lambda_{\rm SM}}{4}h^4, \quad \lambda_{\rm SM} = \lambda_h - \frac{\sigma_{h\phi}^2}{2m_\phi^2}. \tag{5.1.14}$$

It is clear that $\lambda_{\rm SM}$ in the low-energy effective theory is different from λ_h.

Up to the energy scale of m_ϕ, the running of $\lambda_{\rm SM}$ is just that of the SM, and hence it turns to negative at around $10^{10}\,$GeV as we saw in Sec. 2.2. For simplicity, we again approximate it as

$$\lambda_{\rm SM} = -0.01 \times {\rm sgn}\,(M - M_{\rm inst}) \quad \text{for} \quad M < m_\phi, \tag{5.1.15}$$

where M is the energy scale of the system and $M_{\rm inst}$ is the instability scale of the Higgs potential which we take $M_{\rm inst} = 10^{10}\,$GeV. If $m_\phi < M_{\rm inst}$, λ_h is positive at least up to at around $M = M_{\rm inst}$.[b4] Thus, to overcome the potential barrier, the Higgs must be enhanced as $\langle h^2\rangle \gtrsim M_{\rm inst}^2 > m_\phi^2$. However, such an enhancement requires large $\lambda_{h\phi}$ and $\sigma_{h\phi}$ which are likely to spoil Eq. (5.1.11).[b5] Therefore, we concentrate on the opposite case:

$$m_\phi > M_{\rm inst}. \tag{5.1.16}$$

By matching at $M = m_\phi$, the boundary condition for λ_h is roughly given as

$$\lambda_h|_{M=m_\phi} = -0.01 + \left.\frac{\sigma_{h\phi}^2}{2m_\phi^2}\right|_{M=m_\phi}. \tag{5.1.17}$$

If $\sigma_{\phi h}^2/m_\phi^2 \gtrsim 0.01$, it may significantly affect λ_h so that it helps to stabilize the Higgs potential at the high-energy region.[b6] In such a case, t here may be another minimum at around $h \simeq m_\phi$ and $\varphi \simeq -\sigma_{\phi h}$ because of Eqs. (5.1.13) and (5.1.16), and it may affect the dynamics of the Higgs in the early universe. Instead of being involved in such a complexity, here we simply concentrate on the case[b7]

$$\frac{\sigma_{h\phi}^2}{m_\phi^2} \ll 0.01. \tag{5.1.18}$$

Then, we may approximate the quartic coupling as

$$\lambda_h = -0.01 \times {\rm sgn}\,(M - M_{\rm inst})\,. \tag{5.1.19}$$

We take the renormalization scale as $M = \max\left(H, \sqrt{\langle h^2\rangle}\right)$ during preheating as in Chap. 4. Namely, we again simply use the tree-level Higgs potential with the renormalization scale chosen as the typical energy scale of the system.

[b4] The potential can be even absolutely stable depending on $\sigma_{h\phi}^2/m_\phi^2$ and the sign of $\lambda_{h\phi}$ [60–62].

[b5] The hilltop model ($n = 6$) with $m_\phi < M_{\rm inst}$ cannot have large resonance parameters because of Eq. (5.4.2).

[b6] If $\lambda_{\phi h}$ is negative, the potential may not be absolutely stable anyway, depending on the details of $V(\phi)$.

[b7] In principle, the same argument can be applied for the high-scale inflation case we studied in Chap. 4 if $\sigma_{h\phi}$ is present. In practical, the upper bound on $\sigma_{h\phi}$ from the EW vacuum stability during the preheating is much below this value ($|\sigma_{h\phi}| \lesssim 10^9\,$GeV and $m_\phi \simeq 10^{12}$-$10^{13}\,$GeV), and hence we safely ignore it.

5.2 Higgs dynamics during inflation

Before studying the preheating stage, we summarize the Higgs dynamics during inflation in this section. As we saw in Chap. 3, the EW vacuum can be destabilized during inflation if the inflation scale is too high. It is instructive to see what happens if the inflation scale is so low that $H_{\rm inf} \ll M_{\rm inst}$. In the present model, since $\phi \ll v_\phi$ during inflation, the Higgs potential during inflation is approximately given by

$$V(h) \simeq \frac{m_h^2}{2}h^2 + \frac{\lambda_h}{4}h^4, \tag{5.2.1}$$

where m_h^2 satisfies Eq. (5.1.8). There are two possibilities: $m_h^2 < 0$ and $m_h^2 > 0$.

First, let us consider the case with $m_h^2 < 0$, or $\tilde{\sigma}_{h\phi} + \lambda_{h\phi} v_\phi > 0$. In this case, the parameters must satisfy

$$|\lambda_h| M_{\rm inst}^2 > |m_h^2|, \tag{5.2.2}$$

since otherwise the potential decreases monotonically toward large h and the Higgs may roll down to the deeper minimum during inflation. As long as Eq. (5.2.2) is satisfied, the EW vacuum is stable during inflation if $H_{\rm inf} \ll M_{\rm inst}$. Otherwise, the de-Sitter fluctuation of the Higgs field is too large to stay at the local minimum of the potential. Next, let us consider the opposite case: $m_h^2 > 0$, or $\tilde{\sigma}_{h\phi} + \lambda_{h\phi} v_\phi < 0$. In this case, $h = 0$ is always a local minimum of the potential, and it is stable against the de-Sitter fluctuation if

$$H_{\rm inf}^2 \ll \max\left[M_{\rm inst}^2,\ m_h^2/|\lambda_h|\right]. \tag{5.2.3}$$

If the condition (5.2.2) or (5.2.3) is satisfied, the EW vacuum is stable during inflation. However, it does not guarantee the vacuum stability *after* inflation, since the Higgs fluctuation can be resonantly enhanced during the preheating stage as studied in detail from now.

5.3 Particle production after inflation

In this section, we describe the preheating dynamics of our system. We first discuss resonant inflaton production in Sec. 5.3.1. Since the inflaton potential at around the minimum is far from quadratic in the present case, inflaton particles are also resonantly produced. In fact, the inflaton particles can be even tachyonic, and hence the inflaton production is so efficient that the backreaction kills the inflaton condensation within several times of the oscillation. It sets the end of the preheating epoch, which is the time until which we follow in this chapter. Then we discuss resonant Higgs production in Sec. 5.3.2. There we use a crude approximation that the inflaton potential is quadratic. It is still useful to understand the Higgs production qualitatively, and to make an order estimation of the constraints on the couplings. More rigorous analysis is performed numerically in the next section.

5.3.1 Inflaton dynamics during tachyonic oscillation

The inflaton oscillation for a low-scale inflation model is typically dominated by the flat part of the potential just after inflation, and it causes a so-called tachyonic preheating phenomenon. Below we closely follow the discussion in Ref. [63].

There are two stages of the tachyonic preheating. The first stage is from the beginning of the tachyonic growth to the first passage of $\phi = v_\phi$, and the second stage is tachyonic inflaton oscillation regime. The first stage is further divided into the epoch between the point $|\eta| = 1$ and $\epsilon = 1$, and the interval between $\epsilon = 1$ and the first passage of $\phi = v_\phi$. Here ϵ and η are the slow-roll parameters: $\epsilon \equiv M_{\rm Pl}^2 (V'/V)^2/2$, $\eta \equiv M_{\rm Pl}^2 V''/V$, where V is the inflaton potential and the prime denotes the derivative with respect to ϕ.

The inflaton fluctuations with $k/a \lesssim H_{\rm inf}$ start to develop after $|\eta| \gtrsim 1$. Note that still $\epsilon \ll 1$ is satisfied at the beginning of this stage since there is a large hierarchy between $|\eta|$ and ϵ in low-scale inflation models. While the inflaton is rolling down the potential, higher momentum modes with $H_{\rm inf} < k/a \lesssim m_\phi$ also experience tachyonic growth, but the modes with low k/a ($\lesssim H_{\rm inf}$) are most enhanced since they have more time to develop. For the inflaton fluctuatiosn with momentum as low as $k/a \lesssim H_{\rm inf}$, the linearized equation of motion is the same as that of the velocity of the homogenous mode. Hence we estimate the enhancement factor from $|\eta| = 1$ to the first passage of $\phi = v_\phi$ as

$$\frac{\delta\phi_k(\phi(t) = v_\phi)}{\delta\phi_k(|\eta| = 1)} = \frac{\dot\phi(\phi(t) = v_\phi)}{\dot\phi(|\eta| = 1)} \sim \left(\frac{M_{\rm Pl}}{v_\phi}\right)^{n/(n-2)}. \tag{5.3.1}$$

where we have used $\phi(|\eta| = 1) \sim (v_\phi/M_{\rm Pl})^{2/(n-2)}$ and the slow-roll approximation to estimate $\dot\phi(|\eta| = 1)$. The condition for $\delta\phi$ to remain perturbative after the first passage of $\phi = v_\phi$ reads

$$\left\langle \delta\phi^2 \right\rangle \sim \frac{\Lambda^4}{M_{\rm Pl}^2}\left(\frac{M_{\rm Pl}}{v_\phi}\right)^{2n/(n-2)} \lesssim v_\phi^2, \quad \text{or} \quad \frac{\Lambda}{v_\phi} \lesssim \left(\frac{v_\phi}{M_{\rm Pl}}\right)^{1/(n-2)}. \tag{5.3.2}$$

Using the CMB normalization, it translates into

$$\frac{v_\phi}{M_{\rm Pl}} \gtrsim 10^{-6}\text{-}10^{-5}, \tag{5.3.3}$$

independently of n. Otherwise, even within one inflaton oscillation, the inflaton condensate may be broken, and the subsequent inflaton-Higgs dynamics would be too complicated. To avoid this complexity, we focus on the case where the above condition is satisfied so that we can reliably discuss the Higgs dynamics in the second stage.

The second stage is tachyonic inflaton oscillation regime. During this stage, the inflaton oscillation is far from harmonic since the most oscillation period is consumed at the flat part of the potential $\phi \ll v_\phi$. We first estimate the lower endpoint field value of the inflaton after j-th oscillation ϕ_j, and the time t_j at which $\phi = \phi_j$. From the energy conservation, it satisfies

$$V(\phi_j) - V(\phi_{j+1}) = \int_{t_j}^{t_{j+1}} dt\, 3H\dot\phi^2. \tag{5.3.4}$$

The integrand is dominated by the potential minimum where $|dt\dot{\phi}| \sim v_\phi$ and $|\dot{\phi}| \sim \Lambda$. Thus we obtain

$$\frac{\phi_j}{v_\phi} \sim \left(\frac{j v_\phi}{M_{\rm Pl}}\right)^{1/n}. \tag{5.3.5}$$

Note that $\phi_{j=1} > \phi(\epsilon = 1)$ where $\phi(\epsilon = 1) \sim v_\phi (v_\phi/M_{\rm Pl})^{1/(n-1)}$. The mass scale at $\phi = \phi_j$ is much smaller than the mass scale at the bottom of the potential $m_\phi \sim \Lambda^2/v_\phi$. Hence the period of the oscillation is mostly determined by this region as

$$t_{j+1} - t_j \sim \sqrt{\frac{1}{\left|V''(\phi_j)\right|}} \sim \frac{1}{m_\phi}\left(\frac{v_\phi}{\phi_J}\right)^{(n-2)/2}. \tag{5.3.6}$$

It is much longer than m_ϕ^{-1}, as clearly seen in the numerical results in the next section. Now we consider the growth of the inflaton particles $\delta\phi_k$ with the momentum k in the linear regime during $t_j < t < t_{j+1}$. We further divide it into three phases: (a) $t_j < t < t_m^-$, (b) $t_m^- < t < t_m^+$, and (c) $t_m^+ < t < t_{j+1}$, where $t_m^\pm$ denotes the time when $\phi = \phi_m$, with ϕ_m being the field value at which V'' takes negative maximum value, or

$$\frac{\phi_m}{v_\phi} = \left(\frac{n-2}{2(2n-1)}\right)^{1/n}. \tag{5.3.7}$$

First, in the stage (a), modes with $k \lesssim m_\phi$ experience tachyonic instability within $\phi_{\rm tac} < \phi < \phi_m$, where

$$\frac{\phi_{\rm tac}}{v_\phi} \simeq \frac{\phi_j}{v_\phi} \times \max\left[1, \left(\frac{k}{k_*}\right)^{\frac{2}{n-2}}\right], \tag{5.3.8}$$

with $k_* \sim m_\phi (j v_\phi/M_{\rm Pl})^{(n-2)/2n}$ being the tahcyonic mass scale at $\phi = \phi_j$. Then $\delta\phi_k$ is enhanced by a factor of e^{X_k} with

$$X_k = \int_{\phi_{\rm tac}}^{\phi_m} \frac{\sqrt{|V''| - k^2}}{\dot{\phi}} d\phi \sim \sqrt{\frac{n(n-1)}{2}} \log\left(\frac{\phi_m}{\phi_{\rm tac}}\right). \tag{5.3.9}$$

Here it should be noticed that the same mode experiences exponential decay in the stage (c) in the limit $k \to 0$.[b8] Thus a phase shift in the stage (b) is crucial to obtain a net growth of the fluctuations. Schematically, the phase of $\delta\phi_k$ is rotated during the stage (b) as

$$\exp\left(i\sqrt{m_\phi^2 + k^2}\,(t_m^+ - t_m^-)\right) \sim e^{i m_\phi t}\left(1 + \frac{ik^2}{m_\phi^2}\right), \tag{5.3.10}$$

[b8] The linearized equation of motion of $\delta\phi_k$ in the limit $k \to 0$ is the same as $\dot{\phi}$ as we said before, and the latter indeed decreases during the stage (c).

where we have used $k \ll m_\phi$ and $t_m^+ - t_m^- \sim m_\phi^{-1}$. Thus the fraction k^2/m_ϕ^2 is connected to the growing mode in the stage (c), and hence the net enhancement factor within one oscillation F_k is estimated as

$$F_k \equiv \left| \frac{\delta\phi_k(t_{j+1})}{\delta\phi_k(t_j)} \right| \sim \left| 1 + \frac{ik^2}{m_\phi^2} e^{2X_k} \right|. \tag{5.3.11}$$

It is peaked at $k \simeq k_*$ as

$$F_{k_*} \sim \left(\frac{m_\phi^2}{k_*^2} \right)^{x_n - 1}, \quad x_n \equiv \frac{\sqrt{2n(n-1)}}{n-2}. \tag{5.3.12}$$

It is much larger than unity, and hence $\delta\phi_{k_*}$ is enhanced by orders of magnitude within one oscillation for $v_\phi \ll M_{\rm Pl}$. The variance of the inflaton after the j-th oscillation is now estimated as

$$\left\langle \delta\phi^2 \right\rangle \sim k_*^2 F_{k_*}^{2j} \sim m_\phi^2 \left(\frac{M_{\rm Pl}}{v_\phi} \right)^{(n-2)(2j(x_n-1)-1)/n}. \tag{5.3.13}$$

It is valid for $x_n > 3/2$ or $n < 27$. It indicates that the fluctuation becomes nonlinear, *i.e.*, $\langle \delta\phi^2 \rangle \sim v_\phi^2$, within several times of oscillation.

In summary, the inflaton sector becomes nonlinear within several times of oscillation due to the tachyonic preheating. To avoid complications arising from the nonlinearity and thermalization, in this dissertation we just require that the EW vacuum remains stable at least until the inflaton fluctuation becomes nonlinear. Otherwise we cannot avoid the catastrophe anyway. Thus, the tachyonic production of the inflaton particles sets the upper limit of the time until which we follow the dynamics in this chapter.

5.3.2 Higgs dynamics during preheating

Now we study the Higgs particle production during the preheating stage. In this subsection, we crudely approximate the inflaton potential as quadratic, although the actual inflaton potential is typically far from quadratic for low-scale inflation models. Nevertheless, it helps us to understand the numerical results at least qualitatively.

The potential of the inflaton and the Higgs at the inflaton oscillation phase is

$$U(\phi, h) = \frac{m_\phi^2}{2}\varphi^2 + \frac{\lambda_{h\phi}}{4}h^4 + \frac{\sigma_{h\phi}}{2}\varphi h^2 + \frac{\lambda_{\phi h}}{2}\varphi^2 h^2. \tag{5.3.14}$$

The inflaton potential is (crudely) approximated as quadratic around the potential minimum. We study resonant Higgs particle production due to the inflaton oscillation in this system. The linearized equation of motion of the Higgs is

$$\ddot{h}_k + \left(k^2 + \sigma_{h\phi}\varphi + \lambda_{h\phi}\varphi^2 \right) h_k = 0. \tag{5.3.15}$$

We have moved to the momentum space with k being the momentum, and ignored the Hubble expansion because of Eq. (5.1.5). The inflaton oscillation is described as

$$\varphi = \varphi_{\rm ini} \cos\left(m_\phi t\right), \tag{5.3.16}$$

under the quadratic approximation. Here $\varphi_{\rm ini}$ is the initial inflaton oscillation amplitude, which is roughly $\varphi_{\rm ini} \sim v_\phi$ (remember that $\varphi \equiv v_\phi - \phi$). By substituting it to Eq. (5.3.15), we obtain the Whittaker-Hill equation:

$$h_k'' + \left[A_k + 2p\cos 2z + 2q\cos 4z\right] h_k = 0, \tag{5.3.17}$$

where

$$A_k \equiv \frac{4k^2}{m_\phi^2} + 2q, \quad p \equiv \frac{2\sigma_{h\phi}\varphi_{\rm ini}}{m_\phi^2}, \quad q \equiv \frac{\lambda_{h\phi}\varphi_{\rm ini}^2}{m_\phi^2}, \quad z \equiv \frac{m_\phi t}{2}, \tag{5.3.18}$$

and the prime denotes the derivative with respect to z. In Fig. 4.9 in Sec. 4.5, we showed the stability/instability charts of the Whittaker-Hill equation. If the parameters are in the instability region (the unshaded region), Eq. (5.3.17) has exponentially growing solutions, resulting in the resonant Higgs production. The resonance parameters p and q are useful for estimating the strength of the resonance even for a potential that is far from quadratic, as in the case of the hilltop potential. In terms of the resonance parameters, the condition

$$p + 2q \geq 0, \tag{5.3.19}$$

is necessary for the Higgs not to be tachyonic during inflation. Although it does not necessarily cause a problem as long as Eq. (5.2.2) is fulfilled, we will assume that Eq. (5.3.19) holds in the following for simplicity.

Once the resonant Higgs production occurs, it forces the EW vacuum to decay into the deeper minimum in the same way as we studied in Chap. 4: the produced Higgs particles induce the following tachyonic mass from the Higgs self-quartic coupling:

$$m_{\rm tac}^2 \simeq 3\lambda_h \langle h^2 \rangle, \tag{5.3.20}$$

where we have used the mean-field approximation. Note that the dispersion is $\langle h^2 \rangle \gtrsim m_\phi^2$ for the resonant particle production, and thus we expect $\lambda_h < 0$ as can be seen from Eqs. (5.1.16) and (5.1.19). Thus we can constrain the resonance parameters, or the couplings, by requiring that the EW vacuum is stable during the preheating. The tachyonic resonance is effective if $|p|$ exceeds of order unity (see Fig. 4.9), so we may require

$$\left|p\right| \lesssim O(1), \tag{5.3.21}$$

for the EW vacuum stability during the preheating. We will confirm this expectation by means of the classical lattice simulation with a full hilltop inflaton potential in the next section. Note that Eq. (5.3.21) implies $|q| \lesssim O(1)$ without any accidental cancellation between $\sigma_{\phi h}$ and $\lambda_{\phi h}$. However, we will also discuss the case $|p| \lesssim O(1)$ and $|q| \gg O(1)$ at the end of the next section for completeness.[b9]

[b9] Note that $q \gtrsim -O(1)$ from Eqs. (5.3.19) and (5.3.21).

d	N_g	L	dt	dk
2+1	2048	$1500 m_\phi^{-1}$	$5 \times 10^{-3} m_\phi^{-1}$	$4.2 \times 10^{-3} m_\phi$

Table 5.1: The parameters of the classical lattice simulation, where d is the spacetime dimension, N_g is the number of grid in each spatial dimension, L is the size of the lattice, dt is the size of the each time step, $dk \equiv 2\pi/L$ is the resolution of the momentum.

5.4 Numerical simulation and constraints on couplings

In this section we perform classical lattice simulations to study the EW vacuum stability during the preheating epoch. Note that the results in this section include effects of the anharmonicity of the inflaton potential as well as the Hubble expansion, although we ignored them in the previous subsection. For concreteness, we take $n = 6$ in the inflaton potential (5.1.3). The CMB normalization implies

$$\left(\frac{\Lambda}{M_{\rm Pl}}\right)^4 \simeq 7 \times 10^{-14} \left(\frac{v_\phi}{M_{\rm Pl}}\right)^3 \left(\frac{N}{60}\right)^{-5/2} . \tag{5.4.1}$$

See App. C.2.3 for more details. For instance, $\Lambda/M_{\rm Pl} \simeq 2 \times 10^{-5}$, $H_{\rm inf} \simeq 4 \times 10^8\,{\rm GeV}$ and $m_\phi \simeq 5 \times 10^{11}\,{\rm GeV}$ for $v_\phi/M_{\rm Pl} = 10^{-2}$, and $\Lambda/M_{\rm Pl} \simeq 3 \times 10^{-6}$, $H_{\rm inf} \simeq 10^7\,{\rm GeV}$ and $m_\phi \simeq 2 \times 10^{11}\,{\rm GeV}$ for $v_\phi/M_{\rm Pl} = 10^{-3}$. Thus the parameters satisfy $H_{\rm inf} \ll M_{\rm inst} < m_\phi$, and hence this model is indeed a good example of our general argument in the previous sections. The condition (5.1.11) is given in terms of p and q as

$$|p| \lesssim \frac{v_\phi}{m_\phi}\left(\frac{v_\phi}{M_{\rm Pl}}\right)^{5/4}, \qquad |q| \lesssim \frac{v_\phi}{m_\phi}\left(\frac{v_\phi}{M_{\rm Pl}}\right)^{5/4} . \tag{5.4.2}$$

For $n = 6$, the right-hand sides are larger than unity for $v_\phi/M_{\rm Pl} \gtrsim 10^{-4}$.

We numerically solved the discretized version of the classical equations of motion derived from Eq. (5.1.1) as well as the Friedmann equations. We start to solve the equations when $\epsilon = 1$. It corresponds to $\varphi_{\rm ini} \simeq 0.74 v_\phi$ for $v_\phi = 10^{-2} M_{\rm Pl}$, and $\varphi_{\rm ini} \simeq 0.84 v_\phi$ for $v_\phi = 10^{-3} M_{\rm Pl}$. We took the initial velocity of the inflaton as zero. We also introduced initial Gaussian fluctuations that mimic the quantum fluctuations for the inflaton and the Higgs. We have assumed that they are in the vacuum state initially. This is justified for $v_\phi/M_{\rm Pl} \gtrsim 10^{-6}$-$10^{-5}$ since we can safely neglect inflaton particle production at the first stage in this case as discussed in Sec. 5.3.1. We have also added h^6 term in the Higgs potential just for numerical convergence. We have checked that it does not modify the dynamics before the EW vacuum decay. The parameters of our lattice simulations are summarized in Tab. 5.1. Since we have two different momentum scales (k_* and m_ϕ), we must take the number of grids N_g to be large. This is why we took the spatial dimension to be two instead of three (see Tab. 5.1). As far as the linear regime is concerned, the results are not expected to change drastically for different numbers of spatial dimensions. For more details, see App. E.3.

We show our numerical results for $v_\phi = 10^{-2} M_{\rm Pl}$ and $v_\phi = 10^{-3} M_{\rm Pl}$ in Figs. 5.1 and 5.2, respectively. We have followed the dynamics until $m_\phi t = 150$ and 250 for $v_\phi = 10^{-2} M_{\rm Pl}$ and

$10^{-3}M_{\rm Pl}$, respectively, since the inflaton condensation is broken slightly before these times. The black line is $\langle\varphi\rangle^2$, the red line is $\langle\varphi^2\rangle - \langle\varphi\rangle^2$, and the blue line is $\langle h^2\rangle$, where the angle brackets denote the spatial average. They are normalized by $\varphi_{\rm ini}$. The values of p and q are written at the tops of these figures.

In the upper panels in Figs. 5.1 and 5.2, $p \gtrsim O(1)$ and both $q > 0$ and $q < 0$ cases are considered. As we can see, the EW vacuum is actually destabilized during the preheating for these cases. On the other hand, we have taken $p = q \lesssim O(1)$ in the lower left panels in Figs. 5.1 and 5.2. In these cases, the EW vacuum survives the preheating. Thus the numerical results are consistent with our expectation in Sec. 5.3.2:

$$|p| = \frac{2\sigma_{h\phi}\varphi_{\rm ini}}{m_\phi^2} \lesssim O(1), \tag{5.4.3}$$

is required for the stability of the EW vacuum during the preheating. We have checked that this criterion is indeed satisfied for several other values of p and q. In particular, we have also calculated the case $p < 0$. In this case, the Higgs becomes tachyonic in the region $\varphi > 0$, where it takes more time for the inflaton to oscillate. Hence the Higgs is more likely to be enhanced and the EW vacuum decays faster compared to the case $p > 0$.[þ10] In any case, the EW vacuum is stable during the preheating as long as Eq. (5.4.3) holds and $|q| \sim |p|$. The bound (5.4.3) does not strongly depend on v_ϕ since it is expressed solely by the resonance parameters. It is consistent with the numerical results with two different values of v_ϕ.

Eq. (5.4.3) is our main result in this chapter, and it also implies $|q| \lesssim O(1)$ if there is no tuning of the parameters. Still, we have also considered the case $|p| \ll q$ for completeness. Note again that an accidental cancellation between $\sigma_{h\phi}$ and $\lambda_{h\phi}$ is necessary to achieve $q \gg O(1)$ while satisfying Eq. (5.4.3) (see the footnote þ9). In this case, the situation is more complicated. When the broad resonance is dominant, the condition for the EW vacuum destabilization is estimated as

$$|\lambda_h| \left\langle h^2 \right\rangle \gtrsim p_*^2, \tag{5.4.4}$$

where $p_* \equiv m_\phi q^{1/4}$ as we discussed in Sec. 4.2. The growth factor $\mu_{\rm qtc}$ depends little on q for the parametric resonance, and hence the value of q is not so important in this condition. As a result, it is likely that the EW vacuum does not decay during the linear regime even if we take q to be larger, since we have restricted the number of times of the inflaton oscillations in our analysis (only several times) to avoid complications associated with the nonlinear behavior of the inflaton. However, as the inflaton fluctuations grow and become nonlinear, they can also produce the Higgs particles through the scatterings. It corresponds to the beginning of the thermalization, which is studied in detail in, *e.g.*, Ref. [64]. In this regime, the variances of the inflaton and the Higgs tend to converge to a similar value though the scattering. Therefore, as q (or $\lambda_{h\phi}$) becomes larger, $\langle h^2\rangle$ approaches to $\langle\varphi^2\rangle$ faster. In the present case, it might destabilize the EW vacuum since $|\lambda_h| \gg \lambda_{h\phi}$. Actually, in the lower right panels in Figs. 5.1 and 5.2, the EW vacuum is destabilized at almost the same time as

[þ10] Note that p necessarily dominates over q as the inflaton approaches to the minimum of its potential.

the system becomes nonlinear for $q \gtrsim O(10)$. Thus, it might be expected that

$$q = \frac{\lambda_{h\phi}\varphi_{\rm ini}^2}{m_\phi^2} \lesssim O(10) \quad \text{if} \quad \left|p\right| \lesssim O(1), \tag{5.4.5}$$

is at least necessary for the stability of the EW vacuum during and also after the preheating. Eqs. (5.4.3) and (5.4.5) are translated to upper bounds on $\lambda_{h\phi}$ and $\sigma_{h\phi}$ as

$$\left|\sigma_{h\phi}\right| \lesssim 10^8\,{\rm GeV}\left(\frac{m_\phi}{10^{12}\,{\rm GeV}}\right)^2\left(\frac{10^{16}\,{\rm GeV}}{\varphi_{\rm ini}}\right), \tag{5.4.6}$$

$$\left|\lambda_{h\phi}\right| \lesssim 10^{-7}\left(\frac{m_\phi}{10^{12}\,{\rm GeV}}\right)^2\left(\frac{10^{16}\,{\rm GeV}}{\varphi_{\rm ini}}\right)^2. \tag{5.4.7}$$

Note that the initial inflaton amplitude $\varphi_{\rm ini}$ is of order the inflaton VEV v_ϕ.

If we follow the thermalization process for a longer time, the constraints probably become tighter than Eqs. (5.4.3) and (5.4.5). In this sense, Eqs. (5.4.3) and (5.4.5) are just necessary conditions, and we must also follow the dynamics after the preheating to determine an ultimate fate of the EW vacuum. In order to address this issue, however, we should take into account the couplings between Higgs and the SM particles, which might stabilize the EW vacuum. It seems interesting to study further on this direction although it is more complicated.

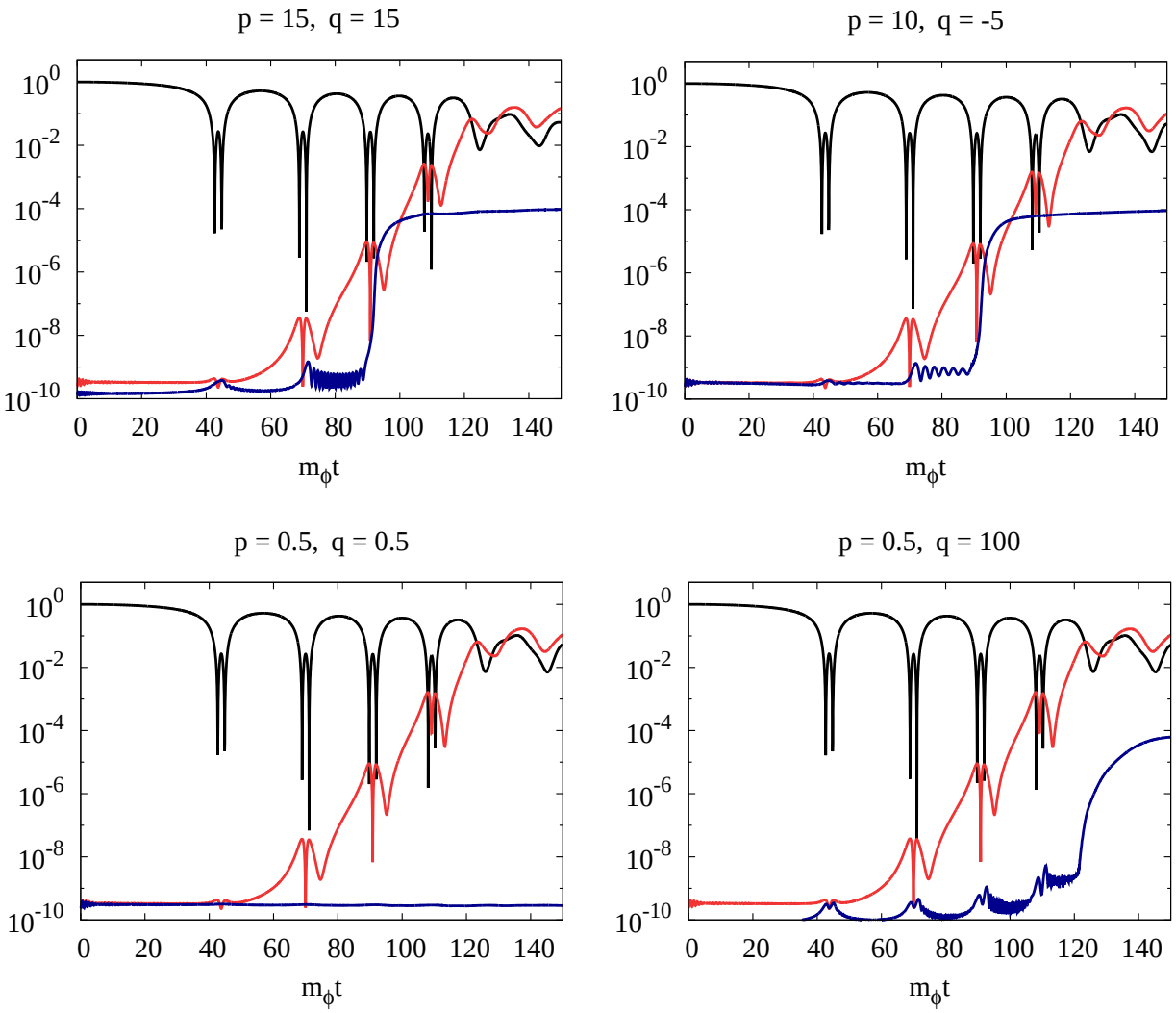

Figure 5.1: The time evolution of the inflaton and the Higgs for $v_\phi = 10^{-2} M_{\rm Pl}$ up to $m_\phi t = 150$. The black line is the inflaton condensation $\langle\varphi\rangle^2$, the red line is the inflaton two point function $\langle\varphi^2\rangle - \langle\varphi\rangle^2$ and the blue line is the Higgs two point function $\langle h^2\rangle$, where the angle brackets denote the spatial average. They are normalized by the initial inflaton amplitude $\varphi_{\rm ini}$. The EW vacuum is stable for $(p, q) = (0.5, 0.5)$, while it is destabilized during the preheating for the other cases. The lower right panel corresponds to the case with an accidental cancellation between $\sigma_{h\phi}$ and $\lambda_{h\phi}$.

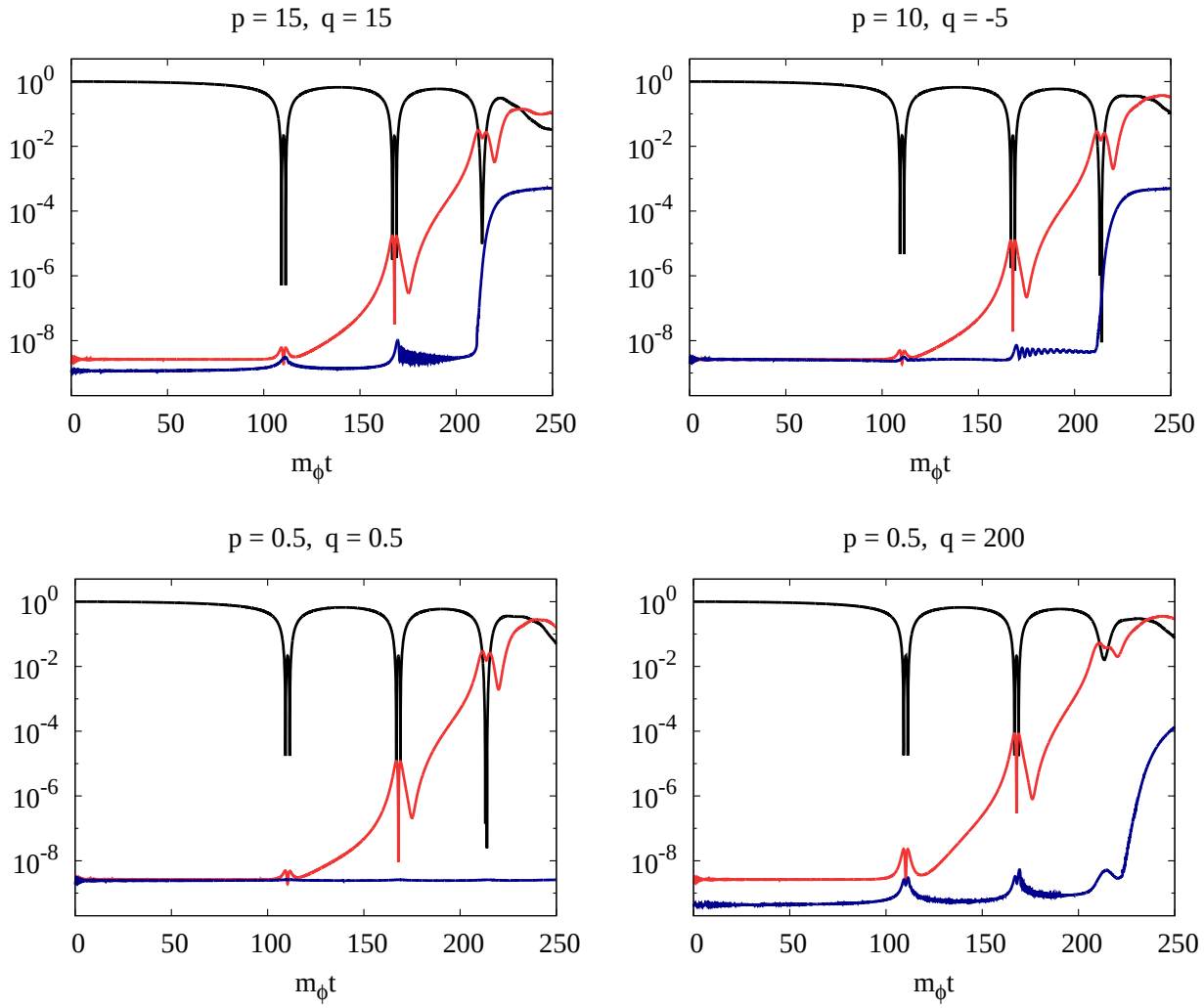

Figure 5.2: The time evolution of the inflaton and Higgs for $v_\phi = 10^{-3} M_{\rm Pl}$ up to $m_\phi t = 250$. The black line is the inflaton condensation $\langle\varphi\rangle^2$, the red line is the inflaton two point function $\langle\varphi^2\rangle - \langle\varphi\rangle^2$ and the blue line is the Higgs two point function $\langle h^2\rangle$, where the angle brackets denote the spatial average. They are normalized by the initial inflaton amplitude $\varphi_{\rm ini}$. The EW vacuum is stable for $(p, q) = (0.5, 0.5)$, while it is destabilized during the preheating for the other cases. The lower right panel corresponds to the case with an accidental cancellation between $\sigma_{h\phi}$ and $\lambda_{h\phi}$.

Chapter 6

Summary and future directions

In this dissertation, we have investigated the cosmological implications of the EW vacuum metastability in the context of the inflationary cosmology. According to the current measurement of the SM parameters, the Higgs potential may develop a true minimum deeper than the EW vacuum, called the EW vacuum metastability. It has interesting consequences on the cosmology, especially in its early stage. In this dissertation, we pay special attention to the Higgs-inflaton dynamics during the inflaton oscillation epoch after inflation. If there are sizable couplings between the inflaton/gravity sector and the Higgs sector, resonant Higgs particle production occurs during the inflaton oscillation epoch, which we call the preheating. The typical energy scale of this process is the inflaton mass scale. Hence, as long as the inflaton mass scale is higher than the instability scale of the Higgs potential, the produced Higgs particles may push the Higgs itself to roll down to the true minimum due to the finite density effect. We have specified the parameter region where the EW vacuum destabilization indeed happens during the preheating epoch for both high-scale and low-scale inflation models. See Eqs. (4.2.17), (4.3.14), (4.5.3), (5.3.21), and Figs. 4.1, 4.3, 4.8, 4.10, 5.1, 5.2.

As concluding remarks, we list some possible future directions here. First of all, it is definitely interesting to implement the SM gauge bosons to the classical lattice simulation as well. The SM Higgs inevitably couples to the gauge bosons, and hence they are expected to be produced during the preheating epoch at least to some amount. We have imitated their effects by introducing a light scalar field χ in Sec. 4.6, and found that its effect is rather minor. However, it is of course just an approximation, and it is mandatory to include the gauge bosons without any approximation in order to judge whether it is truly ineffective or not. Such a study is partly done by Ref. [51] that supports our argument that the effect is minor, but the authors considered the case with only the non-minimal coupling ξ_h. As we saw in Sec. 4.2, it takes more time for the EW vacuum to be destabilized for the case with the quartic coupling $\lambda_{h\phi}$. Hence the gauge bosons may have larger impacts on the case with $\lambda_{h\phi}$. It is still worth investigating further on this direction.

Another direction may be to investigate the inflationary model dependence of our results. In Chaps. 4 and 5, we take the quadratic and the hill-top type potentials as examples, but it is interesting to see how results change quantitatively or even qualitatively once we consider different types of the inflaton potential. One example may be to consider the inflation model with the non-minimal coupling to the gravity [65,66], or the R^2-type inflation models [67–70].

For these models, once we move to the Einstein frame, the inflaton has interaction with the Higgs that is not described by Eq. (1.1.1) we have considered in this thesis. Another example may be to consider the quartic inflaton potential instead of the quadratic one. In this case the system has classical scale invariance. Hence the Hubble expansion does not kill the resonance since the scale factor decouples from the equation of motion by redefining the inflaton and the Higgs fields properly [71]. The resonance is terminated only by the backreaction, and such a situation is quite dangerous for the EW vacuum. This is because the absolute value of the Higgs quartic coupling is typically larger than the Higgs-inflaton coupling and the inflaton quartic self coupling.

Finally, we comment on the EW vacuum stability *after* the preheating epoch. We have discussed the EW vacuum stability during the inflationary and the preheating epoch, but the Higgs dynamics after the preheating could be quite non-trivial as well. The EW vacuum is likely to be stable once the system is in thermal equilibrium [23, 72]. However, it is still non-trivial under what condition the EW vacuum is stable from the end of the preheating to the end of thermalization. The Higgs momentum distribution at the end of the preheating is far from thermal equilibrium, and it evolves due to the scatterings towards thermal equilibrium. It is possible that the EW vacuum decay is activated during this thermalization process depending on the detailed shape of the momentum distribution. For instance, if the Higgs fluctuations are larger than the other SM particles at some time, the EW vacuum decay can be enhanced. The resonant Higgs production may be viewed as an extreme example of this case. This issue is worth investigating in detail since it determines an ultimate fate of the EW vacuum. Thus, we still have a lot to do to completely understand the cosmological implications of the EW vacuum metastability.

Acknowledgement

First of all, I would like to thank my supervisor, Takeo Moroi, who provided stimulating discussions, helpful comments, fruitful suggestions.

I would also like to appreciate my collaborators Kazunori Nakayama, Kyohei Mukaida, Mindaugas Karčiauskas, Oleg Lebedev and Marco Zatta, without whom this work would never complete.

I am grateful to all the members of the particle physics group at the University of Tokyo. It was truly exciting and stimulating to discuss physics as well as other things with them.

I am also grateful to all the members of the theoretical high energy physics group at the University of Helsinki and the theoretical physics group at the Imperial College London for their hospitality during my stay.

Last but not least, I would like to express my gratitude to my family and friends for their continuous support, and to the bouldering wall in the Gotenshita Memorial Arena.

Appendix A

Notations and conventions

In this appendix we summarize the notations and conventions used in this dissertation.

A.1 Unit

In this dissertation we take the natural unit where the speed of light c, the reduced Planck constant $\hbar$ and the Boltzmann constant k_B are all taken to be unity: $c = \hbar = k_B = 1$. We retain the Planck mass explicitly. We denote the reduced Planck mass as $M_{\rm Pl}$.

A.2 Metric

We take the almost-plus convention for the metric in this dissertation. Thus the metric in the Minkowski space is given by

$$\eta_{\mu\nu} = \mathrm{diag}\,(-1, 1, 1, 1)\,, \tag{A.2.1}$$

while that in the Friedmann-Lemaître-Robertson-Walker (FLRW) space is given by

$$g_{\mu\nu} = \mathrm{diag}\left(-1, a^2, a^2, a^2\right), \tag{A.2.2}$$

where a is the scale factor of the universe. We denote the Hubble parameter as $H \equiv \dot{a}/a$, where the dot denotes the derivative with respect to time.

A.3 Clifford algebra

We define the gamma matrices as

$$\{\gamma^\mu, \gamma^\nu\} = -2\eta^{\mu\nu}, \tag{A.3.1}$$

where $\{...\}$ denotes the anti-commutator. Thus, with our almost-plus convention of $\eta^{\mu\nu}$, γ^0 is hermitian while γ^i is anti-hermitian. In this convention, in particular, we obtain

$$\not{a}\not{b} = -a \cdot b, \tag{A.3.2}$$

where the slashed variables are contracted with γ^μ. This convention is the same as Refs. [73, 74], and opposite to Ref. [75]. Indeed, we can easily go back and forth between our convention and that in Refs. [73, 74] just by changing the sign in front of quantities contracted by $\eta^{\mu\nu}$, such as p^2 with p^μ being the four-momentum. Note that a factor of i difference often appears in literature due to these differences. We define γ_5 as

$$\gamma_5 \equiv i\gamma^0\gamma^1\gamma^2\gamma^3. \tag{A.3.3}$$

It anti-commutes with γ^μ, and is hermitian. The projection operators to the left-handed and right-handed components are respectively defined as

$$P_L \equiv \frac{1-\gamma_5}{2}, \quad P_R \equiv \frac{1+\gamma_5}{2}. \tag{A.3.4}$$

We define the Dirac conjugate as

$$\bar{\psi} \equiv \psi^\dagger\gamma^0. \tag{A.3.5}$$

It is again the same as Refs. [73, 74], and different by a factor of i from Ref. [75]. The latter difference is because our γ^0 is hermitian while their γ^0 is anti-hermitian due to the different conventions of the Clifford algebra.

A.4 Couplings and fields

Here we summarize the notations for the couplings and fields used in this dissertation. The U(1), SU(2) and SU(3) SM gauge couplings are g', g and g_s, respectively. The top Yukawa coupling is y_t, and the Higgs quartic self coupling is λ_h. The Higgs-inflaton quartic and trilinear couplings are $\lambda_{h\phi}$ and $\sigma_{h\phi}$, respectively. The Higgs-curvature non-minimal coupling is ξ_h. The Higgs SU(2) doublet is decomposed as

$$H = \frac{1}{\sqrt{2}}\begin{pmatrix} \varphi_+ \\ h + i\varphi_Z \end{pmatrix}. \tag{A.4.1}$$

We also use h to denote the radial component of the Higgs field. We use ϕ as the inflaton. The inflaton mass is denoted as m_ϕ. We often denote a light scalar field other than the inflaton and the Higgs as χ.

Appendix B

More on EW vacuum metastability

In this appendix we derive the one-loop beta functions and anomalous dimensions within the SM. We also derive the 1-loop Higgs effective potential.

B.1 One-loop contributions

Here we give formulae of the scalar, fermion and gauge/Goldstone bosons' one-loop contributions to the effective potential.

B.1.1 Scalar

We start with a scalar field contribution. Suppose that the Lagrangian for the scalar fluctuation is given by

$$\mathcal{L}_s = \frac{1}{2}\chi\left(\Box - m_s^2(h)\right)\chi, \tag{B.1.1}$$

where the mass term m_s depends on the background Higgs field value h. Then the Gaussian integration is performed as

$$\begin{aligned}\int \mathcal{D}\chi \exp\left[i\int d^4x \mathcal{L}_x\right] &\propto \left[\mathrm{Det}\left(\Box - m_s^2\right)\right]^{-1/2} \\ &\propto \exp\left[-\frac{1}{2}\int \frac{d^4x d^4k}{(2\pi)^4}\ln\left(1+\frac{m_s^2}{k^2}\right)\right],\end{aligned} \tag{B.1.2}$$

where we have not cared the overall constant, and used the relation $\mathrm{Tr}\ln = \ln\mathrm{Det}$. Thus, the scalar one-loop contribution is

$$V_s = -\frac{i}{2}\int \frac{d^4k}{(2\pi)^4}\ln\left(1+\frac{m_s^2}{k^2}\right) = \frac{1}{2}\int \frac{d^4k_E}{(2\pi)^4}\ln\left(1+\frac{m_s^2}{k_E^2}\right), \tag{B.1.3}$$

where we have performed the Wick rotation with $k_E^0 \equiv -ik^0$ in the second line. It is divergent, and hence we need to regularize it. Here we just use the hard cut-off regularization, and then the effective potential is given by

$$V_s = \frac{1}{16\pi^2}\int_0^\Lambda dk_E k_E^3 \ln\left(1+\frac{m_s^2}{k_E^2}\right). \tag{B.1.4}$$

The integration is performed as

$$\begin{aligned}\int_0^\Lambda dk_E k_E^3 \ln\left(1+\frac{m_s^2}{k_E^2}\right) &= \frac{\Lambda^4}{2}\int_0^1 dx\, x\left[\ln\left(x+\frac{m_s^2}{\Lambda^2}\right)-\ln x\right] \\ &= \frac{\Lambda^4}{2}\left[\frac{m_s^2}{\Lambda^2}+\frac{1}{2}\left(\ln\left(\frac{m_s^2}{\Lambda^2}-\frac{1}{2}\right)-\frac{1}{2}\right)\frac{m_s^4}{\Lambda^4}+O\left(\frac{m_s^6}{\Lambda^6}\right)\right],\end{aligned} \tag{B.1.5}$$

and hence the scalar contribution before renormalization is given by

$$V_s = \frac{\Lambda^2}{32\pi^2}m_s^2 + \frac{m_s^4}{64\pi^2}\left[\ln\left(\frac{m_s^2}{\Lambda^2}\right)-\frac{1}{2}\right]. \tag{B.1.6}$$

After the renormalization, the quadratic divergent term is subtracted, while Λ in the logarithmic is replaced by the renormalization scale M.

B.1.2 Fermion

Next we consider a fermion contribution. Suppose that the Lagrangian is given by

$$\mathcal{L}_f = \bar{\psi}\left[i\partial\!\!\!/ - m_f(h)\right]\psi, \tag{B.1.7}$$

where ψ is the Dirac field. The mass $m_f(h)$ is assumed to be dependent on the Higgs field value h. Then the integration for the Grassmannian variables is performed as

$$\begin{aligned}\int \mathcal{D}\bar{\psi}\mathcal{D}\psi \exp\left[i\int d^4x\mathcal{L}_f\right] &\propto \mathrm{Det}\left[i\partial\!\!\!/ - m_f\right] \\ &\propto \exp\left[\mathrm{Tr}\int\frac{d^4xd^4k}{(2\pi)^4}\ln\left(k\!\!\!/ - m_f\right)\right],\end{aligned} \tag{B.1.8}$$

where the trace in the last line is taken over the spinor indices. Here it is useful to note that

$$\int d^4k \ln\left(k\!\!\!/ - m_f\right) = \int d^4k \ln\left(-k\!\!\!/ - m_f\right), \tag{B.1.9}$$

since they are connected by the change of the integration variable, and hence we obtain

$$\begin{aligned}\int d^4k \ln\left(k\!\!\!/ - m_f\right) &= \frac{1}{2}\int d^4k\left[\ln\left(k\!\!\!/ - m_f\right)+\ln\left(-k\!\!\!/ - m_f\right)\right] \\ &= \frac{1}{2}\int d^4k \ln\left(1+\frac{m_f^2}{k^2}\right) + \text{(const.)}.\end{aligned} \tag{B.1.10}$$

Then, the fermion contribution to the effective potential before renormalization is obtained in the same as the scalar one, and the result is

$$V_f = -\frac{\Lambda^2}{8\pi^2} m_f^2 - \frac{m_f^4}{16\pi^2}\left[\ln\left(\frac{m_f^2}{\Lambda^2}\right) - \frac{1}{2}\right], \tag{B.1.11}$$

where the factor 4 difference comes from the fact that the Dirac field has 4 components. We should multiply instead 2 in the case of a Weyl/Majorana fermion. Note that the overall sign is opposite to the scalar case due to the Grassmannian (or fermionic) nature of the field.

B.1.3 Gauge/Goldstone bosons

Finally we discuss the gauge/Goldstone boson contributions. We shall work with the Landau gauge in this subsection and also the next section. Here we consider the abelian Higgs model for simplicity, but it is straightforward to extend the discussion to the electroweak SU(2)×U(1) case. Thus we assume that the Lagrangian is given by

$$\mathcal{L}_{A+H} = -D_\mu H^* D^\mu H - \frac{1}{4} F^{\mu\nu} F_{\mu\nu} - m_h^2 |H|^2 - \lambda_h |H|^4 , \tag{B.1.12}$$

where the covariant derivative and the field strength are respectively given as

$$D_\mu H = \left(\partial_\mu - ieA_\mu\right) H \quad \text{and} \quad F_{\mu\nu} = \partial_\mu A_\nu - \partial_\nu A_\mu. \tag{B.1.13}$$

We expand the Higgs field as

$$H = \frac{h + \chi + i\varphi}{\sqrt{2}}, \tag{B.1.14}$$

where h is the background Higgs field value, χ is the Higgs fluctuation and φ is the (would-be) Goldstone boson. Then the Higgs kinetic term is given as

$$-D_\mu H^* D^\mu H \simeq -\frac{1}{2}\left[\partial_\mu \chi \partial^\mu \chi + \partial_\mu \varphi \partial^\mu \varphi + e^2 h^2 A_\mu A^\mu\right] + ehA_\mu \partial^\mu \varphi, \tag{B.1.15}$$

up to quadratic in the fields. We choose the R_ξ-gauge, where the gauge fixing term is given by

$$\mathcal{L}_{\rm GF} = -\frac{1}{2\xi}\left(\partial^\mu A_\mu + ev\varphi\right)^2 , \tag{B.1.16}$$

with ξ and v being a gauge fixing parameter. Note that the Lagrangian should be defined before introducing the external classical field h, and hence it may be inconsistent to take $v = \xi h$. In this gauge, there is generally a kinetic mixing between the divergence part of the gauge boson and φ except the Landau gauge where $v = 0$ and $\xi \to 0$. For this reason,

we work with the Landau gauge in the following. Then the quadratic Lagrangian for the gauge/Goldstone bosons is given by

$$\begin{aligned}\mathcal{L}_{A+H} + \mathcal{L}_{\rm GF} =& \frac{1}{2}\chi\left(\Box - m_\chi^2(h)\right)\chi + \frac{1}{2}\varphi\left(\Box - m_\varphi^2(h)\right)\varphi \\ &+ \frac{1}{2}A_\mu\left(\eta^{\mu\nu}\,\Box - \left(1-\frac{1}{\xi}\right)\partial^\mu\partial^\nu - \eta^{\mu\nu}m_A^2(h)\right)A_\nu,\end{aligned} \tag{B.1.17}$$

where the mass terms are respectively given by

$$m_\chi^2 = 3\lambda_h h^2 + m_h^2, \quad m_\varphi^2 = \lambda_h h^2 + m_h^2, \quad m_A^2 = e^2h^2. \tag{B.1.18}$$

Note that we have ignored the term linear in χ since it is cancelled with the source term. The contributions from χ and φ can be computed by using the result in App. B.1.1. The coefficient of the kinetic term of the gauge boson in the momentum space is given by

$$-\eta^{\mu\nu}\left(k^2 + m_A^2\right) + \left(1-\frac{1}{\xi}\right)k^\mu k^\nu = -\left(\eta^{\mu\nu} - \frac{k^\mu k^\nu}{k^2}\right)\left(k^2 + m_A^2\right) - \frac{1}{\xi}\frac{k^\mu k^\nu}{k^2}\left(k^2 + \xi m_A^2\right), \tag{B.1.19}$$

where the latter part corresponds to the mode $A_\mu \propto \partial_\mu\theta$. It decouples in the Landau gauge with $\xi \to 0$, and thus we need to consider only the contribution from the former part. Hence we obtain the effective potential as

$$V_{A+H} = \frac{1}{2}\int\frac{d^4k}{(2\pi)^4}\left[\mathrm{Tr}\ln\left(\left(\eta^{\mu\nu} - \frac{k^\mu k^\nu}{k^2}\right)\left(1 + \frac{m_A^2}{k^2}\right)\right) + \ln\left(1 + \frac{m_\chi^2}{k^2}\right) + \ln\left(1 + \frac{m_\varphi^2}{k^2}\right)\right]. \tag{B.1.20}$$

Note that

$$\mathrm{Tr}\ln\left(\left(\eta^{\mu\nu} - \frac{k^\mu k^\nu}{k^2}\right)\left(1 + \frac{m_A^2}{k^2}\right)\right) = \eta_{\mu\nu}\left(\eta^{\mu\nu} - \frac{k^\mu k^\nu}{k^2}\right)\ln\left(1 + \frac{m_A^2}{k^2}\right) = 3\ln\left(1 + \frac{m_A^2}{k^2}\right), \tag{B.1.21}$$

where we have used the fact that $\eta^{\mu\nu} - k^\mu k^\nu/k^2$ is a projection operator. Hence we obtain

$$\begin{aligned}V_{A+H} =& \frac{\Lambda^2}{32\pi^2}\left(3m_A^2 + m_\varphi^2 + m_\chi^2\right) \\ &+ \frac{1}{64\pi^2}\left[3m_A^4\left(\ln\left(\frac{m_A^2}{\Lambda^2}\right) - \frac{1}{2}\right) + m_\chi^4\left(\ln\left(\frac{m_\chi^2}{\Lambda^2}\right) - \frac{1}{2}\right) + m_\varphi^4\left(\ln\left(\frac{m_\varphi^2}{\Lambda^2}\right) - \frac{1}{2}\right)\right]\end{aligned} \tag{B.1.22}$$

before renormalization, where the mass terms are given in Eq. (B.1.18). In general we should also consider the ghost sector, but in the Landau gauge it decouples from the scalar sector at least at the one-loop level, and hence we do not discuss it here.

B.2 RG evolutions of SM parameters

In this section we derive one-loop renormalization group equations of the SM parameters. We work in the Landau gauge with the dimensional regularization and the $\overline{\rm MS}$ scheme in this section, but the results do not change in other gauge/scheme at least up to the 1-loop level, as we discuss at the end of this section. The resultant one-loop RG running of the SM parameters are shown in Fig. B.1.

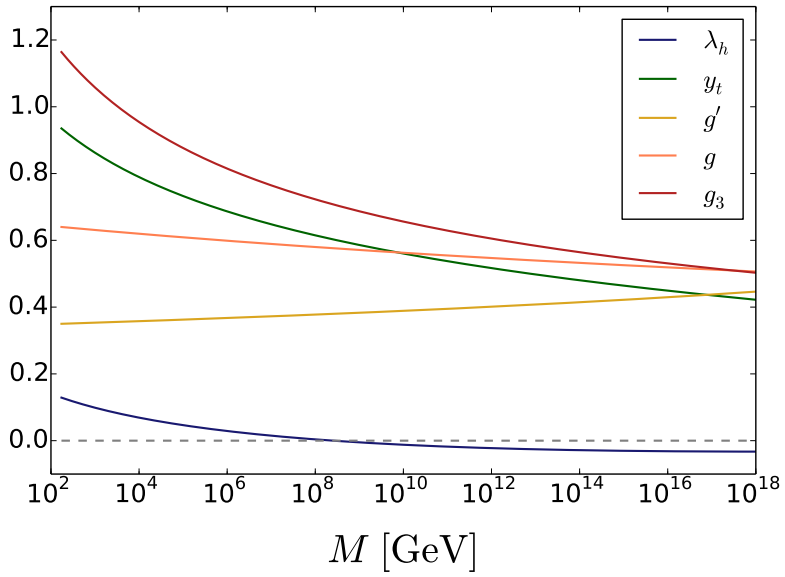

Figure B.1: The RG evolution of the SM parameters within the one-loop beta functions. We have used Eqs. (B.2.39), (B.2.48) and (B.2.49) with $m_h = 125\,\text{GeV}$, $m_t = 173.1\,\text{GeV}$, $g'(M = m_t) = 0.35$, $g(M = m_t) = 0.64$ and $g_3(M = m_t) = 1.16$. Note that g_1 and g_2 often used in literature are related to g' and g as $g_1 = \sqrt{5/3}g'$ and $g_2 = g$.

B.2.1 Anomalous dimensions

First we compute the anomalous dimensions of the Higgs and the top quark. In order to obtain the anomalous dimensions, we fix divergent parts of the wave function renormalization, and hence we concentrate on the divergent parts of the two point functions that depend on external momenta. For this reason, we only need to consider diagrams whose superficial degrees of divergence are two, since the degree of divergence of the momentum dependent parts should be lower than the leading part by two.

■ Higgs

Here we compute the anomalous dimension of the Higgs field. The relevant diagrams are shown in Fig. B.2. We first consider the scalar contribution, whose diagrams are given in (a) and (b) in Fig. B.2. They actually do not contribute to the anomalous dimension, since the superficial degree of divergence of (a) is zero, while the loop integral of (b) does not depend on the external momentum.

Next we consider the top quark contribution whose diagram is given in (c) in Fig. B.2. It is given as

$$\begin{aligned}(\text{c}) &= -N_c\left(\frac{iy_t}{\sqrt{2}}\right)^2\int\frac{d^4q}{(2\pi)^4}\text{Tr}\left[\frac{i\not{q}}{-q^2+i\delta}\frac{i\left(\not{q}-\not{p}\right)}{-(q-p)^2+i\delta}\right]\\ &= 2N_c y_t^2\int\frac{d^4q}{(2\pi)^4}\frac{q\cdot(q-p)}{(-q^2+i\epsilon)\left(-(q-p)^2+i\delta\right)}\end{aligned}\tag{B.2.1}$$

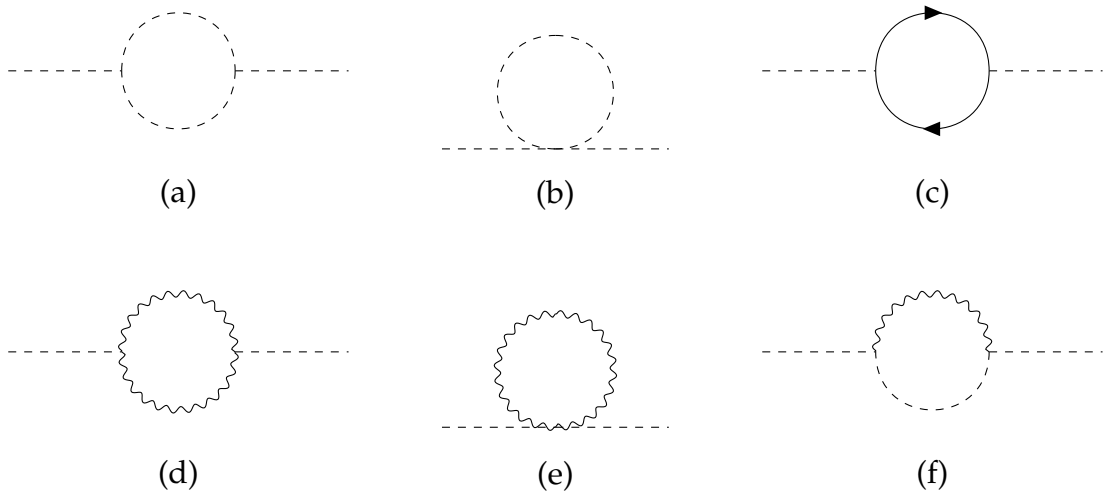

Figure B.2: The diagrams that may contribute to the Higgs anomalous dimension at the one-loop level. The dashed line is the Higgs and the would-be Goldstone bosons, the solid line is the top quark and the wavy line is the gauge boson, respectively. The Feynman diagrams here and below are produced by `TikZ-Feynman` [76].

where the minus sign comes from the fermion loop and $N_c = 3$ is the color degree of freedom. Here we ignored the top quark mass since it is irrelevant for the anomalous dimension. By using the relation

$$\frac{1}{AB} = \int_0^1 dx \frac{1}{[A + (B - A)\, x]^2}, \tag{B.2.2}$$

we obtain

$$\begin{aligned}
\text{(c)} &= 2N_c y_t^2 \int_0^1 dx \int \frac{d^4q}{(2\pi)^4} \frac{q \cdot (q - p)}{\left(-(q - xp)^2 - \Delta + i\delta\right)^2} \\
&= 2N_c y_t^2 M^{4-d} \int_0^1 dx \int \frac{d^dq}{(2\pi)^d} \frac{q^2 - \Delta}{(-q^2 - \Delta + i\delta)^2} \quad \text{with} \quad \Delta \equiv x(1 - x)p^2,
\end{aligned} \tag{B.2.3}$$

where we have dropped odd parts in q since they vanish after integration, and used the dimensional regularization with the dimensionful parameter M being introduced to make the total mass dimension intact. The d-dimensional integrations are given by

$$\int \frac{d^dq}{(2\pi)^d} \frac{1}{(-q^2 - \Delta + i\delta)^2} = \frac{i}{(4\pi)^{d/2}} \frac{1}{\Delta^{2-d/2}} \Gamma\left(2 - \frac{d}{2}\right), \tag{B.2.4}$$

$$\int \frac{d^dq}{(2\pi)^d} \frac{q^2}{(-q^2 - \Delta + i\delta)^2} = \frac{d}{2} \frac{i}{(4\pi)^{d/2}} \frac{1}{\Delta^{1-d/2}} \Gamma\left(1 - \frac{d}{2}\right), \tag{B.2.5}$$

and hence the integration is easily performed to give

$$\text{(c)} = -\frac{4i}{(4\pi)^{d/2}} \left(\frac{d - 1}{d - 2}\right) N_c y_t^2 M^{4-d} \Gamma\left(2 - \frac{d}{2}\right) \int_0^1 dx \Delta^{d/2-1}. \tag{B.2.6}$$

We now take $d = 4 - \epsilon$ and treat ϵ as small. Then the divergence appears as a pole in ϵ:

$$(\mathrm{c})_{\mathrm{div.}} = -\frac{iN_c y_t^2}{8\pi^2}\frac{p^2}{\epsilon}. \tag{B.2.7}$$

Finally we consider the gauge/Goldstone boson contributions, whose diagrams are given by (d), (e) and (f) in Fig. B.2. Actually we need to care only (f), since the superficial degree of divergence of (d) is just zero while the loop integrand of (e) does not depend on the external momentum. Note that the interaction in (f) includes derivatives that make the superficial degree of divergence higher. We first compute the kinetic part of (f), and then sum up the result over the possible couplings. It is given by

$$(\mathrm{f})_{\mathrm{kin.}} = \int \frac{d^4q}{(2\pi)^4}(q-2p)_\mu(-q+2p)_\nu \frac{i}{-q^2+i\delta}\left(\eta^{\mu\nu} - \frac{q^\mu q^\nu}{q^2}\right)\frac{i}{-(q-p)^2+i\delta} \tag{B.2.8}$$

$$= -\int \frac{d^4q}{(2\pi)^4}\frac{q^2(q-2p)^2 - (q\cdot(q-2p))^2}{(-q^2+i\delta)^2\left(-(q-p)^2+i\delta\right)}. \tag{B.2.9}$$

By using the relation

$$\frac{1}{A^2B} = \int_0^1 dx \frac{2(1-x)}{[A+x(B-A)]^3}, \tag{B.2.10}$$

it is rewritten as

$$(\mathrm{f})_{\mathrm{kin.}} = -\int_0^1 dx \int \frac{d^4q}{(2\pi)^4}\frac{8(1-x)\left(p^2q^2 - (p\cdot q)^2\right)}{[-q^2-\Delta+i\delta]^3}. \tag{B.2.11}$$

We can replace $(p\cdot q)^2 \to p^2q^2/4$ inside the integration due to the Lorentz symmetry, and hence we obtain

$$(\mathrm{f})_{\mathrm{kin.}} = -6\int_0^1 dx\,(1-x)\,p^2M^{4-d}\int \frac{d^dq}{(2\pi)^d}\frac{q^2}{[-q^2-\Delta+i\delta]^3}, \tag{B.2.12}$$

where we have used the dimensional regularization. The relevant integration is given by

$$\int \frac{d^dq}{(2\pi)^d}\frac{q^2}{[-q^2-\Delta+i\delta]^3} = -\frac{d}{4}\frac{i}{(4\pi)^{d/2}}\frac{1}{\Delta^{2-d/2}}\Gamma\left(2-\frac{d}{2}\right), \tag{B.2.13}$$

and hence it is now trivial to obtain the pole of ϵ after replacing $d = 4-\epsilon$. The result is

$$(\mathrm{f})_{\mathrm{kin.,div.}} = \frac{3i}{8\pi^2}\frac{p^2}{\epsilon}. \tag{B.2.14}$$

After taking into account the couplings, we obtain

$$(\mathrm{f})_{\mathrm{div.}} = -\frac{3i}{32\pi^2}\frac{p^2}{\epsilon}\left[3g^2 + g'^2\right]. \tag{B.2.15}$$

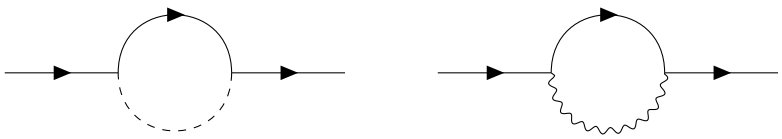

(a) (b)

Figure B.3: The diagrams that contribute to the top quark anomalous dimension.

We define the wave function renormalization of the Higgs as $h_b = Z_h^{1/2} h$, where h_b is the bare Higgs field, and expand it as $Z_h = 1 + \delta_h$. Then the divergent part of δ_h at the one-loop level is given by

$$\delta_h = \frac{1}{32\pi^2\epsilon}\left[-12y_t^2 + 9g^2 + 3g'^2\right]. \tag{B.2.16}$$

The bare Higgs field does not depend on M, and hence we obtain

$$\gamma_h \equiv -\frac{d\ln h}{d\ln M} = \frac{1}{2}\frac{d\delta_h}{d\ln M}. \tag{B.2.17}$$

By counting the mass dimension and using the fact that the bare couplings do not depend on M, we obtain

$$\frac{d\ln y_t^2}{d\ln M} \simeq \frac{d\ln g^2}{d\ln M} \simeq \frac{d\ln g'^2}{d\ln M} \simeq -\epsilon, \tag{B.2.18}$$

to the leading order in the couplings, and hence we finally obtain the Higgs anomalous dimension as

$$\gamma_h = \frac{1}{64\pi^2}\left[12y_t^2 - 9g^2 - 3g'^2\right]. \tag{B.2.19}$$

■ **Top quark**

Next we compute the anomalous dimension of the top quark. The relevant diagrams are shown in Fig. B.3. We first consider the diagram (a) with h and φ_Z running in the loop. It is given as

$$\begin{aligned}(\mathrm{a})_{h,\varphi_Z} =& \left(-i\frac{y_t}{\sqrt{2}}\right)^2 \int \frac{d^4q}{(2\pi)^4}\frac{i\not{q}}{-q^2+i\delta}\frac{i}{-(q-p)^2+i\delta} \\ &+ \left(-\frac{y_t}{\sqrt{2}}\right)^2 \int \frac{d^4q}{(2\pi)^4}\gamma_5\frac{i\not{q}}{-q^2+i\delta}\gamma_5\frac{i}{-(q-p)^2+i\delta} \\ =& y_t^2 \int \frac{d^4q}{(2\pi)^4}\frac{\not{q}}{(-q^2+i\delta)\,(-(q-p)^2+i\delta)}.\end{aligned} \tag{B.2.20}$$

The computation is quite similar to the case of the Higgs, and the divergent part is given by

$$(\mathrm{a})_{h,\varphi_Z,\mathrm{div.}} = \frac{iy_t^2}{16\pi^2}\frac{\not{p}}{\epsilon}. \tag{B.2.21}$$

In the same way we can compute the contribution from $\varphi_\pm$, and we obtain as a total

$$(\mathrm{a})_{\mathrm{div.}} = \frac{iy_t^2}{16\pi^2}\frac{\not{p}}{\epsilon}\left[2P_R + P_L\right]. \tag{B.2.22}$$

Next we consider the contributions from the gauge boson, whose diagram is given by (b) in Fig. B.3. We first pay attention only to the kinetic part, getting rid of the contributions from the couplings. It is given as

$$(\mathrm{b})_{\mathrm{kin.}} = M^{4-d}\int\frac{d^dq}{(2\pi)^d}\gamma_\mu\frac{i\left(\not{q}-\not{p}\right)}{-(q-p)^2+i\delta}\gamma_\nu\frac{i}{-q^2+i\delta}\left[\eta^{\mu\nu}-\frac{q^\mu q^\nu}{q^2}\right]. \tag{B.2.23}$$

After using the Feynman parameter, we obtain the divergent part as

$$\begin{aligned}(\mathrm{b})_{\mathrm{kin.,div.}} &= 3\not{p}\int_0^1 dxM^{4-d}\int\frac{d^dq}{(2\pi)^d}\frac{(x-1)(3x-1)q^2}{\left[-q^2-\Delta+i\delta\right]^3}\\ &= -\frac{3i}{8\pi^2}\frac{\not{p}}{\epsilon}\int_0^1 dx\,(x-1)(3x-1).\end{aligned} \tag{B.2.24}$$

It vanishes after integrating over x, and hence we conclude that

$$(\mathrm{b})_{\mathrm{div.}} = 0. \tag{B.2.25}$$

We define the wave function renormalization of the top quark as $t_{L/R,b} = Z_{t_{L/R}}^{1/2}t_{L/R}$, where $t_{L/R,b}$ is the bare top quark, and expand it as $Z_{t_{L/R}} = 1+\delta_{t_{L/R}}$. Then the divergent part of $\delta_{t_{L/R}}$ at the one-loop level is given by

$$\delta_{t_L} = -\frac{y_t^2}{16\pi^2}\frac{1}{\epsilon}, \tag{B.2.26}$$

$$\delta_{t_R} = -\frac{y_t^2}{8\pi^2}\frac{1}{\epsilon}. \tag{B.2.27}$$

In the same way as the Higgs, we obtain the anomalous dimension of the top quark as

$$\gamma_{t_L} = \frac{y_t^2}{32\pi^2}, \tag{B.2.28}$$

$$\gamma_{t_R} = \frac{y_t^2}{16\pi^2}. \tag{B.2.29}$$

These results are used to compute the beta function of the Higgs quartic coupling and the top Yukawa coupling below.

B.2.2 Higgs quartic coupling

We use the effective potential to compute the beta function of the Higgs quartic coupling. The necessary ingredients are already given in App. B.1, and hence we summarize the mass terms of the relevant particles as functions of the Higgs field value h below. Here we care only the top quark among the SM fermions since the other Yukawa couplings are small.

■ **Top quark**

The mass term is given by

$$m_t = \frac{y_t h}{\sqrt{2}}. \tag{B.2.30}$$

Note that we should count the color degree of freedom $N_c = 3$.

■ **Gauge boson**

In the case of our interest, $W^\pm$ and Z are relevant. Their mass terms are given as

$$m_{W^\pm}^2 = \frac{g^2}{4}h^2, \quad m_Z^2 = \frac{g^2 + g'^2}{4}h^2. \tag{B.2.31}$$

■ **Higgs + Goldstone bosons**

We may expand the Higgs field as

$$H = \frac{1}{\sqrt{2}}\begin{pmatrix} \varphi_1 + i\varphi_2 \\ h + \chi + i\varphi_Z \end{pmatrix}. \tag{B.2.32}$$

Then the mass terms are given respectively by

$$m_\chi^2 = 3\lambda_h h^2 + m_h^2, \quad m_{\varphi_1}^2 = m_{\varphi_2}^2 = m_{\varphi_Z}^2 = \lambda_h h^2 + m_h^2. \tag{B.2.33}$$

Thus the one-loop SM Higgs effective potential is

$$\begin{aligned} V_{\rm eff}(h) \simeq & \frac{m_h^2}{2}h^2 + \frac{\lambda_h}{4}h^4 + \frac{1}{64\pi^2}\left[\frac{3}{16}\left(3g^4 + 2g^2g'^2 + g'^2\right) - 3y_t^4\right]h^4 \ln\left(\frac{h^2}{M^2}\right) \\ & + \frac{\left(m_h^2 + 3\lambda_h h^2\right)^2}{64\pi^2}\ln\left(\frac{m_h^2 + 3\lambda_h h^2}{M^2}\right) + \frac{3\left(m_h^2 + \lambda_h h^2\right)^2}{64\pi^2}\ln\left(\frac{m_h^2 + \lambda_h h^2}{M^2}\right), \end{aligned} \tag{B.2.34}$$

after the renormalization, where we have concentrated only on the terms that depend logarithmically on h. By substituting it to

$$M\frac{dV_{\rm eff}}{dM} = 0, \tag{B.2.35}$$

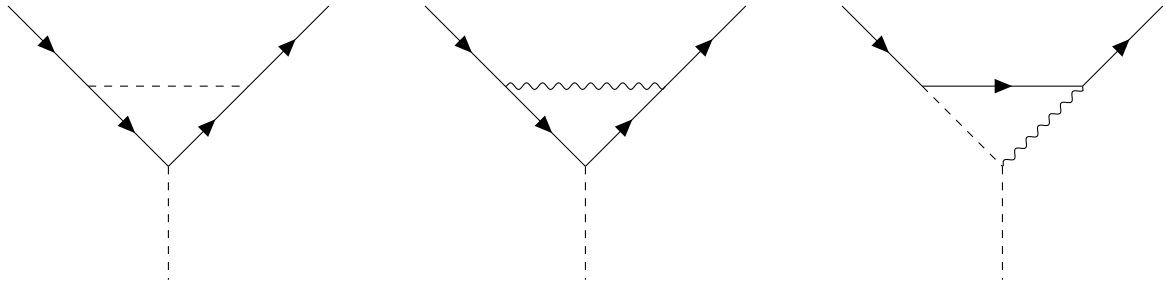

Figure B.4: The diagrams that contribute to the divergent part of the top Yukawa vertex correction. There is also a digram with the wavy and dashed lines being inverted within the loop compared to the diagram (c).

and comparing the first order terms in $g^2, g'^2, y_t^2, \lambda_h$, we obtain

$$\gamma_{m_h} \equiv \frac{d \ln m_h^2}{d \ln M} = \frac{3\lambda_h}{4\pi^2} + 2\gamma_h, \tag{B.2.36}$$

$$\beta_{\lambda_h} = \frac{1}{16\pi^2}\left[24\lambda_h^2 - 6y_t^4 + \frac{3}{8}\left(3g^4 + 2g^2 g'^2 + g'^2\right)\right] + 4\lambda_h \gamma_h, \tag{B.2.37}$$

where γ_h is the anomalous dimension of the Higgs. We know from App. B.2.1 that

$$\gamma_h = \frac{1}{64\pi^2}\left[12y_t^2 - 9g^2 - 3g'^2\right], \tag{B.2.38}$$

and thus we finally obtain the one-loop beta function of the Higgs quartic self coupling as

$$\beta_{\lambda_h} = \frac{1}{16\pi^2}\left[24\lambda_h^2 - 6y_t^4 + \frac{3}{8}\left(3g^4 + 2g^2 g'^2 + g'^2\right) + \left(12y_t^2 - 9g^2 - 3g'^2\right)\lambda_h\right]. \tag{B.2.39}$$

Note that the coefficient of the y_t^4 term is negative due to the fermionic nature of the top quark. It is this y_t^4 term that forces λ_h to be negative in the high energy region.

B.2.3 Top Yukawa coupling

We now compute the beta function of the top Yukawa coupling. The anomalous dimensions of the Higgs and the top quark are already computed in the previous subsection, and hence we compute the vertex correction here. The relevant diagrams are shown in Fig. B.4.

We first consider (a) in Fig. B.4. We consider only the top Yukawa coupling among the Yukawa couplings, and hence only h and φ_Z propagate the loop. It is given as

$$\begin{aligned}(\mathrm{a})_{\mathrm{div.}} = &\left(-i\frac{y_t}{\sqrt{2}}\right)^3 \int \frac{d^4q}{(2\pi)^4}\left(\frac{i\not{q}}{-q^2+i\delta}\right)^2 \frac{i}{-q^2+i\delta} \\ &+ \left(-\frac{y_t}{\sqrt{2}}\right)^2\left(-i\frac{y_t}{\sqrt{2}}\right)\int \frac{d^4q}{(2\pi)^4}\gamma_5\left(\frac{i\not{q}}{-q^2+i\delta}\right)^2 \gamma_5 \frac{i}{-q^2+i\delta} = 0.\end{aligned} \tag{B.2.40}$$

Thus the divergent part cancels between h and φ_Z. Note that we can safely ignore the external momentum as well as the mass term as long as we focus on the divergent part. Next we consider (b) in Fig. B.4. We first compute the kinetic part, and then include the couplings to obtain the result. The kinetic part is given as

$$(\mathrm{b})_{\mathrm{kin.}} = \int \frac{d^4q}{(2\pi)^4}\gamma_\mu \left(\frac{i\not{q}}{-q^2+i\delta}\right)^2 \gamma_\nu \frac{i}{-q^2+i\delta}\left[\eta^{\mu\nu} - \frac{q^\mu q^\nu}{q^2}\right]. \tag{B.2.41}$$

After the dimensional regularization with $d = 4-\epsilon$, we obtain the divergent part as

$$(\mathrm{b})_{\mathrm{kin.,div.}} = -\frac{3}{8\pi^2}\frac{1}{\epsilon}. \tag{B.2.42}$$

The gauge boson that propagates the loop can be the gluon, photon or Z,[b1] and hence we obtain after including the couplings as

$$(\mathrm{b})_{\mathrm{div.}} = \left(-i\frac{y_t}{\sqrt{2}}\right)\frac{1}{24\pi^2}\frac{1}{\epsilon}\left[12g_s^2 + g'^2\right]\delta_{ij}, \tag{B.2.43}$$

where i and j are the color indices of the top quark. Finally we consider (c) in Fig. B.4. Actually the divergent part vanishes since the loop integrand is proportional to

$$\left(\eta^{\mu\nu} - \frac{q^\mu q^\nu}{q^2}\right)q_\mu = 0. \tag{B.2.44}$$

Thus we conclude that

$$(\mathrm{c})_{\mathrm{div.}} = 0. \tag{B.2.45}$$

Collecting them together, we obtain the vertex correction at the one-loop level as

$$\delta_{y_t} = -\frac{12g_s^2 + g'^2}{24\pi^2\epsilon}, \tag{B.2.46}$$

where we have defined $y_{t;b}h_b\bar{t}_b t_b = M^{\epsilon/2}Z_{y_t}y_t h\bar{t}t$, and $Z_{y_t} = 1+\delta_{y_t}$. Then the beta function is obtained from the requirement that the bare coupling $y_{t;b}$ does not depend on the renormalization scale:

$$0 = \frac{d}{d\ln M}\left[M^{\epsilon/2}Z_{y_t}Z_h^{-1/2}Z_{t_L}^{-1/2}Z_{t_R}^{-1/2}y_t\right]. \tag{B.2.47}$$

Thus we finally obtain

$$\beta_{y_t} = \frac{y_t}{16\pi^2}\left[\frac{9}{2}y_t^2 - 8g_s^2 - \frac{9}{4}g^2 - \frac{17}{12}g'^2\right], \tag{B.2.48}$$

in the limit $\epsilon \to 0$, where we have used the results in App. B.2.1

[b1] The contribution from $W^\pm$ is suppressed by the bottom Yukawa coupling.

B.2.4 Gauge couplings

The derivation of the beta functions for the gauge couplings are explained in detail in literature. Hence we just write down the results here:

$$\beta_{g_s} = -\frac{7}{16\pi^2} g_s^3, \quad \beta_g = -\frac{19}{96\pi^2} g^3, \quad \beta_{g'} = \frac{41}{96\pi^2} g'^3. \tag{B.2.49}$$

B.2.5 Gauge/scheme (in)dependence

In this subsection, we study the gauge/scheme (in)dependence of the beta functions. Suppose that we have two set of the couplings $\{g\}$ and $\{\tilde{g}\}$ defined in different gauges and/or schemes.[b2] In a perturbative theory, they should be related as

$$\tilde{g}_i = g_i + a_i{}^{jk} g_j g_k + O(g^3), \tag{B.2.50}$$

where the latin indices run over the couplings. It is inverted as

$$g_i = \tilde{g}_i - a_i{}^{jk} \tilde{g}_j \tilde{g}_k + O(\tilde{g}^3). \tag{B.2.51}$$

We assume that the beta function for $\{g\}$ is given as

$$\beta_i \equiv \frac{dg_i}{d\ln M} = b_i{}^{jk} g_j g_k + b'_i{}^{jkl} g_j g_k g_l + O(g^4), \tag{B.2.52}$$

where M is the renormalization scale. Then the beta function for $\{g'\}$ is given as

$$\begin{aligned} \tilde{\beta}_i \equiv \frac{d\tilde{g}_i}{d\ln M} &\simeq \left(\delta_i^k + 2a_i{}^{jk} g_j\right)\beta_k \\ &= b_i{}^{jk} \tilde{g}_j \tilde{g}_k + b'_i{}^{jkl} \tilde{g}_j \tilde{g}_k \tilde{g}_l + 2\left(a_i{}^{jk} b_j{}^{lm} - b_i{}^{jk} a_j{}^{lm}\right) \tilde{g}_k \tilde{g}_l \tilde{g}_m + O(g^4). \end{aligned} \tag{B.2.53}$$

Thus, the 1-loop part is the same for $\{g\}$ and $\{g'\}$ [77]. It depends on $a_i{}^{jk}$ and $b_i{}^{jk}$ whether or not the 2-loop part is dependent on the gauge and/or scheme choices. For instance, the 2-loop part is also independent if there is only one coupling [78], as

$$a_i{}^{jk} b_j{}^{lm} - b_i{}^{jk} a_j{}^{lm} = 0, \tag{B.2.54}$$

is trivially satisfied in such a case. In general, however, we may need to examine detailed structures of $a_i{}^{jk}$ and $b_i{}^{jk}$ for each theory concerning two or higher loop parts.

It may be worth noting that the beta functions are gauge-invariant to all orders once we use the MS or $\overline{\text{MS}}$ renormalization scheme [79]. In these schemes, we subtract only divergent parts after the dimensional regularization. Hence the relations between bare couplings $g_i^{(B)}$ and renormalized couplings $g_i^{(R)}$ are given by

$$g_i^{(B)} = M^{c_i \epsilon} g_i^{(R)} \left[1 + \frac{a_1(g^{(R)}, \xi)}{\epsilon} + \frac{a_2(g^{(R)}, \xi)}{\epsilon^2} + \cdots\right], \tag{B.2.55}$$

[b2] In the SM of our interest, the couplings $y_t^2, \lambda_h, g_s^2, g^2$ and g'^2 correspond to these sets.

where ξ is a gauge parameter, M is some renormalization scale, c_i is some numerical constant and $d = 4 - \epsilon$ as usual for the MS scheme. For the $\overline{\text{MS}}$ scheme, ϵ should be replaced by $\bar{\epsilon} \equiv (1/\epsilon - \gamma_E + \log(4\pi))^{-1}$ with γ_E being the Euler constant. Note that the ϵ^0-th order term in the bracket is unity just because we have used the MS or $\overline{\text{MS}}$ scheme.[b3] We take the derivative with respect to ξ with ϵ, M and $g_i^{(B)}$ being fixed, and obtain

$$0 = \frac{dg_i^{(R)}}{d\xi} + \frac{1}{\epsilon}\frac{d}{d\xi}\left(g_i^{(R)} a_1\right) + \frac{1}{\epsilon^2}\frac{d}{d\xi}\left(g_i^{(R)} a_2\right) \cdots . \tag{B.2.56}$$

We may regard it to be valid for general d, and thus we conclude from the first term that

$$\frac{dg_i^{(R)}}{d\xi} = 0. \tag{B.2.57}$$

In other words, the renormalized couplings are gauge invariant in the MS or $\overline{\text{MS}}$ scheme. It trivially follows that the beta functions in these schemes are also gauge invariant, since the derivative with respect to M commutes with that with respect to ξ as M is independent of ξ. We can easily extend the above discussion for anomalous dimensions of any gauge invariant operators, since bare operators do not depend on ξ as long as they are gauge invariant. Hence an anomalous dimension of a gauge invariant operator (such as the Higgs mass term) is also independent of ξ to all orders in the MS or $\overline{\text{MS}}$ scheme. On the other hand, the anomalous dimension of the radial direction of the Higgs h does depend on the gauge choice since it is not gauge invariant, so is the effective potential. For some particular choices of the gauge fixing term, we can show that a change of the effective potential due to the change of the gauge parameter is compensated by a corresponding rescaling of the external Higgs field, which is called the Nielsen identity [80]. For more details, see *e.g.* Refs. [80–84] and references therein.

[b3] In other schemes, the ϵ^0-th order term generally has contributions of the form $(g^{(R)})^n \xi^m$, and hence the following discussion does not apply.

Appendix C

Review on inflation

In this appendix we review inflation. We first describe the slow-roll inflation models, and then compute the power spectra of the scalar and the tensor modes. We also discuss the dynamics of a light/heavy spectator scalar field during inflation.

C.1 Inflation

Here we describe the main idea of inflation. We pay particular attention to the so-called slow-roll inflation models.

C.1.1 Main idea

Our universe is known to be homogeneous and isotropic at least in the large scale, and hence we approximate the metric as the the FLRW one:

$$ds^2 = -dt^2 + a^2(t)dx^i dx^i, \tag{C.1.1}$$

where a is the scale factor, with spatial curvature being neglected. The idea of inflation is closely connected to the causal structure of this metric. In order to understand the causal structure, it is most instructive to work with the comoving time η defined as

$$d\eta \equiv \frac{dt}{a}. \tag{C.1.2}$$

Its integrated form is given by

$$\eta = \int^t \frac{dt}{a} = \int^a \frac{d\log a}{aH}. \tag{C.1.3}$$

Hence the comoving distance over which massless particles can travel within one e-folding is $\sim 1/aH$. It is called the comoving Hubble radius, and offers a rough estimation of the comoving size of causally connected regions (or the Hubble patches).[b1] In order to determine

[b1] As we will see below, the integration is dominated by the late time if the universe is dominated by matter/radiation.

the time evolution of the comoving Hubble radius, we must specify the matter contents of the universe. We assume that it is given by a perfect isotropic fluid, where the energy stress tensor is given by

$$T^{\mu}{}_{\nu} = \mathrm{diag}\left(-\rho(t), p(t), p(t), p(t)\right), \tag{C.1.4}$$

with ρ and p being the energy density the pressure, respectively, that depend only on time. We further assume that it satisfies the following equation of state:

$$p = w\rho, \tag{C.1.5}$$

where w is some numerical constant. For instance, it is given by $w = 1/3$ in the radiation-dominated era (RD), while $w = 0$ in the matter-dominated era (MD). The time evolution of the system is governed by the Friedmann equations (the Einstein equation with the FLRW metric) and the conservation law ($\nabla_{\mu} T^{\mu}{}_{\nu} = 0$):

$$H^2 = \frac{\rho}{3M_{\mathrm{Pl}}^2}, \tag{C.1.6}$$

$$0 = \dot{\rho} + 3H\left(\rho + p\right). \tag{C.1.7}$$

where $H \equiv \dot{a}/a$ is the Hubble parameter and M_{Pl} is the reduced Planck mass. We obtain $\rho \propto a^{-3(1+w)}$ from the last equation, and hence the comoving Hubble radius scales as

$$\frac{1}{aH} \propto a^{(1+3w)/2}. \tag{C.1.8}$$

Thus it increases with time and the integration in Eq. (C.1.3) is dominated by the late time as long as $w > -1/3$. Here comes an essential point. In the standard big-bang cosmology, the universe is dominated by the radiation ($w = 1/3$) or the matter ($w = 0$),[♭2] and hence the comoving Hubble radius is always increasing with time. In other words, the Hubble patch we see today consists of many causally disconnected patches in the past. Then a question is why the universe we see today is so homogeneous and isotropic. For instance, the CMB stops interacting with each other well before today, and hence it is weird that the CMB we see today is isotropic to high precision. It is the so-called horizon problem, one of the problems of the standard big-bang cosmology.

The solution to this problem is also simple once we understand the causal structure. If there exists an epoch in which the universe is dominated by a matter with $w < -1/3$, the comoving Hubble radius *decreases* with time. In other words, the region we can see shrinks with time in that epoch. Then causally disconnected regions in a later epoch can be connected in the earlier stage, and hence it is natural that they look quite similar. This epoch is called the *inflation*. It is enough to have $w < -1/3$ for inflation (if we define the inflation as above). In the following, however, we concentrate on the case with $w \simeq -1$ since it is at least supported by the CMB observation.

[♭2] The recent dark energy dominated era is irrelevant in our discussion below.

C.1.2 Slow-roll inflation

In this subsection we review the slow-roll inflation. As a simplest case, we consider the Einstein-Hilbert action with a real scalar field:

$$S = \int d^4x \sqrt{-g}\left[\frac{M_{\rm Pl}^2}{2}R - \frac{1}{2}\left(\partial\phi\right)^2 - V\left(\phi\right)\right], \tag{C.1.9}$$

where ϕ is the real scalar field, or the inflaton, $V(\phi)$ is the inflaton potential, and R is the Ricci scalar. We consider only the homogeneous and isotropic part in this subsection. Perturbations around this background are the subject of the next section. We take the metric as the FLRW one. The equations of motion are given by

$$H^2 = \frac{1}{3M_{\rm Pl}^2}\left(\frac{1}{2}\dot{\phi}^2 + V\right), \tag{C.1.10}$$

$$\dot{H} = -\frac{\dot{\phi}^2}{2M_{\rm Pl}^2}, \tag{C.1.11}$$

$$0 = \ddot{\phi} + 3H\dot{\phi} + V', \tag{C.1.12}$$

where the prime denotes the derivative with respect to ϕ. They are equivalent to identify

$$\rho = \frac{1}{2}\dot{\phi}^2 + V, \tag{C.1.13}$$

$$p = \frac{1}{2}\dot{\phi}^2 - V, \tag{C.1.14}$$

in the language of the previous subsection. It is clear from these expressions that we have $w \simeq -1$ as long as $V \gg |\dot{\phi}|^2$. In other words, inflation occurs when the potential energy is much larger than the kinetic energy, or the inflaton slowly rolls down its potential. It is the so-called slow-roll inflation paradigm. It is characterized by the following conditions:

$$\epsilon \ll 1, \quad \left|\eta\right| \ll 1, \quad \text{where} \quad \epsilon \equiv \frac{M_{\rm Pl}^2}{2}\left(\frac{V'}{V}\right)^2, \quad \eta \equiv \frac{M_{\rm Pl}^2 V''}{V}. \tag{C.1.15}$$

They are called the slow-roll conditions with ϵ and η being called slow-roll parameters. We can also consider conditions on higher derivatives of the potential, but it is usually enough to require the above two conditions to have sufficient number of e-folds. In this case the Hubble friction term dominates the scalar equation of motion, and hence we can approximate it as

$$\dot{\phi} \simeq -\frac{V'}{3H}. \tag{C.1.16}$$

We can show that it is indeed an attractor solution. Then the number of e-folds N of inflation is related to the inflaton field value by

$$N(\phi) \equiv \int_t^{t_e} H dt \simeq -\int_\phi^{\phi_e} \frac{V}{M_{\rm Pl}V'}\frac{d\phi}{M_{\rm Pl}}, \tag{C.1.17}$$

where the subscript "e" indicates the end of inflation, which is usually taken as the field value at which $\epsilon = 1$. Here we have assumed that $\dot{\phi}$ does not change its sign during inflation, and hence we can use ϕ as a clock. It must be at least larger than 50-60 depending on the reheating temperature of the universe. We will use this relation extensively when we constrain the inflation models by the CMB observation in the next section.

C.2 Perturbations

The most important feature of inflation is that it can produce perturbations that seed the large scale structure of the present universe. It also supplies the initial conditions for the CMB anisotropy, and hence is useful to distinguish different inflation models from the observations. Thus, in this section, we compute the curvature and tensor power spectra generated during inflation, and compare it with the observation. We work with the following action for simplicity:

$$S = \int d^4x \sqrt{-g} \left[\frac{M_{\rm Pl}^2}{2} R - \frac{1}{2} \left(\partial\phi\right)^2 - V\left(\phi\right) \right], \tag{C.2.1}$$

and mainly follow the procedure in Ref. [85]. The results of this section are used to determine the parameters of the inflaton potential in Chaps. 4 and 5.

C.2.1 Curvature perturbation

First we compute the quadratic action for the curvature perturbation. Since the scalar part of the perturbation decouples from the vector and tensor ones up to the quadratic order, we concentrate only on the scalar part of the perturbations in this subsection. Note that the terminologies "scalar," "vector" and "tensor" in this section are defined with respect to the spatial rotation, not the Lorentz transformation.

We work with the following ADM decomposition of the metric [86]:

$$ds^2 = -N^2 dt^2 + h_{ij} \left(dx^i + \beta^i dt\right) \left(dx^j + \beta^j dt\right), \tag{C.2.2}$$

where N is the lapse function (do not confuse with the number of e-folds), β^i is the shift vector and h_{ij} is the three-dimensional space metric. In terms of them, the action is given by

$$S = \frac{1}{2} \int d^4x \sqrt{h} \left[M_{\rm Pl}^2 N R^{(3)} - 2NV + \frac{M_{\rm Pl}^2}{N} \left(E_{ij}E^{ij} - E^2\right) + \frac{1}{N} \left(\dot{\phi} - \beta^i \partial_i \phi\right)^2 - N h^{ij} \partial_i \phi \partial_j \phi \right], \tag{C.2.3}$$

where

$$E_{ij} = \frac{1}{2} \left(\dot{h}_{ij} - \nabla_i^{(3)} \beta_j - \nabla_j^{(3)} \beta_i \right) = N K_{ij}, \tag{C.2.4}$$

with K_{ij} being the extrinsic curvature, and $R^{(3)}$ and $\nabla_i^{(3)}$ are the Ricci scalar and the covariant derivative with respect to h_{ij}, respectively. The latin indices $i, j, \ldots$ run the spatial coordinates,

and are contracted by h_{ij}. It is clear that N and β_i do not have any time derivatives, and hence their equations of motion are constraint equations. It is the main virtue of the ADM decomposition. Here it may be instructive to count the number of scalar degrees of freedom (d.o.f). We have initially 5 d.o.f: one from the inflaton, and four from the metric (g_{00}, the divergence parts of g_{0i} and g_{ij}, and the trace part of g_{ij}). We can eliminate two of them by using the general coordinate transformation ($t \to t'(t,x)$ and the divergence part of $x \to x'(t,x)$). We can further eliminate two of them by the constraint equations. As a result, we have one gauge-invariant dynamical scalar d.o.f for a single field inflation model. It is the power spectrum of this d.o.f that we calculate from now.

Now we compute the quadratic action of the scalar d.o.f. We work in the unitary gauge[b3]

$$\phi(t,x) = \phi(t), \quad h_{ij} = a^2(t) e^{2\zeta(t,x)} \delta_{ij}. \tag{C.2.5}$$

In other words, we eliminate the inflaton fluctuation and the divergence part of h_{ij}. In this gauge the action is given by

$$S = \frac{1}{2} \int d^4x\, a^3 e^{3\zeta} \left[M_{\rm Pl}^2 N R^{(3)} - 2NV(\phi(t)) + \frac{M_{\rm Pl}^2}{N} \left(E_{ij} E^{ij} - E^2 \right) + \frac{1}{N} \dot{\phi}^2 \right], \tag{C.2.6}$$

and hence the constraint equations are given by

$$0 = M_{\rm Pl}^2 R^{(3)} - 2V - \frac{M_{\rm Pl}^2}{N^2} \left(E_{ij} E^{ij} - E^2 \right) - \frac{1}{N^2} \dot{\phi}^2, \tag{C.2.7}$$

$$0 = \nabla_j^{(3)} \left(\frac{1}{N} \left(E_i^j - \delta_i^j E \right) \right). \tag{C.2.8}$$

So far no perturbative expansion is made. Now we expand the metric as

$$N = 1 + \alpha, \quad \beta_i = a^2 \partial_i \psi, \tag{C.2.9}$$

and solve the constraint equations to the first order in ζ. Note that the first order solution in ζ is enough to obtain the quadratic (or actually even cubic) action, since the second order contribution couples to the zero-th order part of the constraint equations (*i.e.* the Friedmann equations). Up to the first order, the relevant geometric quantities are given by

$$R^{(3)} = -\frac{4}{a^2} \partial_i \partial_j \zeta, \tag{C.2.10}$$

$$E_{ij} = a^2 \left[\left(H(1 + 2\zeta) + \dot{\zeta} \right) \delta_{ij} - \partial_i \partial_j \psi \right]. \tag{C.2.11}$$

Then the zero-th order solution is just the Friedmann equation:

$$3 M_{\rm Pl}^2 H^2 = \frac{1}{2} \dot{\phi}^2 + V. \tag{C.2.12}$$

[b3] This gauge choice is possible as long as $\dot{\phi}(t) \neq 0$, which is the case during the slow-roll inflation.

At the first order in ζ, the solutions are given by

$$\alpha = \frac{\dot{\zeta}}{H}, \quad \psi = -\frac{\zeta}{a^2 H} + \chi, \quad \text{where} \quad \partial_i \partial_i \chi = \frac{\dot{\phi}^2}{2M_{\rm Pl}^2 H^2}\dot{\zeta}. \tag{C.2.13}$$

By substituting them into the action and expand it up to the second order in ζ, we finally obtain the quadratic action as

$$S_2^{(\zeta)} = \frac{1}{2}\int d^4x \frac{a^3\dot{\phi}^2}{H^2}\left[\dot{\zeta}^2 - \frac{1}{a^2}(\partial_i\zeta)^2\right]. \tag{C.2.14}$$

The prefactor $\dot{\phi}$ just indicates that the unitary gauge is ill-defined in the limit $\dot{\phi} \to 0$. Note that so far no slow-roll approximation is used. Now we rely on the slow-roll approximation. To the leading order in the slow-roll approximation, the prefactor $\dot{\phi}^2/H^2$ can be regarded just as a constant. Then, by using the results below in App. C.3, the power spectrum of ζ at the horizon crossing is given by

$$P_\zeta(k) = \frac{H_*^2}{4\pi^2}\frac{H_*^2}{\dot{\phi}_*^2} = \frac{1}{8\pi^2}\frac{H_*^2}{M_{\rm Pl}^2 \epsilon_*}, \tag{C.2.15}$$

where the subscript "$*$" indicates that the quantities are evaluated at the horizon crossing $k = aH$. The amplitude of ζ is frozen after the horizon crossing, as we can see from the quadratic action (take the limit $k \ll aH$). Thus the above expression for the power spectrum is valid even well after the horizon crossing. The power spectrum slightly depends on k through different values of H_* and ϵ_*. It is parametrized by the spectral index n_s as

$$n_s - 1 \equiv \frac{d}{d\log k}\log P_\zeta(k) = -6\epsilon + 2\eta. \tag{C.2.16}$$

In principle there can be contributions from higher derivatives of the potential, but they are usually small and hence we ignore them here. The power spectrum and the spectral index are the primary observables of the inflation. The CMB anisotropy observation by the Planck satellite [87] fixes these quantities as

$$\log\left(10^{10} P_\zeta(k_0)\right) = 3.064 \pm 0.023, \tag{C.2.17}$$

$$n_s = 0.968 \pm 0.006, \tag{C.2.18}$$

where the quantities are evaluated at $k_0 = 0.05\,\mathrm{Mpc}^{-1}$, corresponding to 50–60 e-folds before the end of the inflation. Note that n_s supports a slightly scale-dependent spectrum.

C.2.2 Tensor perturbation

Next we consider the quadratic action for the tensor mode, *i.e.* the transverse traceless part of the spatial metric h_{ij}. Since it decouples from the scalar perturbation at the quadratic level,

we need to consider only the background part for the scalar sector. Thus we expand the metric as

$$ds^2 = -dt^2 + a^2 \left(e^{\gamma}\right)_{ij} dx^i dx^j, \tag{C.2.19}$$

where $\gamma_{ii} = \partial_i \gamma_{ij} = 0$, and find the quadratic action for γ_{ij}. Up to total derivatives, the relevant geometric quantities are given by

$$R^{(3)} = -\frac{1}{4a^2} \partial_l \gamma_{ij} \partial_l \gamma_{ij}, \tag{C.2.20}$$

$$E_{ij}E^{ij} - E^2 = -6H^2 + \frac{1}{4}\dot{\gamma}_{ij}\dot{\gamma}_{ij}, \tag{C.2.21}$$

to the second order in γ_{ij}, and hence the quadratic action is

$$S_2^{(\gamma)} = \frac{M_{\rm Pl}^2}{8} \int d^4x\, a^3 \left[\dot{\gamma}_{ij}\dot{\gamma}_{ij} - \frac{1}{a^2}\partial_l \gamma_{ij} \partial_l \gamma_{ij}\right]. \tag{C.2.22}$$

We find the power spectrum for the tensor mode from this action as

$$P_\gamma(k) = \frac{2}{\pi^2}\frac{H_*^2}{M_{\rm Pl}^2}, \tag{C.2.23}$$

where we have summed over the two polarization modes. Thus the tensor-to-scalar ratio r is given by

$$r \equiv \frac{P_\gamma}{P_\zeta} = 16\epsilon_*. \tag{C.2.24}$$

Since the normalization of the curvature perturbation is fixed by the CMB observation, it is related to the inflation scale as

$$V^{1/4} \simeq 1.4 \times 10^{16}\,\text{GeV} \left(\frac{r}{0.1}\right)^{1/4}, \tag{C.2.25}$$

$$\text{or}\ \ H_* \simeq 7.6 \times 10^{13}\,\text{GeV} \left(\frac{r}{0.1}\right)^{1/2}, \tag{C.2.26}$$

as long as the inflaton is the dominant source of the curvature perturbation. It implies that high-scale inflation models generically predict a sizable tensor-to-scalar ratio. So far only an upper bound on r is obtained [88]:

$$r < 0.07, \tag{C.2.27}$$

where it is again evaluated at $k = k_0$. Future experiments aim to detect r of $O(10^{-3})$ [89].

C.2.3 Comparison with observation

The normalization and the spectral index of the curvature power spectrum are used to determine inflation model parameters once we fix an inflation model. They are further constrained by the upper bound on the scalar-to-tensor ratio. We see how it works with some specific inflation models in this subsection. The results are used in Chaps. 4 and 5.

Chaotic inflation model

First we consider the chaotic inflation model, where the scalar potential is given by

$$V = \frac{\lambda}{n}\phi^n, \tag{C.2.28}$$

with n being some numerical constant. In this case the slow-roll parameters are given by

$$\epsilon = \frac{n^2}{2}\frac{M_{\rm Pl}^2}{\phi^2}, \quad \eta = n(n-1)\frac{M_{\rm Pl}^2}{\phi^2}. \tag{C.2.29}$$

The number of e-foldings is given by

$$N \simeq -\frac{1}{2n}\left[\frac{\phi_e^2}{M_{\rm Pl}^2} - \frac{\phi^2}{M_{\rm Pl}^2}\right] \simeq \frac{1}{2n}\frac{\phi^2}{M_{\rm Pl}^2}, \tag{C.2.30}$$

where $\phi^2 \gg \phi_e^2$ holds for sufficiently large N. Then the spectral index and the tensor-to-scalar ratio are given in terms of N as

$$n_s - 1 = -\frac{n+2}{2N}, \tag{C.2.31}$$

$$r = \frac{4n}{N}. \tag{C.2.32}$$

The model parameter λ is fixed by the CMB normalization as

$$\frac{\lambda}{M_{\rm Pl}^{4-n}} \simeq 1.2 \times 10^{-7}\,\frac{n^2}{N}\,(2nN)^{-n/2}\,. \tag{C.2.33}$$

To be more specific, we take $n = 2$ (where $\lambda = m_\phi^2$ is the inflaton mass), and $N = 60$. In this case the inflaton mass is fixed from the CMB normalization as

$$m_\phi \simeq 1.4 \times 10^{13}\,{\rm GeV}, \tag{C.2.34}$$

while n_s and r are given by

$$n_s \simeq 0.967, \tag{C.2.35}$$

$$r \simeq 0.13. \tag{C.2.36}$$

Thus the spectral index is consistent with the CMB observation, while the tensor-to-scalar ratio is somewhat larger than the upper bound. If we consider a non-minimal coupling between the inflaton and Ricci scalar, we can avoid it for $n = 4$ [44]. In that case the mass scale at around the minimum is $m_\phi \simeq 10^{12}\,{\rm GeV}$. For this reason we take $m_\phi = 10^{12}$-$10^{13}\,{\rm GeV}$ when we consider the preheating dynamics after high-scale inflation in Chap. 4.

Hill-top inflation model

Next we consider the hill-top inflation model, where the potential is given by

$$V = \Lambda^4 \left[1 - \left(\frac{\phi}{v_\phi}\right)^n\right]^2, \tag{C.2.37}$$

where n is again some constant. In this model, the scalar spectral index and tensor-to-scalar ratio are given in terms of N as

$$n_s - 1 \simeq -\frac{2}{N}\frac{n-1}{n-2}, \tag{C.2.38}$$

$$r \simeq \frac{16n}{N(n-2)}\left[\frac{1}{2Nn(n-2)}\frac{v_\phi^2}{M_{\rm Pl}^2}\right]^{\frac{n}{n-2}}. \tag{C.2.39}$$

Thus r is negligibly small in small-field models for $v_\phi \ll M_{\rm Pl}$ as long as $n > 2$. It originates form a larger hierarchy between $|\eta|$ and ϵ, which is typically present for low-scale inflation models. The CMB normalization implies

$$2.2 \times 10^{-9} \simeq \frac{\left[2n((n-2)N)^{n-1}\right]^{\frac{2}{n-2}}}{12\pi^2}\frac{\Lambda^4}{(v_\phi^n M_{\rm Pl}^{n-4})^{\frac{2}{n-2}}}. \tag{C.2.40}$$

It relates Λ and v_ϕ and hence there remains essentially one parameter, which we take v_ϕ in Chap. 5. For a reasonable value of n, the spectral index is slightly outside the observationally favored range. This discrepancy is resolved if there exists the following Planck suppressed operator [56, 57]:

$$\delta V = -\Lambda^4 \frac{k}{2}\frac{\phi^2}{M_{\rm Pl}^2}, \tag{C.2.41}$$

with $k \lesssim O(1/nN)$. While it is too small to change the inflaton dynamics significantly, it can shift the slow-roll parameter η for a certain range of k. If $n \geqslant 6$, it is possible to shift the spectral index within 68% confidence level for $N = 50$-60. See Fig. C.1 and Ref. [90]. Since the suitable value of k is small, it is safely ignored during the preheating epoch.

C.3 Spectator field dynamics

In this section we consider the dynamics of a light scalar field, which we call a spectator field, during inflation. We do not consider fermions or vector fields since they are Weyl-invariant in the massless limit, and hence are not much amplified during inflation in general. The Higgs is an example of such a spectator field if it is light enough during inflation. We have used the results of this section in Chap. 3.

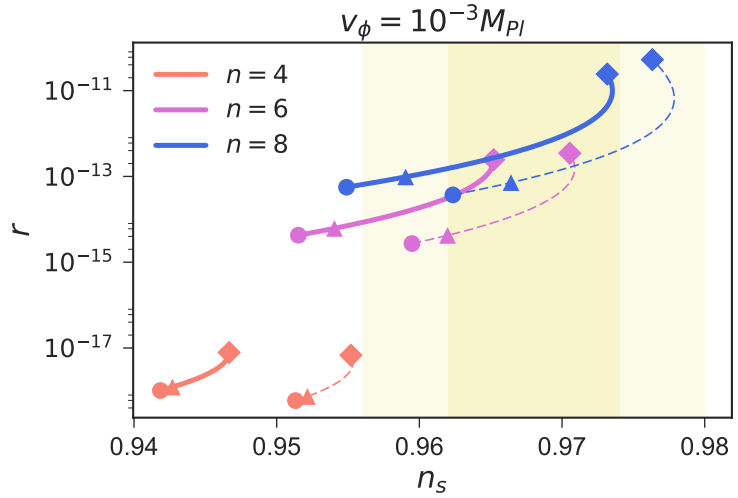

Figure C.1: The n_s-r plane for $n = 4, 6, 8$ with varying k from 10^{-4} to 10^{-2}. The solid (dashed) lines correspond to $N = 50$ (60). The circle, triangle, and square represent points at $k = 10^{-4}, 10^{-3}, 10^{-2}$ respectively. The yellow shaded region stands for one and two sigma regions of n_s [91].

C.3.1 Power spectrum

First we compute the power spectrum of a spectator field for super-horizon modes. We consider the following action:

$$S_\chi = \int d^4x \sqrt{-g} \left[-\frac{1}{2} (\partial\chi)^2 - \frac{1}{2} \left(m_\chi^2 + \xi_\chi R \right) \chi^2 \right], \tag{C.3.1}$$

where χ is a real scalar field, or the spectator field, m_χ is the mass of χ and ξ_χ is the non-minimal coupling. At present we do not assume χ as light during inflation to make the discussion generic. We assume that the background is the de-Sitter spacetime, where the energy density is sourced by the inflaton.

The equation of motion of χ is given by

$$\ddot{\chi} + 3H\dot{\chi} - \frac{\partial_i^2}{a^2}\chi + \left(m_\chi^2 + \xi_\chi R \right) \chi = 0, \tag{C.3.2}$$

where the dot denotes the derivative with respect to the time. In the FLRW metric, the Ricci scalar is given by

$$R = 6 \left[\left(\frac{\dot{a}}{a} \right)^2 + \frac{\ddot{a}}{a} \right]. \tag{C.3.3}$$

Thus, after redefining

$$\tilde{\chi} \equiv a\chi, \tag{C.3.4}$$

and using the conformal time $\eta \equiv \int dt/a$, the equation of motion is rewritten as

$$\left[\frac{d^2}{d\eta^2} - \partial_i^2 + m_\chi^2 a^2 + (6\xi_\chi - 1)\frac{a''}{a}\right]\tilde{\chi} = 0. \tag{C.3.5}$$

We now define the mode function of $\tilde{\chi}$ as

$$\tilde{\chi}(\eta, \vec{x}) = \int \frac{d^3k}{(2\pi)^{3/2}}\left[\hat{a}_{\vec{k}} v_k^*(\eta) e^{i\vec{k}\cdot\vec{x}} + \hat{a}_{\vec{k}}^\dagger v_k(\eta) e^{-i\vec{k}\cdot\vec{x}}\right], \tag{C.3.6}$$

where $\hat{a}_{\vec{k}}^\dagger/\hat{a}_{\vec{k}}$ is the creation/annihilation operator and $v_k(\eta)$ is the mode function of $\tilde{\chi}$. The mode function obeys the wave equation

$$\left[\frac{d^2}{d\eta^2} + k^2 + m_\chi^2 a^2 + (6\xi_\chi - 1)\frac{a''}{a}\right] v_k = 0, \tag{C.3.7}$$

and the Wronskian condition

$$v_k' v_k^* - v_k v_k^{*\prime} = i, \tag{C.3.8}$$

while the creation/annihilation operator satisfies the commutation relation

$$\left[\hat{a}_{\vec{k}}, \hat{a}_{\vec{k}'}^\dagger\right] = \delta\left(\vec{k} - \vec{k}'\right), \quad \left[\hat{a}_{\vec{k}}, \hat{a}_{\vec{k}'}\right] = \left[\hat{a}_{\vec{k}}^\dagger, \hat{a}_{\vec{k}'}^\dagger\right] = 0. \tag{C.3.9}$$

If we define a vacuum as a state that is annihilated by $\hat{a}_{\vec{k}}$, the two-point function of χ is calculated as

$$\left\langle \chi(\vec{x}, \eta)\chi(\vec{x}', \eta)\right\rangle = \frac{1}{a^2}\int \frac{d^3k}{(2\pi)^3}\left|v_k\right|^2 e^{i\vec{k}\cdot(\vec{x}-\vec{x}')}. \tag{C.3.10}$$

In particular, if we define the power spectrum $P_\chi(k)$ as

$$\left\langle \chi^2(\vec{x}, \eta)\right\rangle \equiv \int d\log k\, P_\chi(k), \tag{C.3.11}$$

it is given in terms of the mode function as[b4]

$$P_\chi(k) = \frac{k^3}{2\pi^2 a^2}\left|v_k\right|^2. \tag{C.3.12}$$

Now we compute the mode function in the de-Sitter background. In the pure de-Sitter background, the scale factor is given in terms of the conformal time as

$$a = -\frac{1}{H\eta}, \quad -\infty < \eta < 0, \tag{C.3.13}$$

[b4] Here we ignore subtraction of quantum fluctuations just for simplicity.

where H is now constant. Note that $\eta \to -\infty$ (0) corresponds to the infinite past (future). Thus the wave equation for the mode function is

$$\left[\frac{d^2}{d\eta^2} + k^2 - \left(2 - 12\xi_\chi - \frac{m_\chi^2}{H^2}\right)\frac{1}{\eta^2}\right] v_k = 0. \tag{C.3.14}$$

After redefining the mode function as $\tilde{v}_k \equiv v_k/\sqrt{-k\eta}$, we finally obtain the Bessel equation:

$$z^2\frac{d^2\tilde{v}_k}{dz^2} + z\frac{d\tilde{v}_k}{dz} + \left[z^2 - \nu^2\right]\tilde{v}_k = 0, \tag{C.3.15}$$

where

$$\nu \equiv \sqrt{\frac{9}{4} - 12\xi_\chi - \frac{m_\chi^2}{H^2}} \quad \text{and} \quad z \equiv -k\eta. \tag{C.3.16}$$

We analyze the cases with $\nu^2 > 0$ and $\nu^2 < 0$ separately in the following.

Light field case

First we consider the case that χ is a light field, or $\nu^2 > 0$. In the present case, we take the boundary condition of the mode function as

$$v_k \to \frac{1}{\sqrt{2k}}e^{-ik\eta} \quad \text{for} \quad -k\eta \to \infty, \tag{C.3.17}$$

up to some constant phase factor. It corresponds to the Bunch-Davies vacuum. Note that different choices of the boundary condition correspond to different choices of the vacuum. Then the solution is given as

$$v_k(\eta) = \frac{\sqrt{-\pi\eta}}{2}H_\nu^{(1)}(-k\eta), \tag{C.3.18}$$

where $H_\nu^{(1)}$ is the Hankel function of the first kind. By substituting it to Eq. (C.3.12) and using the asymptotic form of the Hankel function, we obtain the power spectrum for the super-horizon modes as

$$P_\chi(k)\big|_{k/a\ll H} = \frac{H^2}{4\pi^2}\left(\frac{k}{2aH}\right)^{3-2\nu}\left(\frac{\Gamma(\nu)}{\Gamma(3/2)}\right)^2, \tag{C.3.19}$$

thus it is slightly scale-dependent.

There are two interesting limits in this formula. First let us consider the case where χ is massless and minimally coupled to the gravity. In this case $\nu = 3/2$, and hence we obtain

$$P_\chi(k)\big|_{k/a\ll H} = \frac{H^2}{4\pi^2}. \tag{C.3.20}$$

Thus the power spectrum becomes scale independent. We have used this formula to obtain the power spectra of the curvature and the tensor perturbations in the previous section. Next let us consider the case where χ is massless but $\xi_\chi = 1/6$. Actually in this case χ is Weyl-invariant, and hence it decouples from the metric sector as we can see from the wave equation of the mode function. In this case $\nu = 1/2$, and hence the mode function is always given as

$$v_k = \frac{1}{\sqrt{2k}} e^{-ik\eta} \tag{C.3.21}$$

Thus there is no amplification even for the super-horizon mode. More generally, if ξ_χ and m_χ^2 satisfy

$$12\xi_\chi + \frac{m_\chi^2}{H^2} = 2, \tag{C.3.22}$$

there is no amplification for the super-horizon mode in the pure de-Sitter spacetime.

Heavy field case

Next we consider the case that χ is a heavy field, or $\nu^2 < 0$. Even in this case, the solution is given in terms of the Hankel function of the first kind as

$$v_k = \frac{\sqrt{-\pi\eta}}{2} e^{-\pi\alpha/2} H_{i\alpha}^{(1)}(-k\eta), \tag{C.3.23}$$

where the ordering of the Hankel function is now imaginary, and we define $\alpha \equiv |\nu|$. The Hankel function of the first kind with the imaginary ordering has an asymptotic form of

$$H_{i\alpha}^{(1)}(z \to 0) \to \frac{1 + \coth(\pi\alpha)}{\Gamma(1 + i\alpha)} \left(\frac{z}{2}\right)^{i\alpha} - \frac{i\Gamma(i\alpha)}{\pi} \left(\frac{z}{2}\right)^{-i\alpha}, \tag{C.3.24}$$

and the fluctuation on the super-horizon scale is

$$\begin{aligned} |v_k|^2 &= \frac{\pi}{4aH} e^{-\pi\alpha} \left|H_{i\alpha}^{(1)}(-k\eta)\right|^2 \\ &= \frac{1}{2\alpha}\frac{1}{aH}\left[1 - e^{-\pi\alpha}\left(1 + \coth(\pi\alpha)\right)\sin\left(2\alpha \log\left(\frac{-k\eta}{2}\right) + \gamma\right)\right], \end{aligned} \tag{C.3.25}$$

where the constant γ is defined as

$$\gamma \equiv \arg\left[\frac{\Gamma(-i\alpha)}{\Gamma(1 + i\alpha)}\right]. \tag{C.3.26}$$

We may disregard the second term since it is oscillating and exponentially suppressed, resulting in

$$|v_k|^2 \simeq \frac{1}{2\alpha}\frac{1}{aH}. \tag{C.3.27}$$

Note that so far we have used only the approximation $k/aH \ll 1$.

The above expression contains contributions from the quantum fluctuation, and hence we need to renormalize it. Here we may rely on the adiabatic subtraction method that is commonly used in the context of the quantum field theory in curved spacetime. The equation of motion of χ is formally solved as

$$v_k = \frac{1}{\sqrt{2aW_k}} \exp\left[-i \int^t W_k dt\right], \tag{C.3.28}$$

where W_k satisfies

$$W_k^2 = \Omega_k^2 + W_k^{1/2} \frac{d^2}{dt^2}\left(W_k^{-1/2}\right), \tag{C.3.29}$$

with Ω_k^2 being defined as

$$\Omega_k^2 = \omega_k^2 + \left(12\xi_\chi - \frac{9}{4}\right)H^2 + \left(6\xi_\chi - \frac{3}{2}\right)\dot{H}, \quad \omega_k^2 = \frac{k^2}{a^2} + m_\chi^2. \tag{C.3.30}$$

We may recursively solve Eq. (C.3.29) by expanding with respect to the number of the time derivatives, and such an expansion is called the adiabatic expansion. Up to the second order in the adiabatic expansion with the limit $k/aH \ll 1$, it is given by

$$W_k \simeq m_{\mathrm{eff};\chi} + \omega^{(2)}, \tag{C.3.31}$$

where

$$m_{\mathrm{eff};\chi} = \sqrt{m_\chi^2 + 12\xi_\chi H^2}, \quad \omega^{(2)} = -\frac{9}{8}\frac{H^2}{m_{\mathrm{eff};\chi}}. \tag{C.3.32}$$

Here we have assumed $\xi_\chi \sim O(m_\chi^2/H^2)$, and hence treated $\xi_\chi H^2$ as the leading order in the adiabatic expansion. In the adiabatic subtraction, we subtract the n-th order adiabatic solution from the bare solution to obtain a physical quantity, where n is taken as the minimal number with which all the divergences in the bare solution are subtracted. The integration diverges quadratically in the case of the power spectrum, and hence we subtract the second order adiabatic solution from it. Thus we may define the physical power spectrum as

$$P_\chi(k) \equiv \frac{k^3}{4\pi^2 a^3}\left[2a\left|v_k\right|^2 - \frac{1}{W_k^{(0)} + W_k^{(2)}}\right], \tag{C.3.33}$$

where $W_k^{(n)}$ is the n-th order term of W_k in the adiabatic expansion. For the super-horizon mode, it is given by

$$P_\chi(k)\big|_{k/a \ll H} \simeq \frac{243H^2}{512\pi^2}\left(\frac{k}{aH}\right)^3\left(\frac{H}{m_{\mathrm{eff};\chi}}\right)^5, \tag{C.3.34}$$

to the leading order in $H/m_{\mathrm{eff};\chi}$ expansion.[b5] It is highly suppressed, and also highly blue-tilted. Hence we can indeed say that χ is stabilized at the origin of its potential when it is massive enough. See, *e.g.* Refs. [93, 94] for more details on the adiabatic subtraction. In principle we should perform the adiabatic subtraction in the case of a light scalar field as well, but the counter term decays rapidly after the horizon exit and we practically ignore it.

C.3.2 Langevin and Fokker-Planck equations

In this subsection we derive the Langevin and Fokker-Planck equations that describe dynamics of a homogeneous mode of a light spectator field χ during inflation. For more details, see *e.g.* Refs. [21, 22].

■ Derivation of Langevin equation

Suppose that a real canonical scalar field χ has a potential $V = V(\chi)$ with $|V''| \ll H^2$ during inflation. Then the equation of motion is given by

$$\ddot{\chi} + 3H\dot{\chi} - \frac{\partial_i^2 \chi}{a^2} + V' = 0. \tag{C.3.35}$$

We now divide χ into the small scale modes and the coarse-grained large scale mode:

$$\chi(\vec{x}, t) = \bar{\chi}(\vec{x}, t) + \int \frac{d^3k}{(2\pi)^{3/2}} \theta(k - a\epsilon H) \left[\hat{a}_{\vec{k}} \chi_{\vec{k}}(t) e^{-i\vec{k}\cdot\vec{x}} + \hat{a}_{\vec{k}}^\dagger \chi_{\vec{k}}^*(t) e^{i\vec{k}\cdot\vec{x}} \right], \tag{C.3.36}$$

where θ is the Heaviside theta function with the numerical factor ϵ satisfying $\epsilon < 1$. We take the time dependence of ϵ such that ϵH is constant even if H is (slightly) time-dependent. Thus $\bar{\chi}$ is the coarse-grained mode averaged over the constant physical size $(\epsilon H)^{-1}$, or the time-decreasing comoving size $(a\epsilon H)^{-1}$, that are slightly larger than the event horizon.

For the short-wavelength modes, we may linearize the equation of motion since they are small. Thus the equation of motion is approximated by

$$\ddot{\chi}_{\vec{k}} + 3H\dot{\chi}_{\vec{k}} + \frac{k^2}{a^2}\chi_{\vec{k}} = 0, \tag{C.3.37}$$

where we have also ignored the potential term since it is negligible compared to the gradient term due to $H^2 \gg |V''|$. The solution is already discussed in App. C.3.1, and is given by

$$\chi_{\vec{k}} = \frac{H}{\sqrt{2k}} \left(\eta - \frac{i}{k} \right) e^{-ik\eta}, \tag{C.3.38}$$

as long as we use the Bunch-Davies vacuum as the initial condition. Note that $\chi_{\vec{k}}$ in this subsection is different from $v_{\vec{k}}$ in App. C.3.1 by a factor of a.

[b5] This expression is different from Ref. [92], which might be originated from differences in subtraction schemes. Anyway, the conclusion that the fluctuation is suppressed when it is massive does not change, and hence we do not pursue the origin of the difference further here.

We now schematically denote the division as $\chi = \bar{\chi} + \theta \cdot \chi_s$, where the subscript "s" stands for the small scale. Then the equation of motion is given by

$$\frac{d^2}{dt^2}(\bar{\chi} + \theta \cdot \chi_s) + 3H\frac{d}{dt}(\bar{\chi} + \theta \cdot \chi_s) + V'(\bar{\chi} + \theta \cdot \chi_s) = 0. \tag{C.3.39}$$

By using the linearized equation of motion of χ_s, we obtain

$$\ddot{\bar{\chi}} - \frac{d}{dt}\left(a\epsilon H^2\delta\right) \cdot \chi_s - 2a\epsilon H^2\delta \cdot \dot{\chi}_s + 3H\left(\dot{\bar{\chi}} - a\epsilon H^2\delta \cdot \chi_s\right) + V'(\bar{\chi}) = 0. \tag{C.3.40}$$

where we have used $\dot{\theta}(k - a\epsilon H) = -a\epsilon H^2\delta(k - a\epsilon H)$, and δ is an abbreviation of $\delta(k - a\epsilon)$. We ignore the first term due to the slow-roll approximation. The second and third terms can also be safely ignored in the slow-roll approximation, since only the over-horizon mode with $k = a\epsilon H$ contribute to the above equation due to the delta function. Note that the above equation should always be multiplied by slowly-rolling variables, and hence we can safely ignore the time derivative of the delta function as well. Thus we obtain

$$\dot{\bar{\chi}} = -\frac{V'(\bar{\chi})}{3H} + f(t, \vec{x}), \tag{C.3.41}$$

where f is defined as

$$f(t, \vec{x}) \equiv \int \frac{d^3k}{(2\pi)^{3/2}} \frac{-ia\epsilon H^2}{\sqrt{2}k^{3/2}} \left[\hat{a}_{\vec{k}} e^{-i\vec{k}\cdot\vec{x}} - \hat{a}^\dagger_{\vec{k}} e^{i\vec{k}\cdot\vec{x}}\right] \delta(k - a\epsilon H), \tag{C.3.42}$$

where we have used Eq. (C.3.38) with $|\eta| \ll 1/k$. Note that now the operators for each $\vec{k}$ appear only in a specific form, and hence are commuting with each other. We may regard the system as classical in this sense. The correlation function of $f(t, \vec{x})$ is computed as

$$\langle f(t, \vec{x}) f(t', \vec{x}') \rangle = \frac{H^3}{4\pi^2}\delta(t - t') j_0(z), \quad z = a\epsilon H|\vec{x} - \vec{x}'|, \tag{C.3.43}$$

where $j_0(z) = (\sin z)/z$ is the first spherical Bessel function of the first kind. In particular, when $\vec{x} = \vec{x}'$, or within the same Hubble patch, we may drop $\vec{x}$ from Eq. (C.3.41), and write it as

$$\dot{\bar{\chi}} = -\frac{V'(\bar{\chi})}{3H} + f(t), \tag{C.3.44}$$

where the correlation function is now given by

$$\langle f(t) f(t') \rangle = \frac{H^3}{4\pi^2}\delta(t - t'). \tag{C.3.45}$$

Eq. (C.3.44) is called the Langevin equation, and f is called the noise term. The physical interpretation is as follows. The comoving horizon is decreasing with time during inflation. Hence a mode that was inside the horizon in an early epoch exits the horizon at some later time, contributing to the coarse-grained mode $\bar{\chi}$. Such a contribution originates from the

quantum fluctuation, and hence acts as a random noise to $\bar{\chi}$. Its size is controlled by H since the size of the quantum fluctuation in the (quasi) de-Sitter space is determined by H.

■ **Derivation of Fokker-Planck equation**

We derived the Langevin equation just above:

$$\dot{\chi} = -\frac{V'(\chi)}{3H} + f(t), \tag{C.3.46}$$

where the noise term $f(t)$ satisfies

$$\langle f(t)f(t')\rangle = \frac{H^3}{4\pi^2}\delta(t-t'), \tag{C.3.47}$$

and $\chi(t)$ should be understood as the coarse-grained mode denoted as $\bar{\chi}$ above. Now we rewrite it as the time evolution equation of a differential probability density function $P(\tilde{\chi}, t)$ defined as

$$P(\tilde{\chi}, t) \equiv \langle \delta(\chi(t) - \tilde{\chi})\rangle, \tag{C.3.48}$$

where $\langle ...\rangle$ denotes the average over possible noise configurations. It satisfies

$$\langle F(\chi(t))\rangle = \int d\tilde{\chi}\, F(\tilde{\chi})P(\tilde{\chi}, t), \tag{C.3.49}$$

and hence $P(\chi, t)d\chi$ is indeed understood as the probability where the spectator field sits within the field value of $[\chi, \chi + d\chi]$. By using the Langevin equation, its time derivative is given as

$$\frac{\partial P(\tilde{\chi}, t)}{\partial t} = \frac{\partial}{\partial \tilde{\chi}}\left[\frac{V'(\tilde{\chi})}{3H}P(\tilde{\chi}, t)\right] - \frac{\partial}{\partial \tilde{\chi}}\langle f(t)\delta(\chi(t) - \tilde{\chi})\rangle. \tag{C.3.50}$$

We may evaluate the last term as follows. First of all, the formal solution of the Langevin equation is given by

$$\chi(t) - \chi_0 = \int_0^t dt'\, f(t') \exp\left[-\int_{t'}^t dt''\, \frac{V'(\chi(t''))}{3H(\chi(t'') - \chi_0)}\right], \tag{C.3.51}$$

where $\chi_0 \equiv \chi(t = 0)$ is the initial value of χ. Hence the correlation between χ and f may be evaluated as

$$\langle f(t)\chi(t)\rangle = \frac{H^3}{8\pi^2}, \tag{C.3.52}$$

where the factor $1/2$ comes from that the integration is taken over only one side. Now we evaluate the relevant correlation as

$$\langle f(t)\delta(\chi(t) - \tilde{\chi})\rangle = \langle f(t)\chi(t)\rangle\left\langle \frac{\partial}{\partial\chi(t)}\delta(\chi(t) - \tilde{\chi})\right\rangle = -\frac{H^3}{8\pi^2}\frac{\partial P}{\partial\tilde{\chi}} \tag{C.3.53}$$

where we decomposed the correlation function since the noise term is Gaussian. Thus we finally obtain the so-called Fokker-Planck equation as

$$\frac{\partial P(\tilde{\chi},t)}{\partial t} = \frac{\partial}{\partial \tilde{\chi}}\left[\frac{V'(\tilde{\chi})}{3H}P(\tilde{\chi},t) + \frac{H^3}{8\pi^2}\frac{\partial P(\tilde{\chi},t)}{\partial \tilde{\chi}}\right]. \tag{C.3.54}$$

It may be useful to change the time variable from t to the e-folds N. Then the Fokker-Planck equation is given as

$$\frac{\partial P(\chi,N)}{\partial N} = \frac{\partial}{\partial \chi}\left[\frac{V'(\chi)}{3H^2}P(\chi,N) + \frac{H^2}{8\pi^2}\frac{\partial P(\chi,N)}{\partial \chi}\right], \tag{C.3.55}$$

where we have dropped the tildes for notational ease. We use it extensively in Chap. 3.

■ **Equilibrium state and relaxation time scale**

Now we study the properties of the Fokker-Planck equation we derived just above. We decompose the probability density function following Ref. [22] as

$$P = e^{-v}\sum_{n=0}^{\infty} a_n P_n e^{-\Lambda_n(t-t_n)}, \tag{C.3.56}$$

where we have defined $v \equiv 4\pi^2 V/3H^4$. Then the equation for P_n is similar to the Schrödinger equation:

$$\frac{1}{2}\left(-\frac{\partial}{\partial\chi}+v'\right)\left(-\frac{\partial}{\partial\chi}+v'\right)^{\dagger} P_n = \frac{4\pi^2\Lambda_n}{H^3}P_n, \tag{C.3.57}$$

where we have used $(\partial/\partial\chi)^{\dagger} = -\partial/\partial\chi$, and ignored the time-dependence of H. From this expression we can see that $\Lambda_n \geq 0$. It means that the system always approaches to an equilibrium state in the pure de-Sitter space, which is obtained by setting $\Lambda_n = 0$, or

$$P_{\rm eq} = \mathcal{N}\exp\left[-\frac{8\pi^2 V}{3H^4}\right], \tag{C.3.58}$$

where $\mathcal{N}$ is a normalization constant, assuming that $P_{\rm eq}$ is normalizable. If $V < 0$ at the large field value region such as the Higgs potential, the scalar field lies in that region in most Hubble patches in the equilibrium state, resulting in difficulty to realize the present universe. Thus the time scale to achieve such a configuration is the most relevant quantity for the discussion of the EW vacuum stability during inflation. In Chap. 3, we have addressed this question by numerically solving the Fokker-Planck equation.

In the case where the potential is monomial, it is easy to estimate the parameter dependence of the relaxation time scale. Suppose that the potential is given by $V = \lambda_p\chi^p/p$. Then v is given as

$$v = \frac{4\pi^2}{3p}\frac{\lambda_p\chi^p}{H^4} = \frac{4\pi^2}{3p}\bar{\chi}^p. \tag{C.3.59}$$

where we have define the dimensionless field $\bar{\chi} \equiv \chi(\lambda_p/H^4)^{1/p}$ (it should not be confused with the coarse-grained mode we have used above). In terms of $\bar{\chi}$ the Schrödinger-like equation is given as

$$\frac{1}{2}\left(-\frac{\partial}{\partial\bar{\chi}}+\frac{dv}{d\bar{\chi}}\right)\left(-\frac{\partial}{\partial\bar{\chi}}+\frac{dv}{d\bar{\chi}}\right)^{\dagger}P_n = 4\pi^2\bar{\Lambda}_n P_n, \quad \bar{\Lambda}_n \equiv \frac{\Lambda_n}{H^3}\left(\frac{H^4}{\lambda_p}\right)^{2/p}. \tag{C.3.60}$$

The equation now has no explicit dependence on λ_p, and hence we obtain the parameter dependence of Λ_n as

$$\Lambda_n \propto H^3\left(\frac{\lambda_p}{H^4}\right)^{2/p}. \tag{C.3.61}$$

Thus the number of e-folds the system takes to achieve equilibrium is estimated as

$$N_{\rm relax} \sim \frac{H}{\Lambda_n} \sim \frac{1}{H^2}\left(\frac{H^4}{\lambda_p}\right)^{2/p}. \tag{C.3.62}$$

For instance, for the quadratic ($\lambda_p = m_\chi^2$) or quartic ($\lambda_p = \lambda_\chi$) potentials, it is given by

$$N_{\rm relax} \sim \frac{H^2}{m_\chi^2} \quad \text{or} \quad \left|\lambda_\chi\right|^{-1/2}. \tag{C.3.63}$$

If it is larger than the time scale of the change of the Hubble parameter ($\sim \epsilon^{-1}$ with ϵ being the slow-roll parameter), the system may deviate from the equilibrium state even in the later epoch [95]. It may be of some use to estimate the relaxation time scale of the Higgs, but nevertheless we need a numerical study to estimate it more precisely for a complicated potential such as the SM Higgs effective potential.

Appendix D

Review on preheating

In this appendix we review the inflaton dynamics after inflation. Especially, we discuss in detail particle production process caused by the inflaton oscillation after inflation. Here we mainly concentrate on the case where the inflaton potential at around its bottom is well approximated by the quadratic one. For low-scale inflation models such as the hill-top model we consider in Chap. 5, anharmonic terms are also important. Still, the discussion with the quadratic potential is useful to understand qualitative features of such a system. We ignore the Higgs self coupling throughout this appendix. It is discussed in detail in Chaps. 4 and 5.

D.1 Inflaton dynamics after inflation

Here we review the background dynamics of the inflaton after inflation. We concentrate on the case where the inflaton potential at around its bottom is given by

$$V(\phi) \simeq \frac{1}{2} m_\phi^2 \phi^2, \tag{D.1.1}$$

where ϕ is again the inflaton, and m_ϕ is the inflaton mass at around the bottom.

Once the inflation ends, the mass scale m_ϕ satisfies $m_\phi > H$, where H is the Hubble parameter of the universe. In this case we can treat the Hubble expansion adiabatically, by assuming the time-dependence of the inflaton as

$$\phi(t) = \Phi(t) \cos\left(m_\phi t\right), \tag{D.1.2}$$

where $\Phi(t)$ is the inflaton oscillation amplitude, satisfying $\dot{\Phi} \sim \mathcal{O}(H\Phi)$. By substituting it to the scalar field equation of motion, we obtain

$$\left(\dot{\Phi} + \frac{3}{2} H\Phi\right) \sin\left(m_\phi t\right) - \frac{1}{2m_\phi} \left(\ddot{\Phi} + 3H\dot{\Phi}\right) \cos\left(m_\phi t\right) = 0. \tag{D.1.3}$$

The second term is suppressed by H/m_ϕ compared to the first term, and hence the inflaton amplitude scales as

$$\Phi(t) \propto a^{-3/2}. \tag{D.1.4}$$

It indeed satisfies $\dot{\Phi} \sim O(H\Phi)$, implying our adiabatic approximation is self-consistent. Thus, the background dynamics of the inflaton is well described by

$$\phi(t) \simeq \frac{\Phi_{\rm ini}}{a^{3/2}} \cos\left(m_\phi t\right), \tag{D.1.5}$$

where $\Phi_{\rm ini}$ is the initial inflaton oscillation amplitude, and we take $a = 1$ at that time. It is also useful to derive the later time behavior of ϕ in terms of the physical time t. The Hubble parameter decreases as

$$H^2 \propto \Phi^2 \propto a^{-3}, \tag{D.1.6}$$

and hence $a \propto t^{2/3}$ and $H = 2/3t$. Then from the Friedmann equation we obtain

$$\frac{m_\phi^2 \Phi^2}{6M_{\rm Pl}^2} \simeq \frac{4}{9}\frac{1}{t^2}, \tag{D.1.7}$$

or

$$\phi(t) \simeq \frac{2}{3}\frac{\sqrt{6}M_{\rm Pl}}{m_\phi t} \cos\left(m_\phi t\right). \tag{D.1.8}$$

As long as the decay/annihilation rate of the inflaton is small enough, the inflaton oscillates at around the potential minimum following Eq. (D.1.8) for a sizable time scale. We call this epoch as an inflaton oscillation epoch. As we will see in the following, the inflaton oscillation causes a resonant particle production if it has sizable couplings with itself/other particles. Once there exists the resonant particle production, we call that epoch as a "preheating" epoch. Eq. (D.1.8) is used to estimate the end of the preheating analytically in Chap. 4.

D.2 Formalism

In the previous section we saw that the inflaton condensation typically oscillates after inflation. It induces an oscillating effective mass term for the Higgs once there are couplings between the inflaton/gravity sector and the Higgs sector. For instance, the Higgs-inflaton quartic coupling induces

$$m_h^2(t) = \lambda_{h\phi}\Phi^2 \cos^2\left(m_\phi t\right), \tag{D.2.1}$$

while the trilinear coupling induces

$$m_h^2(t) = \sigma_{h\phi}\Phi \cos\left(m_\phi t\right). \tag{D.2.2}$$

The Higgs-curvature coupling also induces an oscillating effective mass term as

$$m_h^2(t) = \xi_h m_\phi^2 \frac{\Phi^2}{M_{\rm Pl}^2}\left[3\cos^2\left(m_\phi t\right) - 1\right], \tag{D.2.3}$$

since the Ricci scalar is expressed by the inflaton condensation through the Friedmann equation. In general, if the background is time-dependent, or even oscillating, then it causes a particle production. We review the formalism that deals with such a particle production in this section. In this section we just assume that the Higgs mass term m_h^2 is time-dependent, without specifying an explicit form. In the subsequent sections we discuss effects of the couplings $\lambda_{h\phi}$, ξ_h and $\sigma_{h\phi}$ more explicitly.

Let us start with an equation of motion of the Higgs:

$$\ddot{h} - \frac{1}{a^2}\partial_i^2 h + 3H\dot{h} + m_h^2(t)h = 0, \tag{D.2.4}$$

where m_h^2 is the time-dependent effective mass, and we have neglected the self-interaction of the Higgs here since it is small at the beginning of the particle production. We perform a mode expansion of the Higgs as

$$h(x) = \int \frac{d^3k}{[2\pi a(t)]^{3/2}} \left[\hat{a}_{\vec{k}} h_{\vec{k}}(t) e^{i\vec{k}\cdot\vec{x}} + \text{H.c.}\right], \tag{D.2.5}$$

where $\vec{k}$ is a comoving momentum and $a(t)$ is the scale factor. Then the equation of motion in the Fourier space is given by

$$0 = \ddot{h}_{\vec{k}}(t) + \left[\omega_{k;h}^2(t) + \Delta(t)\right] h_{\vec{k}}(t), \tag{D.2.6}$$

where $\Delta \equiv -9H^2/4 - 3\dot{H}/2$ and $\omega_{k;h}^2(t) = k^2/a^2 + m_h^2(t)$. We impose the Wronskian condition of the Higgs

$$h_{\vec{k}}\dot{h}_{\vec{k}}^* - h_{\vec{k}}^*\dot{h}_{\vec{k}} = i, \tag{D.2.7}$$

that fixes the overall normalization of $h_{\vec{k}}$. It is invariant under the time evolution since the equation of motion is linear in $h_{\vec{k}}$. Then the creation/annihilation operator satisfies

$$\left[\hat{a}_{\vec{k}}, \hat{a}_{\vec{k}'}^\dagger\right] = \delta\left(\vec{k} - \vec{k}'\right), \quad \left[\hat{a}_{\vec{k}}, \hat{a}_{\vec{k}'}\right] = \left[\hat{a}_{\vec{k}}^\dagger, \hat{a}_{\vec{k}'}^\dagger\right] = 0, \tag{D.2.8}$$

due to the commutation relation of the Higgs. Here note that there is a redundancy in Eq. (D.2.6): we can always rewrite it by another set of $(\hat{\tilde{a}}_{\vec{k}}, \tilde{h}_{\vec{k}})$ that satisfies

$$\hat{\tilde{a}}_{\vec{k}} = \alpha_k \hat{a}_{\vec{k}} + \beta_k^* \hat{a}_{-\vec{k}}^\dagger, \quad \tilde{h}_{\vec{k}} = \alpha_k^* h_{\vec{k}} - \beta_k h_{\vec{k}}^*. \tag{D.2.9}$$

It leaves Eq. (D.2.6), the Wronskian and the commutation relation invariant as long as the coefficients satisfy

$$|\alpha_k|^2 - \left|\beta_k\right|^2 = 1. \tag{D.2.10}$$

It is the well-known Bogoliubov transformation. With this redundancy, we can always take the initial condition as

$$h_{\vec{k}}(t \to 0) \to \frac{1}{\sqrt{2\omega_{k;h}(0)}}, \quad \dot{h}_{\vec{k}}(t \to 0) \to -i\sqrt{\frac{\omega_{k;h}(0)}{2}}. \tag{D.2.11}$$

We assume that there is no excitation at the initial time, and hence the initial vacuum state is annihilated by the corresponding operator $\hat{a}_{\vec{k}}$. Here we have omitted contributions from the cosmic expansion since it is suppressed by $O(H^2/\omega_{k;h}^2)$. In other words, we work with the leading order in the WKB approximation.

We now define a comoving number density of the Higgs in the momentum space as

$$n_{k;h}(t) \equiv \frac{1}{2\omega_{k;h}(t)}\left[\left|\dot{h}_{\vec{k}}(t)\right|^2 + \omega_{k;h}^2(t)\left|h_{\vec{k}}(t)\right|^2\right] - \frac{1}{2}, \tag{D.2.12}$$

at the leading order in $H^2/\omega_{k;h}^2$ expansion. It becomes the comoving energy density with the vacuum fluctuation being subtracted once we multiply the frequency $\omega_{k;h}$. It also satisfies $\dot{n}_{k;h} = 0$ when m_h^2 does not depend on time. Finally the initial condition of $h_{\vec{k}}$ implies $n_{k;h}(0) = 0$. These facts support the above definition of the comoving number density. There are two situations where the comoving number density grows rapidly with time: the breakdown of adiabaticity and the tachyonic mass term.

First let us discuss the breakdown of the adiabaticity. Here we assume that $\omega_{k;h}^2 \geq 0$, as is the case for the Higgs-inflaton quartic coupling (see Eq. (D.2.1)). In this case the time derivative of the comoving number density $n_{k;h}$ is

$$\dot{n}_{k;h} \sim O\left(\frac{\dot{\omega}_{k;h}}{\omega_{k;h}^2}\right)\omega_{k;h} n_{k;h}, \tag{D.2.13}$$

where we again keep only the leading order terms in the WKB expansion. Thus, the number density increases drastically with time only if

$$\left|\frac{\dot{\omega}_{k;h}}{\omega_{k;h}^2}\right| \gtrsim 1. \tag{D.2.14}$$

We call this situation as a breakdown of the adiabaticity. Indeed, the WKB solution $h_{\boldsymbol{k}}(t) = e^{-i\int^t d\tau\omega_{k;h}(\tau)}/\sqrt{2\omega_{k;h}(t)}$, which is valid for the adiabatic region $|\dot{\omega}_{k;h}/\omega_{k;h}^2| \ll 1$, leaves the number density invariant up to corrections of $O(\dot{\omega}_{k;h}/\omega_{k;h}^2)$. If $\lambda_{h\phi}$ is large enough, the adiabaticity condition is indeed violated at around when the inflaton crosses the origin of its potential, resulting in resonant Higgs particle production as we see in the next section.

In the above discussion we assume that $\omega_{k;h}^2$ is positive definite. If we have the Higgs-inflaton trilinear coupling and/or the Higgs-curvature non-minimal coupling, the effective mass squared can be negative (see Eqs. (D.2.2) and (D.2.3)), so is $\omega_{k;h}^2$. In this regime the wave function grows exponentially with time, resulting in efficient particle production after the inflaton passes the tachyonic regime.[þ1] In the following sections we first discuss the resonant particle production due to the breakdown of the adiabaticity (corresponding to the Higgs-inflaton quartic coupling $\lambda_{h\phi}$), and then move on to that due to the tachyonic effective mass (corresponding to the Higgs-curvature non-minimal coupling ξ_h and the Higgs-inflaton trilinear coupling $\sigma_{h\phi}$).

[þ1] The comoving number density is ill-defined when the inflaton passes the regime where $\omega_{k;h}^2 < 0$.

D.3 Broad resonance

First we discuss the particle production due to the breakdown of the adiabaticity. In particular, we assume that there is the Higgs-inflaton quartic coupling

$$\mathcal{L}_{\rm int} = -\frac{\lambda_{h\phi}}{2}\phi^2 h^2, \tag{D.3.1}$$

in this section. In this case the time-dependent effective Higgs mass term is given by

$$m_h^2 = \lambda_{h\phi}\phi^2(t). \tag{D.3.2}$$

It is clear that the mass term is large enough at the end-points of the inflaton oscillation, and thus the adiabaticity is likely to be broken only at around when the inflaton crosses the origin of its potential. At around the origin of its potential, the inflaton is approximated as $\phi \simeq \Phi m_\phi (t - t_c)$, where t_c is the time when the inflaton crosses the origin. Hence we obtain

$$\left|\frac{\dot{\omega}_{k;h}}{\omega_{k;h}^2}\right| \sim \left|\frac{\lambda_{h\phi} m_\phi^2 \Phi^2 (t - t_c)}{\left(k^2/a^2 + \lambda_{h\phi} m_\phi^2 \Phi^2 (t - t_c)^2\right)^{3/2}}\right| \lesssim \frac{m_\phi^2 q^{1/2}}{k^2/a^2}, \quad q \equiv \frac{\lambda_{h\phi}\Phi^2}{4m_\phi^2}, \tag{D.3.3}$$

where q is a resonance parameter, and the inequality is saturated when $t - t_c \simeq k/a\lambda_{h\phi}^{1/2} m_\phi \Phi$. Here we ignore effects of the cosmic expansion on the adiabaticity since $m_\phi \gg H$ at least after several oscillations of the inflaton. If $q \ll 1$, the Higgs particles are produced only within narrow bands $k/a \sim m_\phi(1 \pm q)$, and hence the adiabaticity is not broken down. Since the Higgs is boson, bosonic enhancement of the previously produced Higgs particles could still cause a narrow resonance [96–98], but the cosmic expansion soon kills it in a usual case.[þ2] Thus we concentrate on the opposite case: $q \gtrsim 1$. In this case, the adiabaticity is broken at around when the inflaton crosses the origin of its potential for the modes with

$$\frac{k}{a} \lesssim p_*(t), \quad p_*(t) \equiv m_\phi q^{1/4}, \tag{D.3.4}$$

and hence these modes are produced efficiently. The production of these modes are enhanced by the previously produced particles for bosonic particles, and the number density of these modes grows exponentially with time. It is called a broad resonance, since the width of the resonance band is broad compared to the narrow resonance. Due to the phase space factor, the typical energy scale of the produced particles are estimated as $k/a \sim p_*$. Note that $q \gtrsim 1$ implies that $p_* \gtrsim m_\phi$, and hence the typical energy scale ($\sim p_*$) is comparable or larger than the inflaton mass scale.

In order to study the broad resonance quantitatively, it is useful to first ignore the cosmic expansion, and rewrite the equation of motion for the wave functions as

$$\left[\frac{d^2}{dz^2} + A_k + 2q\cos(2z)\right] h_{\vec{k}} = 0, \tag{D.3.5}$$

[þ2] The modes within the resonant band are efficiently red-shifted away if $q^2 m_\phi < H$.

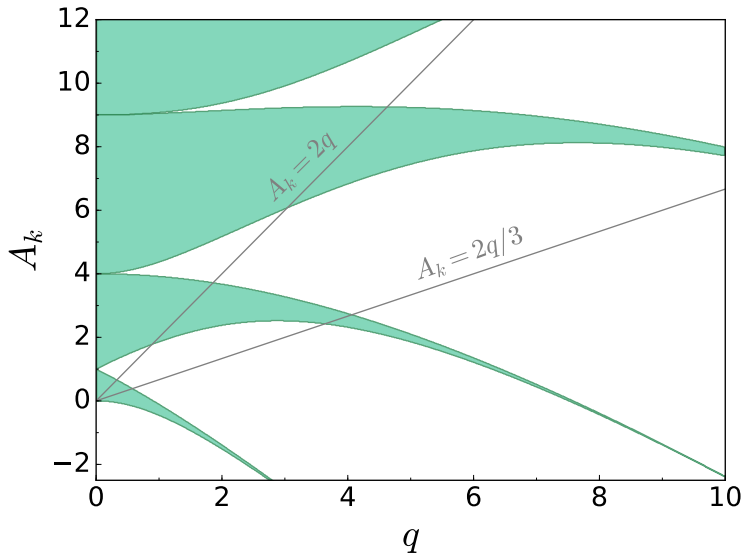

Figure D.1: The stability/instability chart of the Mathieu equation. It is the same as Fig. 4.5.

where we define the parameters as

$$z \equiv m_\phi t, \quad A_k \equiv \frac{k^2}{m_\phi^2} + 2q, \quad q \equiv \frac{\lambda_{h\phi}\Phi^2}{4m_\phi^2}. \tag{D.3.6}$$

It is the Mathieu equation, and is treated by the Floquet theory (see App. D.6). We again show the stability/instability chart of the Mathieu equation in Fig. D.1 for readers' convenience, which is the same as Fig. 4.5. There exists an exponentially growing mode in the white region, which means that a resonant particle production occurs in that parameter region. For the broad resonance case we should concentrate only on the region with $A_k \geq 2q$. As we can see from the figures, the instability bands get broader and broader as we increase q, and this is the reason why the case with $q \gg 1$ is called the broad resonance. The coefficient of the exponent of the growing factor $\mu_{\rm qtc}$ can also be calculated analytically (see Ref. [99] and App. D.6), and it is roughly given by $\mu_{\rm qtc} \sim \mathcal{O}(0.1)$.

Once we switch on the Hubble expansion, the resonance parameters A_k and q decrease with time. They pass several instability bands within the course of the Hubble expansion. This process is called a stochastic resonance in Ref. [99], and is discussed to some extent in App. D.7. Anyway, the resonance persists with the exponent of order $\mu_{\rm qtc} \sim \mathcal{O}(0.1)$ until the parameters enter the stability region at around the origin in Fig. D.1. Thus, the condition

$$p_* \lesssim m_\phi, \quad \text{or} \quad q \lesssim 1, \tag{D.3.7}$$

indicates the end of the preheating epoch. The number density of the Higgs increases as $n_{k;h} \propto e^{2\mu_{\rm qtc} m_\phi t}$ until the above condition is satisfied.

D.4 Tachyonic resonance

Here we consider the case where the resonant particle production is caused by a tachyonic mass term. First we consider the Higgs-curvature non-minimal coupling:

$$\mathcal{L}_{\rm int} = -\frac{\xi_h}{2} R h^2, \tag{D.4.1}$$

where R is the Ricci scalar. It is given in terms of the inflaton condensation as

$$R = 6\left[\dot{H} + 2H^2\right] = \frac{1}{M_{\rm Pl}^2}\left[3m_\phi^2\phi^2 - \dot{\phi}^2\right], \tag{D.4.2}$$

where H is the Hubble parameter, and we have used the Friedmann equation in the second equality. Thus the time-dependent effective Higgs mass term is

$$m_h^2(t) = \xi_h m_\phi^2 \frac{\Phi^2}{2M_{\rm Pl}^2}\left[1 + 3\cos\left(2m_\phi t\right)\right], \tag{D.4.3}$$

where we have ignored terms suppressed by H/m_ϕ. It is clear from this expression that the Higgs effective mass term can be negative during one oscillation of the inflaton. The particle production due to this tachyonic mass is called the tachyonic resonance. In order to study it quantitatively, it is again useful to first ignore the Hubble expansion, and rewrite the equation of motion of the wave function as

$$\left[\frac{d^2}{dz^2} + A_k + 2q\cos\left(2z\right)\right] h_{\vec{k}} = 0, \tag{D.4.4}$$

where we define the parameters as

$$z \equiv m_\phi t, \quad A_k \equiv \frac{k^2}{m_\phi^2} + \frac{2q}{3}, \quad q \equiv \frac{3\xi_h}{4}\frac{\Phi^2}{M_{\rm Pl}^2}. \tag{D.4.5}$$

It is again the Mathieu equation. In the present case we should see the region with $A_k \geq 2q/3$ in the stability/instability chart D.1.[b3] As we can see, the instability band is broader for the tachyonic resonance compared to the broad resonance. In other words, the tachyonic resonance is more efficient than the broad resonance. Indeed, an analytical computation shows that the growth rate of the number density X_k for $q \gg 1$ is given by [37] (see also App. D.6)

$$X_k = -\frac{x}{\sqrt{q}} A_k + 2x\sqrt{q}, \tag{D.4.6}$$

in the case of the tachyonic resonance, where $x \simeq 0.85$. Note that X_k is larger for lager q, as opposed to the case of the broad resonance. It is qualitatively understood as follows. The

[b3] Here we assume $\xi_h > 0$ for the EW vacuum stability during inflation.

time interval Δt_p during which a Higgs mode with (physical) momentum p is tachyonic is estimated as

$$m_\phi \Delta t_p \sim 1 - \frac{p^2}{m_\phi^2 q}, \quad \text{for} \quad p^2 \lesssim m_\phi^2 q. \tag{D.4.7}$$

Within one inflaton oscillation, these modes are enhanced as

$$\exp\left(m_\phi \sqrt{q} \Delta t_p\right) \sim \exp\left(\sqrt{q} - \frac{A_p}{\sqrt{q}}\right), \tag{D.4.8}$$

and hence it is proportional to $\sqrt{q}$. The typical momentum $p_*^{(\mathrm{tac})}$ enhanced by the tachyonic resonance is estimated from $A_{p_*^{(\mathrm{tac})}} = \sqrt{q}/x$, or

$$p_*^{(\mathrm{tac})} \equiv \frac{1}{\sqrt{x}} m_\phi q^{1/4}. \tag{D.4.9}$$

Note that the q dependence of the typical momentum scale is the same as that in the case of the broad resonance.

Next we consider the Higgs-inflaton trilinear coupling:

$$\mathcal{L}_{\mathrm{int}} = -\frac{\sigma_{h\phi}}{2} \phi h^2. \tag{D.4.10}$$

In this case the time-dependent Higgs effective mass term is given by

$$m_h^2 = \sigma_{h\phi} \phi(t), \tag{D.4.11}$$

and hence it is trivial to see that it becomes tachyonic within one oscillation of the inflaton condensation. Once we neglect the Hubble expansion, the equation of motion of the wave function is again written in the form of the Mathieu equation as

$$\left[\frac{d^2}{dz^2} + A_k + 2q\cos(2z)\right] h_{\vec{k}} = 0, \tag{D.4.12}$$

where the parameters are now given by

$$z \equiv \frac{m_\phi t}{2}, \quad A_k \equiv \frac{4k^2}{m_\phi^2}, \quad q \equiv \frac{2\sigma_{h\phi}\Phi}{m_\phi^2}. \tag{D.4.13}$$

Thus now we should see the region with $A_k \geq 0$ in Fig. D.1, and hence the resonance is even stronger compared to the case with the Higgs-curvature non-minimal coupling. The growth rate of the number density is again given by Eq. (D.4.6).

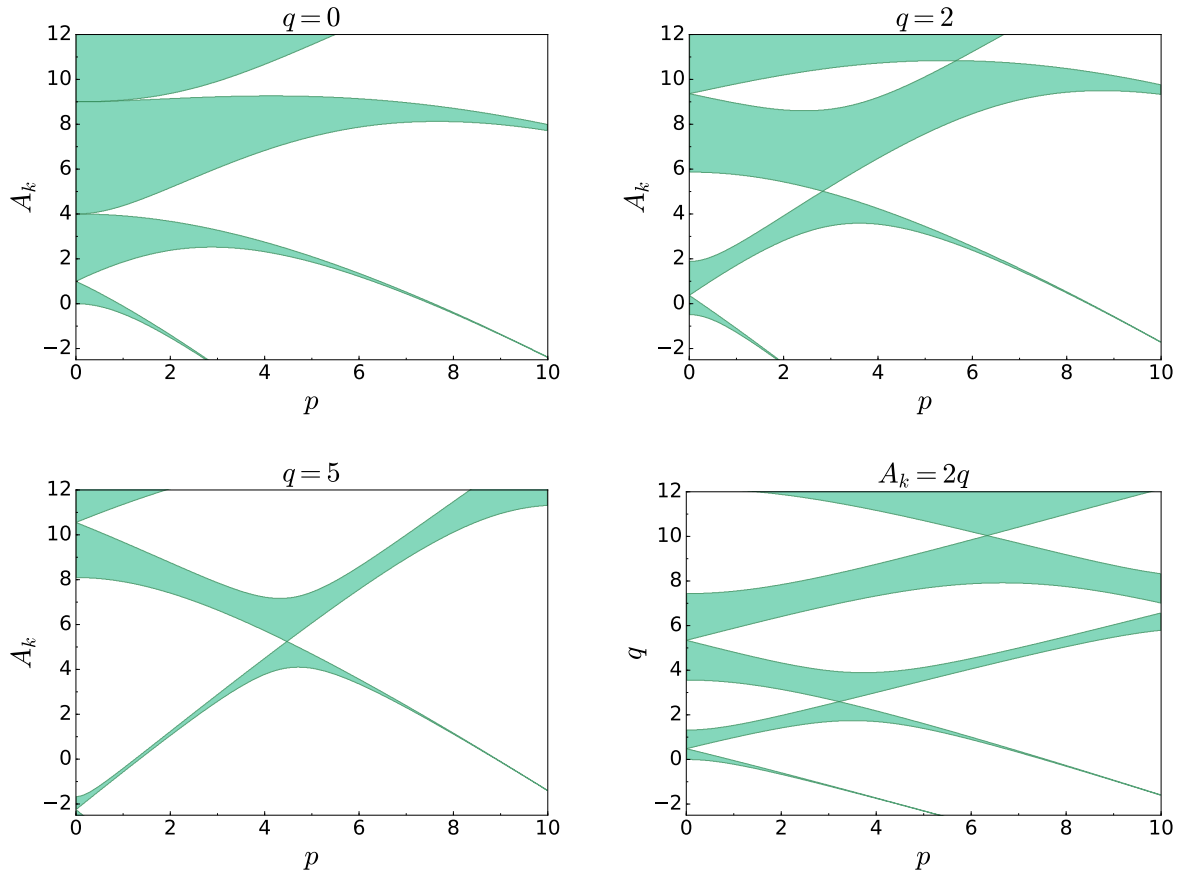

Figure D.2: The stability/instability chart of the Whittaker-Hill equation. It is the same as Fig. 4.9.

D.5 Resonance with all couplings

Now we consider the case with the Higgs-inflaton quartic/trilinear coupling as well as the Higgs-curvature non-minimal coupling:

$$\mathcal{L}_{\rm int} = -\frac{1}{2}\left[\lambda_{h\phi}\phi^2 + \xi_h R + \sigma_{h\phi}\phi\right]h^2. \tag{D.5.1}$$

In this case the time-dependent Higgs effective mass term is given by

$$m_h^2 = \left(\lambda_{h\phi} + \frac{3\xi_h m_\phi^2}{M_{\rm Pl}^2}\right)\phi^2 - \frac{\xi_h \dot{\phi}^2}{M_{\rm Pl}^2} + \sigma_{h\phi}\phi. \tag{D.5.2}$$

It is again instructive to first consider the equation of motion of the wave function with the Hubble expansion being ignored. It is now given by

$$\left[\frac{d^2}{dz^2} + A_k + 2p\cos(2z) + 2q\cos(4z)\right]h_{\vec{k}} = 0, \tag{D.5.3}$$

with the parameters defined as

$$A_k = \frac{4k^2}{m_\phi^2} + 2\left(\lambda_{h\phi} + \frac{\xi_h m_\phi^2}{M_{\rm Pl}^2}\right)\frac{\Phi^2}{m_\phi^2}, \quad z = \frac{m_\phi t}{2},$$
$$p = \frac{2\sigma_{h\phi}\Phi}{m_\phi^2}, \quad q = \left(\lambda_{h\phi} + \frac{3\xi_h m_\phi^2}{M_{\rm Pl}^2}\right)\frac{\Phi^2}{m_\phi^2}. \tag{D.5.4}$$

Note that we have now two different frequencies. This equation is called the Whittaker-Hill equation. Its stability/instability chart can be again obtained following the Floquet theory. We again show it for combinations of (p, q, A_k) in Fig. D.2 for readers' convenience, which is the same as Fig. 4.9. An interesting feature is that A_k, p and q are now independent variables even for fixed k, since we have now three parameters $\lambda_{h\phi}$, ξ_h and $\sigma_{h\phi}$. In particular, the resonance due to $\lambda_{h\phi}$ and ξ_h is strongly suppressed at around the line with

$$\lambda_{h\phi} + \frac{3\xi_h m_\phi^2}{M_{\rm Pl}^2} = 0. \tag{D.5.5}$$

It corresponds to the line $q = 0$ in Fig. D.1 if we ignore $\sigma_{h\phi}$. This case is considered carefully in Sec. 4.4. Even in that case the trilinear coupling causes the resonant particle production. Indeed, once we switch on the Hubble expansion, it dominates over the other terms in the later epoch, since it decreases slower than the other terms (it is proportional to ϕ, not ϕ^2). As the end of the resonance, p and q offer a good criteria:

$$|p| \lesssim O(1), \quad |q| \lesssim O(1). \tag{D.5.6}$$

Indeed, the modes enter the stability region at around the origin once this criteria is satisfied, as we can see from Fig. D.2.

D.6 Floquet theory

Here we summarize some basic facts of the Floquet theory without any proof. For more details, see *e.g.* Refs. [38, 100] and references therein.

D.6.1 Floquet exponent

Suppose we have the following differential equation:

$$\left[\frac{d^2}{dz^2} + A + 2qf(z)\right]h(z) = 0, \tag{D.6.1}$$

where $f(z) = f(z + \pi)$ is a periodic function. As long as the back-reaction and the Hubble expansion are negligible, the equation of motion of the Higgs is indeed this form. The Floquet theorem states that it has a solution of the form

$$h(z) = ae^{\mu z}g(z) + be^{-\mu z}g(-z), \tag{D.6.2}$$

where μ is a complex number called the Floquet exponent, $g(z) = g(z + \pi)$ is a periodic function, and a, b are some numerical constants fixed by initial conditions. The Floquet exponent μ determines the stability/instability behavior of this system: the solution grows exponentially with time as long as $\mathrm{Re}[\mu] \neq 0$.

Now we give a formula for μ. We concentrate on the Whittaker-Hill equation

$$\left[\frac{d^2}{dz^2} + A + 2p\cos(2z) + 2q\cos(4z)\right] h(z) = 0, \tag{D.6.3}$$

in the following for simplicity. Note that the Mathieu equation is just a special case ($q = 0$) of the Whittaker-Hill equation, and hence is included in our discussion below. We consider the solution

$$h(z) = e^{\mu z} g(z). \tag{D.6.4}$$

Since $g(z)$ is periodic, it is expanded as

$$g(z) = \sum_n a_n e^{2inz}. \tag{D.6.5}$$

By inserting it to the Whittaker-Hill equation, we obtain the linear equations for the coefficients as

$$\hat{M}(\mu) \cdot \vec{a} = 0, \tag{D.6.6}$$

where

$$\vec{a} \equiv \begin{pmatrix} \ldots & a_{-2} & a_{-1} & a_0 & a_1 & a_2 & \ldots \end{pmatrix}^t, \tag{D.6.7}$$

and

$$\hat{M}(\mu) \equiv \begin{pmatrix} \ddots & \ddots & \ddots & \ddots & \ddots & & & \\ & \tilde{q}_{n-1} & \tilde{p}_{n-1} & 1 & \tilde{p}_{n-1} & \tilde{q}_{n-1} & 0 & 0 \\ & 0 & \tilde{q}_n & \tilde{p}_n & 1 & \tilde{p}_n & \tilde{q}_n & 0 \\ & 0 & 0 & \tilde{q}_{n+1} & \tilde{p}_{n+1} & 1 & \tilde{p}_{n+1} & \tilde{q}_{n+1} \\ & & & & \ddots & \ddots & \ddots & \ddots & \ddots \end{pmatrix}, \tag{D.6.8}$$

with $\tilde{p}_n$ and $\tilde{q}_n$ being defined as

$$\tilde{p}_n \equiv \frac{p}{A - (i\mu - 2n)^2}, \quad \tilde{q}_n \equiv \frac{q}{A - (i\mu - 2n)^2}. \tag{D.6.9}$$

Thus the Floquet exponent μ is obtained as a solution of the equation

$$\det\left[\hat{M}(\mu)\right] = 0. \tag{D.6.10}$$

Actually we can show that

$$\det\left[\hat{M}(\mu)\right] = 1 + \frac{\left(\det\left[\hat{M}(0)\right] - 1\right)\left(1 - \cos\left(\pi\sqrt{A}\right)\right)}{\cos\left(i\pi\mu\right) - \cos\left(\pi\sqrt{A}\right)}, \tag{D.6.11}$$

from the analyticity of the both sides [100], and hence μ is given by

$$\mu = -\frac{i}{\pi}\arccos\left[1 + \det\left[\hat{M}(0)\right]\left(\cos\left(\pi\sqrt{A}\right) - 1\right)\right]. \tag{D.6.12}$$

The matrix $\hat{M}$ is infinite-dimensional, but we need to retain only several tens components at around M_{00} to compute the determinant numerically, since the off-diagonal parts get smaller as the (absolute value of the) indices get larger. Thus this formula is useful to evaluate μ numerically for given A, p and q.

D.6.2 Boundary of stability/instability regions

Now we discuss how to determine the boundaries of the stability/instability regions of the Whittaker-Hill equation. It is known that

$$\mathrm{Re}\left[\mu\right] = 0, \quad \mathrm{Im}\left[\mu\right] \in \mathbb{Z}, \tag{D.6.13}$$

on the boundaries [38]. Thus we can expand the solution by the harmonic functions as

$$h_1(z) = \sum_{n=0}^{\infty} c_{2n}\cos\left(2nz\right), \tag{D.6.14}$$

$$h_2(z) = \sum_{n=0}^{\infty} s_{2n+1}\sin\left((2n+1)z\right), \tag{D.6.15}$$

$$h_3(z) = \sum_{n=0}^{\infty} c_{2n+1}\cos\left((2n+1)z\right), \tag{D.6.16}$$

$$h_4(z) = \sum_{n=1}^{\infty} s_{2n}\sin\left(2nz\right), \tag{D.6.17}$$

where we have classified the solutions according to the properties under $z \to -z$ and $z \to z + \pi$. By substituting them into the Whittaker-Hill equation, we obtain linear equations for the coefficients as in the previous subsection. Thus, by requiring the determinant of the associated matrices to vanish, we obtain the values of (A, p, q) where the solution takes one of the above forms. It is nothing but a point on the boundaries of the stability/instability regions. We have drawn Figs. 4.5 and 4.9 (and of course Figs. D.1 and D.2) following this method.

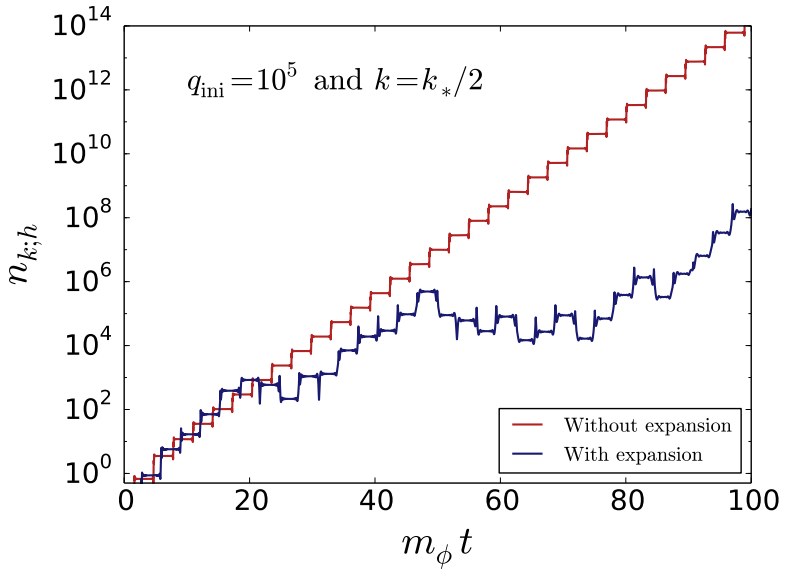

Figure D.3: The time evolution of the number density with and without the cosmic expansion. The parameters are taken as $\Phi_{\rm ini} = \sqrt{2}M_{\rm Pl}$, $q_{\rm ini} = 10^5$ and $k = k_*/2$ with $k_* = m_\phi q_{\rm ini}^{1/4}$. The backreaction to ϕ is ignored.

D.7 Effects of cosmic expansion

In this section we briefly discuss effects of cosmic expansion on the resonant particle productions. We concentrate on the cases with only $\lambda_{h\phi}$ or ξ_h in this section, but a similar argument holds for more general cases.

■ Broad resonance

First we consider the case with only $\lambda_{h\phi}$. In this case, the resonance parameters are given by (see Eq. (D.3.6))

$$A_k = \frac{k^2}{a^2} + \frac{\lambda_{h\phi}\Phi^2}{2m_\phi^2}, \quad q = \frac{\lambda_{h\phi}\Phi^2}{4m_\phi^2}. \tag{D.7.1}$$

Once we include the cosmic expansion, the inflaton oscillation amplitude Φ decreases with time, so do A_k and q. Thus each mode scans the stability/instability chart of the Mathieu equation in the course of the cosmic expansion. An interesting feature is that the number density can even decrease for some time, and hence the resonance may be suppressed compared to the case without the cosmic expansion. In order to see this point, we plot the time evolution of the number density $n_{k;h}$ with/without cosmic expansion in Fig. D.3. We have taken the parameters as $\Phi_{\rm ini} = \sqrt{2}M_{\rm Pl}$, the resonance parameter $q_{\rm ini} \equiv \lambda_{h\phi}\Phi_{\rm ini}^2/4m_\phi^2 = 10^5$, and $k = k_*/2$ where $k_* \equiv m_\phi q_{\rm ini}^{1/4}$. The number density without the cosmic expansion (the red line) always increases with time, while it with the cosmic expansion (the blue line) indeed decreases for some time, resulting in less efficient growth. Nevertheless, the number density

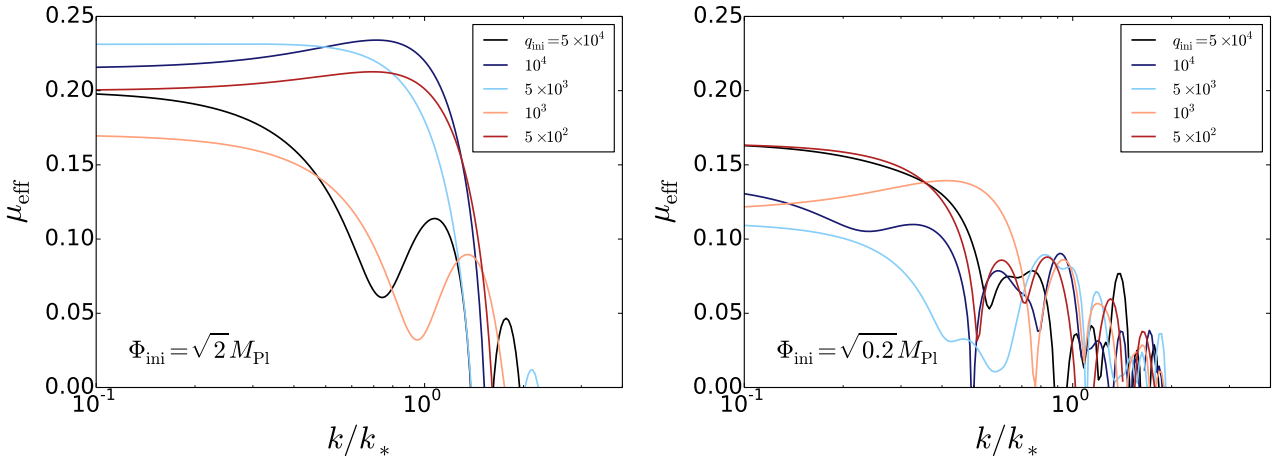

Figure D.4: The effective Floquet exponent $\mu_{\rm eff}$ as a function of q and k. The initial inflaton amplitude is $\Phi_{\rm ini} = \sqrt{2}M_{\rm Pl}$ and $\sqrt{0.2}M_{\rm Pl}$ in the left and right panels, respectively. The average is taken from the beginning of the inflaton oscillation till t_e with which $q(t_{\rm e})/q_{\rm ini} = 10^{-2}$.

grows with time on average. In order to estimate the growth rate with the cosmic expansion, we may define an effective Floquet exponent $\mu_{\rm eff}$ as

$$\mu_{\rm eff}(k, t_{\rm i}, t_{\rm e}) \equiv \frac{\log\left(n_{k;h}(t_{\rm e})/n_{k;h}(t_{\rm i})\right)}{2\,(t_{\rm e} - t_{\rm i})}. \tag{D.7.2}$$

In Fig. D.4 we plot $\mu_{\rm eff}$ for different values of $q_{\rm ini}$ and k. The initial inflaton amplitude is taken as $\Phi_{\rm ini} = \sqrt{2}M_{\rm Pl}$ and $\sqrt{0.2}M_{\rm Pl}$ in the left and right panels, respectively. The time t_i is taken as the beginning of the inflaton oscillation, and t_e is a solution of the equation $q(t_e) = 10^{-2}q_{\rm ini}$. As we can see from Fig. D.4, $\mu_{\rm eff}$ is a complicated function of q. In particular, it does not always increase with q. Still, the order of magnitude does not depend much on the value of q, and hence we may roughly estimate it as $\mu_{\rm eff} \sim O(0.1)$ almost independently of $\Phi_{\rm ini}$ and q. This result is used in Sec. 4.2. Another interesting feature of Fig. D.4 is that, almost all modes with $k \lesssim k_*$ experience the growth since they scan the stability/instability chart. Thus the resonance band itself is broader than the case without the cosmic expansion.

■ Tachyonic resonance

Next we consider the case with only ξ_h. In this case, the resonance parameters are given by (see Eq. (D.4.5))

$$A_k = \frac{k^2}{m_\phi^2} + \frac{2q}{3}, \quad q = \frac{3\xi_h}{4}\frac{\Phi^2}{M_{\rm Pl}^2}, \tag{D.7.3}$$

and hence again they decrease with time one we turn on the cosmic expansion. In Fig. D.5, we show the numerical results of the time evolution of the number density with the cosmic expansion. The number density is defined only around the end points of the inflaton oscillation $\dot\phi = 0$, and hence we evaluated it only at the points $\dot\phi = 0$. As we can see from the

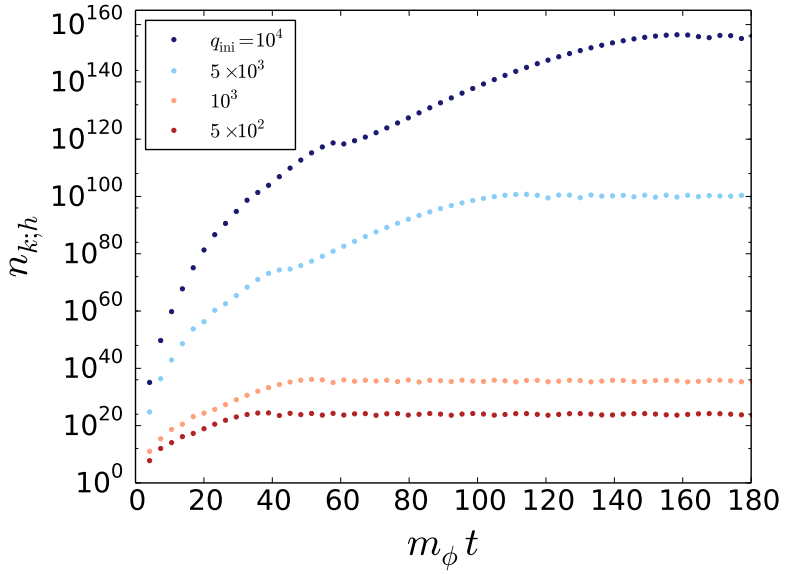

Figure D.5: The time evolution of the number density with ξ_h for several values of $q_{\rm ini}$. The parameters are taken as $\Phi_{\rm ini} = \sqrt{2}M_{\rm Pl}$ and $k = k_*/2$. The number density is evaluated only at the points $\dot{\phi} = 0$. The backreaction to ϕ is ignored.

figure, the number density grows rather in a power-law like way with time until $q \lesssim 1$ once we include the cosmic expansion. It may be understood as follows. As we saw in App. D.4, the growth rate X_k is proportional to $q^{1/2}$ for the modes with $k \lesssim k_*$. Thus, the number density grows as

$$n_k \propto \exp\left[\int^t m_\phi dt\, X_k\right] \simeq \exp\left[2x\sqrt{2\xi_h}\int^t \frac{dt}{t}\right] \simeq \left(\frac{t}{t_{\rm ini}}\right)^{2.4\xi_h}, \tag{D.7.4}$$

where we have used Eq. (D.1.8). In Sec. 4.3, we introduced the effective number of oscillation $n_{\rm eff}$ to include the effect of the time integration in the above expression. Anyway, the resonance parameter q is rather small in the case of our interest since otherwise the EW vacuum is soon destabilized after inflation, and hence only first a few inflaton oscillation is important. Thus, $n_{\rm eff}$ is of order unity in the case of our interest.

Appendix E

Classical lattice simulation

In this appendix we review the basics of the classical lattice simulation. We first show that the classical approximation is valid in the large occupation number limit, and then discuss what initial condition is suitable for the simulation. We explain some details on the practical implementation of the classical lattice simulation in the end.

E.1 Wigner function

Here we review the Winger function, which is a necessary ingredient of the next section. We mainly follow Refs. [35, 101], and consider the quantum mechanics for simplicity in this section. We retain $\hbar$ explicitly in this section to see the meaning of a classical limit.

E.1.1 Definition and characteristics

Let us first define a Weyl transformation $\tilde{A}$ of an operator $\hat{A}$:

$$\tilde{A}(x,p) \equiv \int dy\, e^{-ipy/\hbar} \left\langle x + \frac{y}{2} \right| \hat{A} \left| x - \frac{y}{2} \right\rangle, \tag{E.1.1}$$

where x and p are the position and the momentum, respectively. It is rewritten in terms of the integration over the momentum eigenstates as

$$\tilde{A}(x,p) = \int du\, e^{ixu/\hbar} \left\langle p + \frac{u}{2} \right| \hat{A} \left| p - \frac{u}{2} \right\rangle, \tag{E.1.2}$$

where we have used

$$\langle x|p\rangle = \frac{1}{\sqrt{2\pi\hbar}} \exp\left(\frac{ixp}{\hbar}\right), \quad \int dy\, \exp\left(\frac{iyp}{\hbar}\right) = 2\pi\hbar\delta(p). \tag{E.1.3}$$

Then we obtain

$$\mathrm{Tr}\left[\hat{A}\hat{B}\right] = \frac{1}{2\pi\hbar} \int dxdp\, \tilde{A}(x,p)\tilde{B}(x,p). \tag{E.1.4}$$

In particular, by identifying the operator $\hat{B}$ as the density matrix $\hat{\rho} = |\psi\rangle\langle\psi|$ with $|\psi\rangle$ being a given state, we obtain

$$\langle A \rangle \equiv \mathrm{Tr}\left[\hat{\rho}\hat{A}\right] = \frac{1}{2\pi\hbar}\int dxdp\, \tilde{\rho}\tilde{A}. \tag{E.1.5}$$

We thus define the Wigner function $W(x,p)$ as

$$W(x,p) \equiv \frac{\tilde{\rho}(x,p)}{2\pi\hbar} = \frac{1}{2\pi\hbar}\int dy\, e^{-ipy/\hbar}\psi\left(x+y/2\right)\psi^*\left(x-y/2\right), \tag{E.1.6}$$

where the wave function $\psi(x)$ is defined as $\psi(x) \equiv \langle x|\psi\rangle$. The expectation value of an operator $\hat{A}$ is now given by the convolution of the Weyl transformed function $\tilde{A}$ and the Wigner function:

$$\langle A \rangle = \int dxdp\, \tilde{A}(x,p)W(x,p). \tag{E.1.7}$$

In this sense, the Wigner function is analogous to the classical phase-space probability distribution function.

Before studying the Wigner function in detail, here we also define an inverse Weyl-transformation for later convenience. Let us define the following operator:

$$\Delta(x,p) \equiv \int \frac{dudv}{2\pi\hbar}\exp\left(\frac{i\left(x-\hat{x}\right)u}{\hbar} + \frac{i\left(p-\hat{p}\right)v}{\hbar}\right). \tag{E.1.8}$$

It is equivalent to the following expressions:

$$\Delta(x,p) = \int du\, e^{ixu/\hbar}\left|p-\frac{u}{2}\right\rangle\left\langle p+\frac{u}{2}\right| = \int dy\, e^{ipy/\hbar}\left|x+\frac{y}{2}\right\rangle\left\langle x-\frac{y}{2}\right|. \tag{E.1.9}$$

We now show this statement. By using the Campbell-Baker-Hausdorff (CBH) identity

$$e^{\hat{A}+\hat{B}} = e^{\hat{A}}e^{\hat{B}}e^{-\left[\hat{A},\hat{B}\right]/2}, \tag{E.1.10}$$

we obtain

$$\exp\left(\frac{i\left(x-\hat{x}\right)u}{\hbar} + \frac{i\left(p-\hat{p}\right)v}{\hbar}\right) = \exp\left(\frac{i\left(ux+vp\right)}{\hbar} + \frac{iuv}{2\hbar}\right)e^{-iu\hat{x}/\hbar}e^{-iv\hat{p}/\hbar}. \tag{E.1.11}$$

Then we show that

$$\begin{aligned}\Delta(x,p) &= \int \frac{dudvdu'dv'du''}{2\pi\hbar}e^{i(ux+vp)/\hbar+iuv/2\hbar}e^{-iuv'/\hbar}e^{-u'v/\hbar}\left|u''\right\rangle\left\langle u''\right|\left.v'\right\rangle\left\langle v'\right|\left.u'\right\rangle\left\langle u'\right| \\ &= 2\int du'e^{-2i(p-u')x/\hbar}\left|2p-u'\right\rangle\left\langle u'\right| = \int due^{iux/\hbar}\left|p-\frac{u}{2}\right\rangle\left\langle p+\frac{u}{2}\right|.\end{aligned} \tag{E.1.12}$$

In the same way, we can show the second equality in Eq. (E.1.9). Now it is trivial that

$$\hat{A}(\hat{x},\hat{p}) = \int \frac{dxdp}{2\pi\hbar}\tilde{A}(x,p)\Delta(x,p), \tag{E.1.13}$$

and hence $\Delta(x,p)$ is the inverse Weyl-transformation operator. It is used in Sec. E.1.3. Now we summarize some characteristics of the Wigner function.

■ **Reality**

The Wigner function is real. We can show this as follows:

$$\begin{aligned} W(x,p)^* &= \frac{1}{2\pi\hbar}\int dy\, e^{ipy/\hbar}\psi^*(x+y/2)\psi(x-y/2) \\ &= \frac{1}{2\pi\hbar}\int dy\, e^{-ipy/\hbar}\psi^*(x-y/2)\psi(x+y/2) = W(x,p), \end{aligned} \tag{E.1.14}$$

where we have changed $y \to -y$ at the second line.

■ **Projection onto x-axis (p-axis)**

Once we project the Wigner function onto x-axis (p-axis), it is the probability distribution function for x (p). Indeed, we find that

$$\int dpW(x,p) = \int dy\,\delta(y)\psi(x+y/2)\psi^*(x-y/2) = \left|\psi(x)\right|^2, \tag{E.1.15}$$

and in a similar way for the projection onto the p-axis.

■ **Normalization**

The normalization of the Wigner function is given by

$$\int dxdp\, W(x,p) = \int dx \left|\psi(x)\right|^2 = 1. \tag{E.1.16}$$

■ **Upper bound**

The Wigner function cannot be arbitrary large. Indeed, we obtain from the Cauchy-Schwarz inequality that

$$\begin{aligned} \left|W(x,p)\right| &= \frac{1}{\pi\hbar}\left|\int dy\,\psi_1(y)\psi_2^*(y)\right| \\ &\le \frac{1}{\pi\hbar}\left(\int dy\,\left|\psi_1(y)\right|^2\right)^{1/2}\left(\int dy\,\left|\psi_2(y)\right|^2\right)^{1/2} = \frac{1}{\pi\hbar}, \end{aligned} \tag{E.1.17}$$

where we have defined

$$\psi_1(y) \equiv e^{-ipy/\hbar}\frac{\psi(x+y/2)}{\sqrt{2}}, \quad \psi_2(y) \equiv \frac{\psi(x-y/2)}{\sqrt{2}}. \tag{E.1.18}$$

■ **Necessity of the Weyl transformation**

As we saw above, in order to obtain the expectation value using the Wigner function, the operator must be Weyl-transformed. It sometimes leads $O(\hbar)$ differences from the classical quantity due to the non-commutativity of $(\hat{x}, \hat{p})$. We shall see this in an example shown in the next subsection.

■ **Non-positivity**

The Wigner function is not semi-positive definite in general. In order to see it, let us consider two different states ψ_a and ψ_b that are orthogonal to each other. Then, by denoting the Wigner functions corresponding to $\psi_{a/b}$ as $W_{a/b}$ respectively, we obtain

$$\int dxdp W_a(x,p) W_b(x,p) \propto \mathrm{Tr}\left[\hat{\rho}_a \hat{\rho}_b\right] = 0. \tag{E.1.19}$$

It means that the Wigner function generally takes negative values for some regions in the phase-space, otherwise the right-hand side must be larger than zero.[♭1]

The last three properties are the main differences between the Wigner function and the classical phase-space distribution function. Although the former two can be disregarded in the quasi-classical limit ($\hbar \to 0$), we should carefully examine the last property for state by state. If we are lucky enough so that the Wigner function is semi-positive definite for a given state, then we can regard it as the classical phase-space distribution function in the quasi-classical limit. Fortunately, it is the case for the Wigner function corresponding to the initial state for the preheating epoch as we see in the next section.

E.1.2 Example: harmonic oscillator

In this subsection, we consider the harmonic oscillator in the Wigner-Weyl formalism as an example. The Hamiltonian is given by

$$\hat{H} = \frac{\hat{p}^2}{2m} + \frac{m\omega^2}{2}\hat{x}^2. \tag{E.1.20}$$

The lowest and second lowest energy states are respectively given by

$$\psi_0(x) = \frac{1}{\sqrt[4]{\pi}\sqrt{a}} e^{-x^2/2a^2}, \tag{E.1.21}$$

$$\psi_1(x) = \frac{1}{\sqrt[4]{\pi}} \sqrt{\frac{2}{a}} \frac{x}{a} e^{-x^2/2a^2}, \tag{E.1.22}$$

[♭1] At this point, there is a logical possibility that the Wigner functions corresponding to orthogonal states do not have overlaps. However, as we see in the next subsection, it is not the case.

where a is defined as $a \equiv \sqrt{\hbar/m\omega}$. The corresponding Wigner functions are given by

$$W_0(x,p) = \frac{1}{\pi\hbar}\exp\left[-\frac{x^2}{a^2} - \frac{a^2p^2}{\hbar^2}\right], \tag{E.1.23}$$

$$W_1(x,p) = \frac{1}{\pi\hbar}\left(-1 + \frac{2x^2}{a^2} + \frac{2a^2p^2}{\hbar^2}\right)\exp\left[-\frac{x^2}{a^2} - \frac{a^2p^2}{\hbar^2}\right]. \tag{E.1.24}$$

Note that $W_1(x,p)$ can be negative, while $W_0(x,p)$ is positive definite.

Now we calculate $\langle H\rangle$ and $\langle H^2\rangle$ for the lowest energy state in the Wigner-Weyl formulation. We shall learn the importance of the Weyl transformation from this example. It is trivial to calculate $\langle H\rangle$:

$$\langle H\rangle = \int dxdpW_0(x,p)\left(\frac{p^2}{2m} + \frac{m\omega^2}{2}x^2\right) = \frac{1}{2}\hbar\omega. \tag{E.1.25}$$

If one views $W_0(x,p)$ as the probability distribution function, one may naively expect that the dispersion $\langle H^2\rangle - \langle H\rangle^2 \equiv \Delta E \neq 0$ because the distribution of (x,p) is not restricted to the circle with a constant energy. However, since ψ_0 is the energy eigenstate, the dispersion must vanish. The key to solve this apparent contradiction is the Weyl transformation. In fact, the Weyl-transformed Hamiltonian squared is

$$\tilde{H}^2(x,p) = H^2(x,p) - \left(\frac{\hbar\omega}{2}\right)^2, \tag{E.1.26}$$

that is different from the classical Hamiltonian squared by $O(\hbar^2)$. Then, the expectation value of the Hamiltonian squared is given by

$$\left\langle H^2\right\rangle = \int dxdpW_0(x,p)\left(H^2(x,p) - \frac{\hbar^2\omega^2}{4}\right) = \frac{\hbar^2\omega^2}{4}, \tag{E.1.27}$$

and hence the dispersion is zero as expected. Therefore, the Wigner function is different from the classical probability distribution function even if it is positive-definite in the sense that the operators must be Weyl-transformed to obtain the correct expectation value, which may make differences of order $O(\hbar)$. Of course we can disregard this difference in the quasi-classical limit.

E.1.3 Time evolution

In this subsection, we derive the time evolution equation for the Wigner function. We shall show that, when operators satisfy the following commutation relation

$$i\hbar\hat{C} = \left[\hat{A},\hat{B}\right], \tag{E.1.28}$$

the Weyl-transformed operators satisfy

$$\begin{aligned} i\hbar\tilde{C}(x,p) &= \left\{\tilde{A}(x,p),\tilde{B}(x,p)\right\}_{\mathrm{MB}} \\ &= 2i\sin\left[\frac{\hbar}{2}\left(\frac{\partial}{\partial x_A}\frac{\partial}{\partial p_B} - \frac{\partial}{\partial x_B}\frac{\partial}{\partial p_A}\right)\right]\tilde{A}(x,p)\tilde{B}(x,p), \end{aligned} \tag{E.1.29}$$

where $\partial/\partial x_O$ and $\partial/\partial p_O$ act only on the arguments of a Weyl-transformed operator $\tilde{O}(x,p)$, and the subscript MB is the abbreviation for a "Moyal bracket." Note that

$$\left\{\tilde{A},\tilde{B}\right\}_{\rm MB} = i\hbar\left[\left\{\tilde{A},\tilde{B}\right\}_{\rm PB} + O(\hbar^2)\right], \tag{E.1.30}$$

where $\{O_1,O_2\}_{\rm PB}$ is the Poisson bracket. Now we show the above statement. We use Eq. (E.1.13):

$$\begin{aligned}\left[\hat{A},\hat{B}\right] = &\int \frac{du_a dv_a dx_a dp_a}{(2\pi\hbar)^2}\frac{du_b dv_b dx_b dp_b}{(2\pi\hbar)^2}\\ &\times \tilde{A}(x_a,p_a)\tilde{B}(x_b,p_b)\left[e^{i(x_a-\hat{x})u_a/\hbar+i(p_a-\hat{p})v_a/\hbar}, e^{i(x_b-\hat{x})u_b/\hbar+i(p_b-\hat{p})v_b/\hbar}\right].\end{aligned} \tag{E.1.31}$$

From the CBH identity, we obtain

$$\left[e^{-iu_a\hat{x}/\hbar-iv_a\hat{p}/\hbar}, e^{-iu_b\hat{x}/\hbar-iv_b\hat{p}/\hbar}\right] = 2i\sin\left[\frac{\hbar}{2}(v_au_b - v_bu_a)\right]e^{-i(u_a+u_b)\hat{x}/\hbar-i(v_a+v_b)\hat{p}/\hbar}. \tag{E.1.32}$$

By doing integration by parts, we get

$$\begin{aligned}\left[\hat{A},\hat{B}\right] =&2i\left(\prod_{o=a,b}\int\frac{du_o dv_o dx_o dp_o}{(2\pi\hbar)^2}\right)\left(\sin\left[\frac{\hbar}{2}\left(\frac{\partial}{\partial x_a}\frac{\partial}{\partial p_b}-\frac{\partial}{\partial x_b}\frac{\partial}{\partial p_a}\right)\right]\tilde{A}(x_a,p_a)\tilde{B}(x_b,p_b)\right)\\ &\times\exp\left[\frac{i}{\hbar}(x_au_a+p_av_a+x_bu_b+p_bv_b-(u_a+u_b)\hat{x}-(v_a+v_b)\hat{p})\right].\end{aligned} \tag{E.1.33}$$

After changing the variables as

$$u_1\equiv u_a+u_b,\ v_1\equiv v_a+v_b,\ u_2\equiv u_a-u_b,\ v_2\equiv v_a-v_b, \tag{E.1.34}$$

and integrating over these variables, we obtain

$$\left[\hat{A},\hat{B}\right] = \int\frac{dxdp}{2\pi\hbar}\left(2i\sin\left[\frac{\hbar}{2}\left(\frac{\partial}{\partial x_A}\frac{\partial}{\partial p_B}-\frac{\partial}{\partial x_B}\frac{\partial}{\partial p_A}\right)\right]\tilde{A}(x,p)\tilde{B}(x,p)\right)\Delta(x,p). \tag{E.1.35}$$

We have thus proven Eq. (E.1.29). The density matrix satisfies

$$i\hbar\frac{\partial\hat{\rho}}{\partial t} = \left[\hat{H},\hat{\rho}\right], \tag{E.1.36}$$

and hence, the time evolution of the Winger function is given by

$$\begin{aligned}i\hbar\frac{\partial W(x,p)}{\partial t} =&2i\sin\left[\frac{\hbar}{2}\left(\frac{\partial}{\partial x_H}\frac{\partial}{\partial p_W}-\frac{\partial}{\partial x_W}\frac{\partial}{\partial p_H}\right)\right]\tilde{H}(x,p)W(x,p)\\ =&i\hbar\left[\left\{\tilde{H},W\right\}_{\rm PB}+O(\hbar^2)\right].\end{aligned} \tag{E.1.37}$$

Thus the time evolution equation of the Wigner function results in the classical Liouville equation in the quasi-classical limit ($\hbar\to 0$). In other words, we correctly describe the time evolution of the Winger function in the quasi-classical limit if we follow the classical equation of motion of the variables x and p with the initial distribution function given by the initial Wigner function, as long as the Wigner function is semi-positive definite at the initial time. It is the key background of the quasi-classical treatment of the preheating dynamics.

E.2 Initial condition for classical lattice simulation

Now we study the initial condition for the classical lattice simulation of the preheating dynamics. We follow the discussion in Ref. [35], and take $\hbar = 1$ in this section.

E.2.1 Wave function of a vacuum

We consider the quadratic action of a real scalar field in the FLRW background. We consider the following action for a real scalar

$$S = \int d^4x \sqrt{-g}\left[-\frac{1}{2}g^{\mu\nu}\partial_\mu\phi\partial_\nu\phi - \frac{1}{2}m^2\phi^2\right], \tag{E.2.1}$$

where the metric is taken as

$$ds^2 = dt^2 - a^2(t)dx^i dx^i. \tag{E.2.2}$$

We define the rescaled field φ and the conformal time η as

$$\varphi = a\phi, \tag{E.2.3}$$
$$dt = ad\eta. \tag{E.2.4}$$

The Hamiltonian is given by

$$H = \frac{1}{2}\int d^3k\left[\pi_{\vec{k}}\pi^*_{\vec{k}} + \omega_k^2\varphi_{\vec{k}}\varphi^*_{\vec{k}} + \frac{a'}{a}\left(\varphi_{\vec{k}}\pi^*_{\vec{k}} + \pi_{\vec{k}}y^*_{\vec{k}}\right)\right], \tag{E.2.5}$$

where

$$\pi_{\vec{k}} \equiv \frac{\delta\mathcal{L}(\varphi,\varphi')}{\delta\varphi'_{\vec{k}}} = \varphi'_{\vec{k}} - \frac{a'}{a}\varphi_{\vec{k}}, \tag{E.2.6}$$
$$\omega_k^2 = k^2 + m^2, \tag{E.2.7}$$

and the primes denote derivations with respect to the conformal time. Here the Fourier transformation is defined as

$$\Phi(x) = \frac{1}{(2\pi)^{3/2}}\int d^3k\,\Phi_{\vec{k}}e^{i\vec{k}\cdot\vec{x}}. \tag{E.2.8}$$

Due to the reality of ϕ, the Fourier components satisfy $\varphi_{-\vec{k}} = \varphi^*_{\vec{k}}$. The equation of motion for the Fourier component is

$$\varphi''_{\vec{k}} + \left(\omega_k^2 - \frac{a''}{a}\right)\varphi_{\vec{k}} = 0. \tag{E.2.9}$$

We first treat the time evolution in the Heisenberg picture. We expand φ and π as

$$\varphi_{\vec{k}} = f_k(\eta)a(\vec{k},\eta_0) + f_k^*(\eta)a^\dagger(-\vec{k},\eta_0), \tag{E.2.10}$$
$$\pi_{\vec{k}} = -i\left[g_k(\eta)a(\vec{k},\eta_0) - g_k^*a^\dagger(-\vec{k},\eta_0)\right] \tag{E.2.11}$$

where the initial conditions are taken as $f_k(\eta_0) = 1/\sqrt{2\omega_k}$ and $g_k(\eta_0) = \sqrt{\omega_k/2}$. From the relation between φ and π, the mode function g_k is related to f_k as

$$g_k = i\left(f_k' - \frac{a'}{a} f_k\right). \tag{E.2.12}$$

From the commutation relation

$$\left[\varphi_{\vec{k}}(\eta), \pi^\dagger_{\vec{k}'}(\eta)\right] = i\delta\left(\vec{k} - \vec{k}'\right), \tag{E.2.13}$$

we obtain the following Wronskian condition:

$$g_k f_k^* + g_k^* f_k = i\left(f_k' f_k^* - f_k'^* f_k\right) = 1. \tag{E.2.14}$$

We are interested in the following state defined at a time $\eta = \eta_0$ as

$$a\left(\vec{k}, \eta_0\right)\left|0, \eta_0\right\rangle = 0. \tag{E.2.15}$$

In the Heisenberg picture, the operators satisfy

$$\left\{\varphi_{\vec{k}}(\eta) + i\gamma_k^{-1}(\eta)\pi_{\vec{k}}(\eta)\right\}\left|0, \eta_0\right\rangle_H = 0, \tag{E.2.16}$$

where γ_k is defined as

$$\gamma_k \equiv \frac{g_k^*}{f_k^*} = \frac{1}{2\left|f_k\right|^2}\left(1 - 2iF_k\right), \quad F_k = \mathrm{Im}\left[f_k^* g_k\right]. \tag{E.2.17}$$

On the other hand, in order to connect with the Wigner function, we should move from the Heisenberg picture to the Schrödinger picture. In the Schrödinger picture, the time evolution of the state is determined by

$$Sa\left(\vec{k}, \eta_0\right) S^{-1}\left|0, \eta\right\rangle_S = 0, \tag{E.2.18}$$

or equivalently

$$\left\{\varphi_{\vec{k}}(\eta_0) + i\gamma_k^{-1}(\eta)\pi_{\vec{k}}(\eta_0)\right\}\left|0, \eta\right\rangle_S = 0, \tag{E.2.19}$$

where S is the S-matrix. Note that

$$S^{-1}O(\eta_0)S = O(\eta), \quad \text{or} \quad SO(\eta)S^{-1} = O(\eta_0), \tag{E.2.20}$$

for operators in the Heisenberg picture. Then, since $\pi_{\vec{k}} = -i\partial/\partial\varphi_{-\vec{k}}$ in the coordinate representation, the wave function is given by

$$\begin{aligned}\Psi(\varphi) =& \bar{\mathcal{N}} \exp\left[-\int d^3k\, \gamma_k(\eta)\varphi_{\vec{k}}(\eta_0)\varphi_{-\vec{k}}(\eta_0)\right] \\ =& \bar{\mathcal{N}} \exp\left[-\int d^3k\, \frac{\left|\varphi_{\vec{k}}(\eta_0)\right|^2}{2\left|f_k(\eta)\right|^2}\left(1 - 2iF_k(\eta)\right)\right].\end{aligned} \tag{E.2.21}$$

Thus we obtain the Wigner function as

$$W(\varphi,\pi) = \frac{1}{(2\pi)^2}\int d\psi d\psi^* \exp\left[-i\int d^3k\left(\pi_{\vec{k}}\psi^*_{\vec{k}} + \pi^*_{\vec{k}}\psi_{\vec{k}}\right)\right]\Psi^*\left(\varphi - \frac{\psi}{2}\right)\Psi\left(\varphi + \frac{\psi}{2}\right)$$
$$= \mathcal{N}\exp\left[-\int d^3k \frac{\left|\varphi_{\vec{k}}\right|^2}{\left|f_k(\eta)\right|^2}\right]\exp\left[-\int d^3k \left|f_k(\eta)\right|^2\left|\pi_{\vec{k}} - \frac{F_k\varphi_{\vec{k}}}{\left|f_k(\eta)\right|^2}\right|^2\right], \tag{E.2.22}$$

up to the overall constant. In particular, the Wigner function is positive definite for the vacuum state, and hence we can safely view it as the classical phase-space distribution function in the quasi-classical limit.

E.2.2 Semiclassical behavior

We call the limit

$$f_k \gg \frac{1}{\sqrt{2\omega_k}}, \quad g_k \gg \sqrt{\frac{\omega_k}{2}}, \tag{E.2.23}$$

as the quasi-classical limit. In this limit Eq. (E.2.14) reduces to

$$g_k f_k^* + g_k^* f_k = i\left(f_k' f_k^* - f_k'^* f_k\right) \simeq 0. \tag{E.2.24}$$

It means that the non-commutative behavior of φ and π is suppressed by the factor $1/|g_k f_k|$. The factor $\hbar$ always comes with the commutation relation, and hence it is equivalent to the limit $\hbar \to 0$. As we saw in App. D, the occupation number indeed grows exponentially with time during the preheating epoch, and hence the quasi-classical limit is a good approximation in this epoch. In this limit the Wigner function reduces to[b2]

$$W(\varphi,\pi) = \mathcal{N}\exp\left[-\int d^3k \frac{\left|\varphi_{\vec{k}}\right|^2}{\left|f_k(\eta)\right|^2}\right]\delta\left(\pi_{\vec{k}} - \frac{F_k\varphi_{\vec{k}}}{\left|f_k(\eta)\right|^2}\right), \tag{E.2.25}$$

where we have used

$$\lim_{\sigma\to\infty}\frac{1}{\sqrt{\pi}\sigma}\exp\left[-\frac{x^2}{\sigma^2}\right] = \delta(x). \tag{E.2.26}$$

Here note that f_k can be taken to be real in the quasi-classical limit. This is because

$$f_k' f_k^* \simeq \left(f_k' f_k^*\right)^*, \tag{E.2.27}$$

that means that the complex phase of f_k does not depend on the conformal time. Then, by rotation the phase time-independently, we can take f_k as real. In the same way, g_k can be taken to be pure imaginary. In this case, F_k is given by

$$F_k = f_k f_k' - \frac{a'}{a}f_k^2. \tag{E.2.28}$$

[b2] Note that a factor $|f_k|$ is included in the constant factor $\mathcal{N}$.

By remembering that

$$\pi_{\vec{k}} = \varphi'_{\vec{k}} - \frac{a'}{a}\varphi_{\vec{k}}, \tag{E.2.29}$$

we obtain

$$\pi_{\vec{k}} - \frac{F_k \varphi_{\vec{k}}}{\left|f_k(\eta)\right|^2} = \frac{1}{f_k(\eta)}\left(f_k \varphi'_{\vec{k}} - f'_k \varphi_{\vec{k}}\right). \tag{E.2.30}$$

Therefore we finally obtain

$$W(\varphi, \pi) = \mathcal{N} \exp\left[-\int d^3k \frac{\left|\varphi_{\vec{k}}\right|^2}{\left|f_k(\eta)\right|^2}\right] \delta\left(f_k \varphi'_{\vec{k}} - f'_k \varphi_{\vec{k}}\right), \tag{E.2.31}$$

which is equivalent to the expression given in Ref. [36]. Strictly speaking, the quasi-classical limit is not valid at the very beginning of the preheating epoch, and hence it is not verified that Eq. (E.2.31) is the appropriate initial condition. Thus, in our numerical computation, we have instead used the initial condition where $\dot{\varphi}_{\vec{k}}$ follows a Gaussian distribution with its variance determined by Eq. (E.2.22), independently of $\varphi_{\vec{k}}$. Fortunately, different choices of the initial condition do not change the late time behavior of the system, and hence we may simply disregard this subtlety.

E.3 Practical implementation

In this section we explain how we implemented the classical lattice simulation numerically in some details. In the classical lattice simulation, we divide the space into a lattice, and put scalar fields at each point of the lattice. Then we solve a discretized version of the classical equations of motion in the configuration space on the lattice numerically. In the following, we first explain the spatial discretization method. Of course we should also discretize the time direction, and hence we explain it as well. Finally we discuss how to set the initial condition, in particular in the two dimensional case. For more details on the practical implementation, we refer the readers to Refs. [102, 103].

E.3.1 Spatial discretization

In this subsection, we briefly explain the spatial discretization procedure in our classical lattice simulation. We discretize the Laplacian following `DEFROST` [103]. Suppose that we would like to compute the Laplacian of a scalar field ϕ at the point $\vec{n} = (n_x, n_y, n_z)$. Then the Laplacian at that point is given by

$$\partial_i^2 \phi_{\vec{n}} \equiv \frac{1}{\Delta x^2} \sum_{\vec{m}} c_{\vec{m}} \phi_{\vec{m}}, \tag{E.3.1}$$

$\left\vert\vec{m}-\vec{n}\right\vert$	0	1	$\sqrt{2}$	$\sqrt{3}$	≥ 2
$c_{\vec{m}}$ $(d=3+1)$	-64/15	7/15	1/10	1/30	0
$c_{\vec{m}}$ $(d=2+1)$	-10/3	2/3	1/6	0	0

Table E.1: The coefficients for the discretized version of the Laplacian.

where $c_{\vec{m}}$ is given in Tab. E.1. Here Δx is the size of the lattice spacing, which is given by $\Delta x = L/N_g$, with L and N_g being the size of the simulation box and the number of grids, respectively. The corresponding spatial gradient square operator is given by

$$\left(\partial_i \phi_{\vec{n}}\right)^2 \equiv \frac{1}{2\Delta x^2} \sum_{\vec{m}} \left(\phi_{\vec{m}} - \phi_{\vec{n}}\right)^2 . \tag{E.3.2}$$

Note that the discretized version of the energy density should be fixed to be consistent with the discretization method of the equations of motion.

E.3.2 Time discretization

In order to numerically solve the equations of motion, we also discretize the time direction, and hence we briefly explain the procedure here.

In the case with $\xi_h = 0$, we have used the Leap-frog method. Suppose that we would like to evaluate the time derivatives at the time $t_n = n\Delta t$, where n is the number of step in the time direction, and Δt is the size of each step, respectively. In the Leap-frog method, they are evaluated as [103][b3]

$$\dot{\phi}_{t_n} \equiv \frac{\phi_{t_{n+1}} - \phi_{t_{n-1}}}{2\Delta t}, \tag{E.3.3}$$

$$\ddot{\phi}_{t_n} \equiv \frac{\phi_{t_{n+1}} + \phi_{t_{n-1}} - 2\phi_{t_n}}{\Delta t^2}. \tag{E.3.4}$$

The Leap-frog method has good properties: symplectic and time-symmetric, and hence we have relied on it as long as it is numerically stable.

In the case with $\xi_h \neq 0$, the Leap-frog method is not stable since the equations of motion depend on time derivatives of the scalar fields in a complicated manner. We still have symplectic methods in this case, but they are inevitably implicit and hence time-consuming. Thus we just used the Adams-Bashforth (liner multistep) method. Suppose we have an differential equation $\dot{y} = f(t, y)$. Then, in the Adams-Bashforth method, the time evolution is evaluated as

$$y_{t_{n+2}} = y_{t_{n+1}} + \Delta t \left[\frac{3}{2} f(t_{n+1}, y_{t_{n+1}}) - \frac{1}{2} f(t_n, y_{t_n})\right]. \tag{E.3.5}$$

[b3] Strictly speaking, it is slightly different from the usual Leap-frog method, since we have the Hubble friction terms that depend on the time derivatives of the scalar fields. Still, we know that it works well at least empirically as long as $\xi_h = 0$.

Note that we can make the scalar field equations of motion in this form by defining $v_\phi \equiv \dot{\phi}$ for the inflaton and similarly for the Higgs. It is in general faster than the Runge-Kutta method since we need to evaluate f only once at each step, although it is more memory-consuming since we need to retain f at t_{n+1} and t_n to evaluate quantities at t_{n+2}.

E.3.3 Initial condition and 3d-2d conversion

Here we explain the practical implementation of the initial condition. In particular, we discuss how we implemented the initial condition for the fluctuations in the case with two-dimensional space.

If we start a classical lattice simulation only with a homogenous inflaton condensation, fluctuations are never enhanced, since the classical solution must be homogenous in the later time as long as the initial condition is homogenous. Thus, we must introduce fluctuations that mimic the quantum fluctuations as an initial condition to simulate the preheating dynamics. In the case with $d = 3+1$, we introduced fluctuations in the momentum space whose variances are determined by Eq. (E.2.31), and then Fourier-transformed to obtain the fluctuations in the configuration space.

In the case with $d = 2 + 1$, we assume that the modes are homogenous in the z-direction to reduce the computational cost, and solve the $d = 3 + 1$-dimensional classical equations of motion under that assumption. In this case, we should properly take the normalization of the initial fluctuations to compensate the differences of the phase-space density, since what we would like to study is the dynamics with $d = 3 + 1$ [102]. We take the normalization such that the variance for the fluctuations in the configuration space is the same as $d = 3 + 1$ initially. In the case with $d = 3 + 1$, it is given by

$$\left\langle \chi(x)^2 \right\rangle \simeq \frac{(\Delta k)^6}{(2\pi)^2} \left(\frac{L}{2\pi}\right)^2 \sum_n k_n^2 \left| \chi^{(3d)}_{\vec{k}_n} \right|^2 , \tag{E.3.6}$$

where χ is a scalar field, $\Delta k = 2\pi/L$ is the momentum resolution, and k_n is the norm of the momentum $\vec{k}_n$. Note that we have used the spherical symmetry here, and n parametrizes the radial direction of $\vec{k}$. In the case with $d = 2 + 1$, it is instead given by

$$\left\langle \chi(x)^2 \right\rangle \simeq \frac{(\Delta k)^4}{(2\pi)^2} \left(\frac{L}{2}\right) \sum_n k_n \left| \chi^{(2d)}_{\vec{k}_n} \right|^2 , \tag{E.3.7}$$

and hence we should take the normalization of $\chi^{(2d)}_{\vec{k}_n}$ such that

$$\left| \chi^{(2d)}_{\vec{k}_n} \right|^2 = \frac{2k_n}{L} \left| \chi^{(3d)}_{\vec{k}_n} \right|^2 . \tag{E.3.8}$$

We have used this relation to run the classical lattice simulation in Chap. 5.

E.3.4 Mass renormalization

As we discussed in the previous subsection, we introduce Gaussian fluctuations initially to imitate the quantum fluctuations. They induce effective mass terms to the scalar fields that

are sensitive to the UV cut-off of the lattice. Thus, we need to subtract such mass terms to obtain physical results [104, 105]. It is analogous to the usual renormalization procedure of the quantum field theory.

To be more specific, let us consider the Lagrangian (4.6.14) used to study the effects of the gauge bosons with only $\lambda_{h\phi}$ being present. In this case, the inflaton, the Higgs and χ initially obtains effective mass terms as

$$m^2_{\mathrm{eff};\phi}(0) = m^2_\phi + \lambda_{h\phi}\left\langle h^2(0)\right\rangle + \delta m^2_{R;\phi}(0), \tag{E.3.9}$$

$$m^2_{\mathrm{eff};h}(0) = \lambda_{h\phi}\left\langle \phi^2(0)\right\rangle + 3\lambda_h\left\langle h^2(0)\right\rangle + g^2_{h\chi}\left\langle \chi^2(0)\right\rangle + \delta m^2_{R;h}(0) \tag{E.3.10}$$

$$m^2_{\mathrm{eff};\chi}(0) = g^2_{h\chi}\left\langle h^2(0)\right\rangle + 3g^2_{\chi\chi}\left\langle \chi^2(0)\right\rangle + \delta m^2_{R;\chi}(0), \tag{E.3.11}$$

where $\delta m_{R;i}$ is the counter term for the scalar field i and we have used the mean field approximation. Among these contributions, only m^2_ϕ and the contribution from the initial inflaton condensation is physical, and hence we take the counter terms as

$$\delta m^2_{R;\phi}(0) = -\lambda_{h\phi}\left\langle h^2(0)\right\rangle, \tag{E.3.12}$$

$$\delta m^2_{R;h}(0) = -\lambda_{h\phi}\left(\left\langle \phi^2(0)\right\rangle - \Phi^2_{\mathrm{ini}}\right) - 3\lambda_h\left\langle h^2(0)\right\rangle - g^2_{h\chi}\left\langle \chi^2(0)\right\rangle, \tag{E.3.13}$$

$$\delta m^2_{R;\chi}(0) = -g^2_{h\chi}\left\langle h^2(0)\right\rangle - 3g^2_{\chi\chi}\left\langle \chi^2(0)\right\rangle. \tag{E.3.14}$$

The time evolution of the counter terms is given as

$$\delta m^2_{R;i}(t) = \frac{m^2_{R;i}(0)}{a^2(t)}, \tag{E.3.15}$$

where i is ϕ, h or χ, since the UV cut-off scales as $\Lambda/a(t)$ as we fix the comoving volume in our lattice simulation. We can define mass counter terms in a similar way for other systems.

This renormalization procedure is not important if there are only the inflaton and the Higgs, since the sizes of the couplings are relatively small in such a case. However, it is crucial if we introduce an additional field that couples to other fields with sizable couplings, as it is the case of the scalar field χ in Sec. 4.6. See *e.g.* Ref. [105] for more details on the importance of this mass renormalization procedure.

Bibliography

[1] Y. Ema, K. Mukaida, and K. Nakayama, "Fate of Electroweak Vacuum during Preheating," *JCAP* **1610** no. 10, (2016) 043, arXiv:1602.00483 [hep-ph].

[2] Y. Ema, M. Karciauskas, O. Lebedev, and M. Zatta, "Early Universe Higgs dynamics in the presence of the Higgs-inflaton and non-minimal Higgs-gravity couplings," *JCAP* **1706** no. 06, (2017) 054, arXiv:1703.04681 [hep-ph].

[3] Y. Ema, K. Mukaida, and K. Nakayama, "Electroweak Vacuum Metastability and Low-scale Inflation," *JCAP* **1712** no. 12, (2017) 030, arXiv:1706.08920 [hep-ph].

[4] S. R. Coleman and E. J. Weinberg, "Radiative Corrections as the Origin of Spontaneous Symmetry Breaking," *Phys. Rev.* **D7** (1973) 1888–1910.

[5] G. Degrassi, S. Di Vita, J. Elias-Miro, J. R. Espinosa, G. F. Giudice, G. Isidori, and A. Strumia, "Higgs mass and vacuum stability in the Standard Model at NNLO," *JHEP* **08** (2012) 098, arXiv:1205.6497 [hep-ph].

[6] D. Buttazzo, G. Degrassi, P. P. Giardino, G. F. Giudice, F. Sala, A. Salvio, and A. Strumia, "Investigating the near-criticality of the Higgs boson," *JHEP* **12** (2013) 089, arXiv:1307.3536 [hep-ph].

[7] A. Andreassen, W. Frost, and M. D. Schwartz, "Scale Invariant Instantons and the Complete Lifetime of the Standard Model," arXiv:1707.08124 [hep-ph].

[8] S. Chigusa, T. Moroi, and Y. Shoji, "State-of-the-Art Calculation of the Decay Rate of Electroweak Vacuum in Standard Model," *Phys. Rev. Lett.* **119** no. 21, (2017) 211801, arXiv:1707.09301 [hep-ph].

[9] M. Sher, "Electroweak Higgs Potentials and Vacuum Stability," *Phys. Rept.* **179** (1989) 273–418.

[10] P. B. Arnold, "Can the Electroweak Vacuum Be Unstable?," *Phys. Rev.* **D40** (1989) 613.

[11] G. W. Anderson, "New Cosmological Constraints on the Higgs Boson and Top Quark Masses," *Phys. Lett.* **B243** (1990) 265–270.

[12] P. B. Arnold and S. Vokos, "Instability of hot electroweak theory: bounds on m(H) and M(t)," *Phys. Rev.* **D44** (1991) 3620–3627.

[13] J. R. Espinosa and M. Quiros, "Improved metastability bounds on the standard model Higgs mass," *Phys. Lett.* **B353** (1995) 257–266, arXiv:hep-ph/9504241 [hep-ph].

[14] G. Isidori, G. Ridolfi, and A. Strumia, "On the metastability of the standard model vacuum," *Nucl. Phys.* **B609** (2001) 387–409, arXiv:hep-ph/0104016 [hep-ph].

[15] F. Bezrukov and M. Shaposhnikov, "Standard Model Higgs boson mass from inflation: Two loop analysis," *JHEP* **07** (2009) 089, arXiv:0904.1537 [hep-ph].

[16] J. Ellis, J. R. Espinosa, G. F. Giudice, A. Hoecker, and A. Riotto, "The Probable Fate of the Standard Model," *Phys. Lett.* **B679** (2009) 369–375, arXiv:0906.0954 [hep-ph].

[17] J. Elias-Miro, J. R. Espinosa, G. F. Giudice, G. Isidori, A. Riotto, and A. Strumia, "Higgs mass implications on the stability of the electroweak vacuum," *Phys. Lett.* **B709** (2012) 222–228, arXiv:1112.3022 [hep-ph].

[18] F. Bezrukov, M. Yu. Kalmykov, B. A. Kniehl, and M. Shaposhnikov, "Higgs Boson Mass and New Physics," *JHEP* **10** (2012) 140, arXiv:1205.2893 [hep-ph]. [,275(2012)].

[19] A. V. Bednyakov, B. A. Kniehl, A. F. Pikelner, and O. L. Veretin, "Stability of the Electroweak Vacuum: Gauge Independence and Advanced Precision," *Phys. Rev. Lett.* **115** no. 20, (2015) 201802, arXiv:1507.08833 [hep-ph].

[20] W. E. East, J. Kearney, B. Shakya, H. Yoo, and K. M. Zurek, "Spacetime Dynamics of a Higgs Vacuum Instability During Inflation," *Phys. Rev.* **D95** no. 2, (2017) 023526, arXiv:1607.00381 [hep-ph]. [Phys. Rev.D95,023526(2017)].

[21] A. A. Starobinsky, "STOCHASTIC DE SITTER (INFLATIONARY) STAGE IN THE EARLY UNIVERSE," *Lect. Notes Phys.* **246** (1986) 107–126.

[22] A. A. Starobinsky and J. Yokoyama, "Equilibrium state of a selfinteracting scalar field in the De Sitter background," *Phys. Rev.* **D50** (1994) 6357–6368, arXiv:astro-ph/9407016 [astro-ph].

[23] J. R. Espinosa, G. F. Giudice, and A. Riotto, "Cosmological implications of the Higgs mass measurement," *JCAP* **0805** (2008) 002, arXiv:0710.2484 [hep-ph].

[24] A. Kobakhidze and A. Spencer-Smith, "Electroweak Vacuum (In)Stability in an Inflationary Universe," *Phys. Lett.* **B722** (2013) 130–134, arXiv:1301.2846 [hep-ph].

[25] M. Fairbairn and R. Hogan, "Electroweak Vacuum Stability in light of BICEP2," *Phys. Rev. Lett.* **112** (2014) 201801, arXiv:1403.6786 [hep-ph].

[26] A. Hook, J. Kearney, B. Shakya, and K. M. Zurek, "Probable or Improbable Universe? Correlating Electroweak Vacuum Instability with the Scale of Inflation," *JHEP* **01** (2015) 061, arXiv:1404.5953 [hep-ph].

[27] K. Kamada, "Inflationary cosmology and the standard model Higgs with a small Hubble induced mass," *Phys. Lett.* **B742** (2015) 126–135, arXiv:1409.5078 [hep-ph].

[28] M. Herranen, T. Markkanen, S. Nurmi, and A. Rajantie, "Spacetime curvature and the Higgs stability during inflation," *Phys. Rev. Lett.* **113** no. 21, (2014) 211102, arXiv:1407.3141 [hep-ph].

[29] J. Kearney, H. Yoo, and K. M. Zurek, "Is a Higgs Vacuum Instability Fatal for High-Scale Inflation?," *Phys. Rev.* **D91** no. 12, (2015) 123537, arXiv:1503.05193 [hep-th].

[30] J. R. Espinosa, G. F. Giudice, E. Morgante, A. Riotto, L. Senatore, A. Strumia, and N. Tetradis, "The cosmological Higgstory of the vacuum instability," *JHEP* **09** (2015) 174, arXiv:1505.04825 [hep-ph].

[31] A. Joti, A. Katsis, D. Loupas, A. Salvio, A. Strumia, N. Tetradis, and A. Urbano, "(Higgs) vacuum decay during inflation," *JHEP* **07** (2017) 058, arXiv:1706.00792 [hep-ph].

[32] A. Rajantie and S. Stopyra, "Standard Model vacuum decay in a de Sitter Background," arXiv:1707.09175 [hep-th].

[33] I. L. Buchbinder, S. D. Odintsov, and I. L. Shapiro, *Effective action in quantum gravity*. 1992.

[34] O. Lebedev and A. Westphal, "Metastable Electroweak Vacuum: Implications for Inflation," *Phys. Lett.* **B719** (2013) 415–418, arXiv:1210.6987 [hep-ph].

[35] D. Polarski and A. A. Starobinsky, "Semiclassicality and decoherence of cosmological perturbations," *Class. Quant. Grav.* **13** (1996) 377–392, arXiv:gr-qc/9504030 [gr-qc].

[36] S. Yu. Khlebnikov and I. I. Tkachev, "Classical decay of inflaton," *Phys. Rev. Lett.* **77** (1996) 219–222, arXiv:hep-ph/9603378 [hep-ph].

[37] J. F. Dufaux, G. N. Felder, L. Kofman, M. Peloso, and D. Podolsky, "Preheating with trilinear interactions: Tachyonic resonance," *JCAP* **0607** (2006) 006, arXiv:hep-ph/0602144 [hep-ph].

[38] K. Enqvist, M. Karciauskas, O. Lebedev, S. Rusak, and M. Zatta, "Postinflationary vacuum instability and Higgs-inflaton couplings," *JCAP* **1611** (2016) 025, arXiv:1608.08848 [hep-ph].

[39] G. N. Felder, L. Kofman, and A. D. Linde, "Instant preheating," *Phys. Rev.* **D59** (1999) 123523, arXiv:hep-ph/9812289 [hep-ph].

[40] F. Bezrukov, D. Gorbunov, and M. Shaposhnikov, "On initial conditions for the Hot Big Bang," *JCAP* **0906** (2009) 029, arXiv:0812.3622 [hep-ph].

[41] J. Garcia-Bellido, D. G. Figueroa, and J. Rubio, "Preheating in the Standard Model with the Higgs-Inflaton coupled to gravity," *Phys. Rev.* **D79** (2009) 063531, arXiv:0812.4624 [hep-ph].

[42] K. Mukaida and K. Nakayama, "Dynamics of oscillating scalar field in thermal environment," *JCAP* **1301** (2013) 017, arXiv:1208.3399 [hep-ph].

[43] K. Mukaida and K. Nakayama, "Dissipative Effects on Reheating after Inflation," *JCAP* **1303** (2013) 002, arXiv:1212.4985 [hep-ph].

[44] F. L. Bezrukov and M. Shaposhnikov, "The Standard Model Higgs boson as the inflaton," *Phys. Lett.* **B659** (2008) 703–706, arXiv:0710.3755 [hep-th].

[45] K. Nakayama and F. Takahashi, "Running Kinetic Inflation," *JCAP* **1011** (2010) 009, arXiv:1008.2956 [hep-ph].

[46] R. Kallosh and A. Linde, "Universality Class in Conformal Inflation," *JCAP* **1307** (2013) 002, arXiv:1306.5220 [hep-th].

[47] R. Kallosh, A. Linde, and D. Roest, "Superconformal Inflationary α-Attractors," *JHEP* **11** (2013) 198, arXiv:1311.0472 [hep-th].

[48] G. N. Felder and L. Kofman, "The Development of equilibrium after preheating," *Phys. Rev.* **D63** (2001) 103503, arXiv:hep-ph/0011160 [hep-ph].

[49] D. G. Figueroa, J. Garcia-Bellido, and F. Torrenti, "Decay of the standard model Higgs field after inflation," *Phys. Rev.* **D92** no. 8, (2015) 083511, arXiv:1504.04600 [astro-ph.CO].

[50] K. Enqvist, S. Nurmi, S. Rusak, and D. Weir, "Lattice Calculation of the Decay of Primordial Higgs Condensate," *JCAP* **1602** no. 02, (2016) 057, arXiv:1506.06895 [astro-ph.CO].

[51] D. G. Figueroa, A. Rajantie, and F. Torrenti, "Higgs-curvature coupling and post-inflationary vacuum instability," arXiv:1709.00398 [astro-ph.CO].

[52] A. D. Linde, "A New Inflationary Universe Scenario: A Possible Solution of the Horizon, Flatness, Homogeneity, Isotropy and Primordial Monopole Problems," *Phys. Lett.* **108B** (1982) 389–393.

[53] A. Albrecht and P. J. Steinhardt, "Cosmology for Grand Unified Theories with Radiatively Induced Symmetry Breaking," *Phys. Rev. Lett.* **48** (1982) 1220–1223.

[54] G. Barenboim, E. J. Chun, and H. M. Lee, "Coleman-Weinberg Inflation in light of Planck," *Phys. Lett.* **B730** (2014) 81–88, arXiv:1309.1695 [hep-ph].

[55] L. Boubekeur and D. Lyth, "Hilltop inflation," *JCAP* **0507** (2005) 010, arXiv:hep-ph/0502047 [hep-ph].

[56] K. Kumekawa, T. Moroi, and T. Yanagida, "Flat potential for inflaton with a discrete R invariance in supergravity," *Prog. Theor. Phys.* **92** (1994) 437–448, arXiv:hep-ph/9405337 [hep-ph].

[57] K. I. Izawa and T. Yanagida, "Natural new inflation in broken supergravity," *Phys. Lett.* **B393** (1997) 331–336, arXiv:hep-ph/9608359 [hep-ph].

[58] T. Asaka, K. Hamaguchi, M. Kawasaki, and T. Yanagida, "Leptogenesis in inflationary universe," *Phys. Rev.* **D61** (2000) 083512, arXiv:hep-ph/9907559 [hep-ph].

[59] V. N. Senoguz and Q. Shafi, "New inflation, preinflation, and leptogenesis," *Phys. Lett.* **B596** (2004) 8–15, arXiv:hep-ph/0403294 [hep-ph].

[60] O. Lebedev, "On Stability of the Electroweak Vacuum and the Higgs Portal," *Eur. Phys. J.* **C72** (2012) 2058, arXiv:1203.0156 [hep-ph].

[61] J. Elias-Miro, J. R. Espinosa, G. F. Giudice, H. M. Lee, and A. Strumia, "Stabilization of the Electroweak Vacuum by a Scalar Threshold Effect," *JHEP* **06** (2012) 031, arXiv:1203.0237 [hep-ph].

[62] Y. Ema, M. Karciauskas, O. Lebedev, S. Rusak, and M. Zatta, "Higgs-Inflaton Mixing and Vacuum Stability," arXiv:1711.10554 [hep-ph].

[63] P. Brax, J.-F. Dufaux, and S. Mariadassou, "Preheating after Small-Field Inflation," *Phys. Rev.* **D83** (2011) 103510, arXiv:1012.4656 [hep-th].

[64] D. I. Podolsky, G. N. Felder, L. Kofman, and M. Peloso, "Equation of state and beginning of thermalization after preheating," *Phys. Rev.* **D73** (2006) 023501, arXiv:hep-ph/0507096 [hep-ph].

[65] T. Futamase and K.-i. Maeda, "Chaotic Inflationary Scenario in Models Having Nonminimal Coupling With Curvature," *Phys. Rev.* **D39** (1989) 399–404.

[66] R. Fakir and W. G. Unruh, "Improvement on cosmological chaotic inflation through nonminimal coupling," *Phys. Rev.* **D41** (1990) 1783–1791.

[67] A. A. Starobinsky, "A New Type of Isotropic Cosmological Models Without Singularity," *Phys. Lett.* **91B** (1980) 99–102.

[68] J. D. Barrow and A. C. Ottewill, "The Stability of General Relativistic Cosmological Theory," *J. Phys.* **A16** (1983) 2757.

[69] B. Whitt, "Fourth Order Gravity as General Relativity Plus Matter," *Phys. Lett.* **145B** (1984) 176–178.

[70] J. D. Barrow and S. Cotsakis, "Inflation and the Conformal Structure of Higher Order Gravity Theories," *Phys. Lett.* **B214** (1988) 515–518.

[71] P. B. Greene, L. Kofman, A. D. Linde, and A. A. Starobinsky, "Structure of resonance in preheating after inflation," *Phys. Rev.* **D56** (1997) 6175–6192, arXiv:hep-ph/9705347 [hep-ph].

[72] L. Delle Rose, C. Marzo, and A. Urbano, "On the fate of the Standard Model at finite temperature," *JHEP* **05** (2016) 050, arXiv:1507.06912 [hep-ph].

[73] M. E. Peskin and D. V. Schroeder, *An Introduction to quantum field theory*. Addison-Wesley, Reading, USA, 1995. http://www.slac.stanford.edu/~mpeskin/QFT.html.

[74] M. D. Schwartz, *Quantum Field Theory and the Standard Model*. Cambridge University Press, 2014. http://www.cambridge.org/us/academic/subjects/physics/theoretical-physics-and-mathematical-physics/quantum-field-theory-and-standard-model.

[75] D. Z. Freedman and A. Van Proeyen, *Supergravity*. Cambridge Univ. Press, Cambridge, UK, 2012. http://www.cambridge.org/mw/academic/subjects/physics/theoretical-physics-and-mathematical-physics/supergravity?format=AR.

[76] J. Ellis, "TikZ-Feynman: Feynman diagrams with TikZ," *Comput. Phys. Commun.* **210** (2017) 103–123, arXiv:1601.05437 [hep-ph].

[77] D. J. Gross and F. Wilczek, "Asymptotically Free Gauge Theories. 1," *Phys. Rev.* **D8** (1973) 3633–3652.

[78] S. Weinberg, *The quantum theory of fields. Vol. 2: Modern applications*. Cambridge University Press, 2013.

[79] W. E. Caswell and F. Wilczek, "On the Gauge Dependence of Renormalization Group Parameters," *Phys. Lett.* **49B** (1974) 291–292.

[80] N. K. Nielsen, "On the Gauge Dependence of Spontaneous Symmetry Breaking in Gauge Theories," *Nucl. Phys.* **B101** (1975) 173–188.

[81] R. Fukuda and T. Kugo, "Gauge Invariance in the Effective Action and Potential," *Phys. Rev.* **D13** (1976) 3469.

[82] I. J. R. Aitchison and C. M. Fraser, "Gauge Invariance and the Effective Potential," *Annals Phys.* **156** (1984) 1.

[83] A. Andreassen, W. Frost, and M. D. Schwartz, "Consistent Use of Effective Potentials," *Phys. Rev.* **D91** no. 1, (2015) 016009, arXiv:1408.0287 [hep-ph].

[84] A. Andreassen, W. Frost, and M. D. Schwartz, "Consistent Use of the Standard Model Effective Potential," *Phys. Rev. Lett.* **113** no. 24, (2014) 241801, arXiv:1408.0292 [hep-ph].

[85] J. M. Maldacena, "Non-Gaussian features of primordial fluctuations in single field inflationary models," *JHEP* **05** (2003) 013, arXiv:astro-ph/0210603 [astro-ph].

[86] R. L. Arnowitt, S. Deser, and C. W. Misner, "The Dynamics of general relativity," *Gen. Rel. Grav.* **40** (2008) 1997–2027, arXiv:gr-qc/0405109 [gr-qc].

[87] **Planck** Collaboration, P. A. R. Ade *et al.*, "Planck 2015 results. XIII. Cosmological parameters," *Astron. Astrophys.* **594** (2016) A13, arXiv:1502.01589 [astro-ph.CO].

[88] **BICEP2, Keck Array** Collaboration, P. A. R. Ade *et al.*, "Improved Constraints on Cosmology and Foregrounds from BICEP2 and Keck Array Cosmic Microwave Background Data with Inclusion of 95 GHz Band," *Phys. Rev. Lett.* **116** (2016) 031302, arXiv:1510.09217 [astro-ph.CO].

[89] **CMB-S4** Collaboration, K. N. Abazajian *et al.*, "CMB-S4 Science Book, First Edition," arXiv:1610.02743 [astro-ph.CO].

[90] K. Nakayama and F. Takahashi, "PeV-scale Supersymmetry from New Inflation," *JCAP* **1205** (2012) 035, arXiv:1203.0323 [hep-ph].

[91] **Planck** Collaboration, P. A. R. Ade *et al.*, "Planck 2015 results. XX. Constraints on inflation," *Astron. Astrophys.* **594** (2016) A20, arXiv:1502.02114 [astro-ph.CO].

[92] L. Pilo, A. Riotto, and A. Zaffaroni, "On the amount of gravitational waves from inflation," *Phys. Rev. Lett.* **92** (2004) 201303, arXiv:astro-ph/0401302 [astro-ph].

[93] N. D. Birrell and P. C. W. Davies, *Quantum Fields in Curved Space*. Cambridge Monographs on Mathematical Physics. Cambridge Univ. Press, Cambridge, UK, 1984. http://www.cambridge.org/mw/academic/subjects/physics/theoretical-physics-and-mathematical-physics/quantum-fields-curved-space?format=PB.

[94] L. E. Parker and D. Toms, *Quantum Field Theory in Curved Spacetime*. Cambridge Monographs on Mathematical Physics. Cambridge University Press, 2009. http://www.cambridge.org/de/knowledge/isbn/item2327457.

[95] R. J. Hardwick, V. Vennin, C. T. Byrnes, J. Torrado, and D. Wands, "The stochastic spectator," *JCAP* **1710** (2017) 018, arXiv:1701.06473 [astro-ph.CO].

[96] A. D. Dolgov and D. P. Kirilova, "ON PARTICLE CREATION BY A TIME DEPENDENT SCALAR FIELD," *Sov. J. Nucl. Phys.* **51** (1990) 172–177. [Yad. Fiz.51,273(1990)].

[97] J. H. Traschen and R. H. Brandenberger, "Particle Production During Out-of-equilibrium Phase Transitions," *Phys. Rev.* **D42** (1990) 2491–2504.

[98] Y. Shtanov, J. H. Traschen, and R. H. Brandenberger, "Universe reheating after inflation," *Phys. Rev.* **D51** (1995) 5438–5455, arXiv:hep-ph/9407247 [hep-ph].

[99] L. Kofman, A. D. Linde, and A. A. Starobinsky, "Towards the theory of reheating after inflation," *Phys. Rev.* **D56** (1997) 3258–3295, arXiv:hep-ph/9704452 [hep-ph].

[100] J. Lachapelle and R. H. Brandenberger, "Preheating with Non-Standard Kinetic Term," *JCAP* **0904** (2009) 020, arXiv:0808.0936 [hep-th].

[101] W. B. Case, "Wigner functions and Weyl transforms for pedestrians," *Amer. J. Phys.* **76** (2008) 937–946.

[102] G. N. Felder and I. Tkachev, "LATTICEEASY: A Program for lattice simulations of scalar fields in an expanding universe," *Comput. Phys. Commun.* **178** (2008) 929–932, arXiv:hep-ph/0011159 [hep-ph].

[103] A. V. Frolov, "DEFROST: A New Code for Simulating Preheating after Inflation," *JCAP* **0811** (2008) 009, arXiv:0809.4904 [hep-ph].

[104] A. Rajantie, P. M. Saffin, and E. J. Copeland, "Electroweak preheating on a lattice," *Phys. Rev.* **D63** (2001) 123512, arXiv:hep-ph/0012097 [hep-ph].

[105] J. Berges, K. Boguslavski, S. Schlichting, and R. Venugopalan, "Basin of attraction for turbulent thermalization and the range of validity of classical-statistical simulations," *JHEP* **05** (2014) 054, arXiv:1312.5216 [hep-ph].